Doctoral theses at NTNU, 2012:301

Grunde Olimstad

Characteristics of Reversible-Pump Turbines

Doctoral Thesis

Grunde Olimstad

ISBN 978-82-471-3919-6
ISBN 978-82-471-3920-2
ISSN 1503-8181

NTNU – Trondheim
Norwegian University of Science and Technology

NTNU
Norwegian University of Science and Technology
Thesis for the degree of Philosophiae Doctor
Faculty of Engineering Science & Technology
Department of Energy and Process Engineering

Doctoral theses at NTNU, 2012:301

NTNU

NTNU – Trondheim
Norwegian University of Science and Technology

Grunde Olimstad

Characteristics of Reversible-Pump Turbines

Thesis for the degree of Philosophiae Doctor

Trondheim, 10 2012

Norwegian University of Science and Technology
Faculty of Engineering Science & Technology
Department of Energy and Process Engineering

NTNU – Trondheim
Norwegian University of
Science and Technology

NTNU
Norwegian University of Science and Technology

Thesis for the degree of Philosophiae Doctor

Faculty of Engineering Science & Technology
Department of Energy and Process Engineering

ISBN 978-82-471-3919-6
ISBN 978-82-471-3920-2
ISSN 1503-8181

Doctoral theses at NTNU, 2012:301

Printed by Skipnes Kommunikasjon as

Abstract

The primary goal for this PhD project has been to investigate instability of reversible-pump turbines (RPTs) as a phenomenon and to find remedies to solve it. The instability occurs for turbines with s-shaped characteristics, unfavourable waterways and limited rotating inertia. It is only observed for certain operation points at either high speed or low load. These correspond to either high values of N_{ed} or low values of Q_{ed}. The work done in this PhD thesis can be divided into the three following categories.

Investigate and understand the behaviour of a pump turbine: A model was designed in order to investigate the pump turbine behaviour related to its characteristics. This model was manufactured and measurements were performed in the laboratory. By using throttling valves or torque as input the full s-shaped characteristics was measured. When neither of these techniques is used, the laboratory system has unstable operation points which result in hysteresis behaviour. Global behaviour of the RPT in a power plant system was investigated through analytical stability analysis and dynamic system simulations. The latter included both rigid and elastic representation of the water column.

Turbine internal flow: The flow inside the runner was investigated by computer simulations (CFD). Two-dimensional analysis was used to study the inlet part of the runner. This showed that a vortex forming at the inlet is one of the causes for the unstable characteristics. Three-dimensional analyses were performed and showed multiple complex flow structures in the unstable operation range. Measurements at different pressure levels showed that the characteristics were dependent on the Reynolds number at high N_{ed} values in turbine mode. This means that the similarity of flows is not sufficiently described by constant Q_{ed} and N_{ed} values at this part of the characteristics.

Design modifications: The root of the stability problem was considered to be the runner's geometric design at the inlet in turbine mode. Therefore different design parameters were investigated to find relations to the characteristics. Methods used were measurements, CFD modelling and analytical models. The leading edge profile was altered on the physical model and measurements were performed in the laboratory. Results showed that the profiles have significant influence on characteristics and therewith stability at high speed operation points. Other design parameters were investigated by CFD analysis with special focus on the inlet blade angle.

Keywords: Pump Turbines, Stability, Design, CFD, Measurements

Acknowledgements

I would like to express my gratitude to my supervisors Torbjørn Nielsen and Bjarne Børresen who have been of great support throughout the project. You have been invaluable discussions partners with unique technical insight and understanding of the PhD work. Thanks to Ole Gunnar Dahlhaug and Bård Brandåstrø for helping with the design and manufacturing of the pump turbine and thanks to the laboratory staff, Trygve Opland, Joar Grilstad and Halvor Haukvik for your laboratory assistance. I have been lucky to be part of a very good working environment at the Waterpower Laboratory. Especially I want to thank Eve Cathrin Walseth, for many good discussions, cooperation and encouraging talks. I am grateful to Rainpower for technical discussions, using their computer cluster and advices regarding geometry alterations on the laboratory model runner. I am also grateful to Håkan Nilsson and Olivier Petit at Chalmers University for their help with the CFD tool OpenFOAM. Thanks to the Norwegian power companies, consultants and equipment suppliers that have funded this work through Energy Norway. Finally, I want to express my gratitude to Ingvild for being supportive and encouraging during my work with this thesis.

Contents

List of Figures

List of symbols

Abbreviations and special terms

CFD	Computational fluids dynamic
BEP	Best efficiency point
RPT	Reversible-pump turbine
DNS	Direct numerical simulation
CFL	Courant-Friedrich limit
GGI	General grid interface
OpenFOAM	Open field operation and manipulation, an open source CFD code
Turbine brake mode	Operation area where the flow rate is positive and the efficiency negative
Reverse pump mode	Operation area where the turbine rotation has the same direction as in turbine mode but the flow rate is negative, i.e. the turbine is pumping.

List of physical symbols

Symbols	Description	Dimensions
A	Area	$[m^2]$
a	Linear slope of turbine H-Q curve	[-]
a_1	Slope of flow curve	[-]
α	Flow angle	[-]
α	Guide vane angle	[-]
b_1	Slope of torque curve	[-]
β	Normalized torque	[-]
β	Relative flow angle	[-]
c	Absolute velocity	[m/s]
C	Reference speed	[m/s]
D	Diameter	[m]
ε	Turbulent dissipation	$[m^2/s^3]$
f	Friction factor	[-]
g	Gravitational acceleration	$[m/s^2]$
H	Head	[m]
h	Normalized head	[-]
J	Polar moment of inertia	$[kgm^2]$
k	Friction coefficient	$[s^2/m^5]$
k	Turbulent kinetic energy	$[m^2/s^2]$

L	Length/Reference length	[m]
μ	Viscosity	[kg/ms]
N,n	Speed of rotation	[rev/s]
N_{ed}	Dimensionless speed of rotation	[-]
ω	Speed of rotation	[rad/s]
p	Pressure	[Pa]
P	Reference pressure	[Pa]
Q	Flow rate	[m^3/s]
q	Flow perturbation	[m^3/s]
Q_{ed}	Dimensionless flow rate	[-]
r	Radius	[m]
ρ	Density	[kg/m^3]
τ	Shear stress	[N/m^2]
t	Time	[s]
T	Torque	[Nm]
T	Reference time	[s]
T_a	Machine time scale	[s]
τ_f	Fluid to machine timescale	[-]
T_{ed}	Dimensionless torque	[-]
T_w	Water time scale	[s]
u	Peripheral velocity	[m/s]
u_τ	Friction velocity	[m/s]
v	Normalized flow rate	[-]
w	Relative velocity	[m/s]
y	Wall distance	[m]
y+	Normalized wall distance	[-]
Z,z	Height	[m]

List of mathematical symbols

Mathematical symbols	**Description**
d/dt	Time derivative
∇	Vector differential operator
$\bar{\bar{x}}$	x-vector
$\bar{\bar{A}}$	A-matrix
I	Identity matrix
∂/∂x	Spatial derivative
λ	Eigenvalue

Sub- and superscript

Symbol	Description
1	Inlet
2	Outlet
0	Initial point
f	Friction
t	Turbine
r	Reservoir
h	Hydraulic
g	Generator
*	Best operation point
s	Shaft
u	Peripheral
m	Meridional
i	Index
j	Index
t	Turbulent
delta	Djiracs delta function
abs	Absolute
rel	Relative
n	Nominal
z	Axial direction

1 Introduction

1.1 Introduction to pump turbines

Pumped storage power plants play an important role in stabilizing the electric power system. Traditionally this mainly gets its energy from thermal gas-, coal- or nuclear-power plants or hydropower. Today new renewable energy sources such as wind and sun constitute a larger and larger piece of this energy mixture. These intermittent energy sources have varying and, to some extent, unpredictable production. Therefore they need a collaborator to step in when the production is either too high or too low. In many cases the most efficient collaborator is pumped hydro storage power plants. They can, depending on reservoir size, deliver long term energy storage and they are able to boost production (turbine) or consumption (pump) in peak power situations.

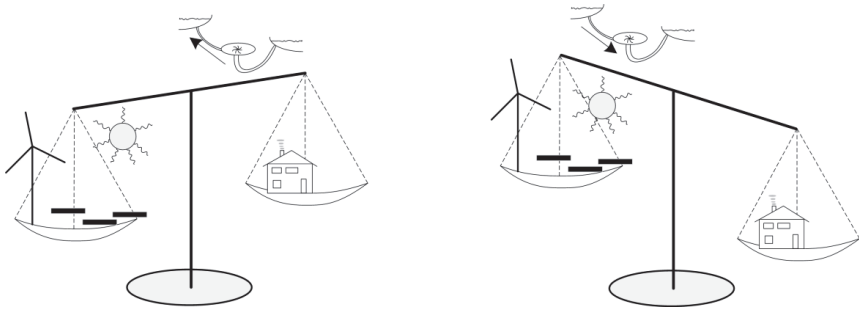

Figure 1 Pumped hydro storage plants balance production and consumption

There are currently many pumped hydro storage power plants in the world, and many more will probably come. In Norway there are in total nine plants, NVE [1], with Ulla-Førre as the largest having an installed capacity of 2000 MW in turbine mode and 340MW in pump mode. Its upper reservoir, Blåsjø, holds an energy reserve of 7.8 TWh. The largest pumped hydro power plant in Europe is Dinorwig [2] in Wales with 1.7 GW generating potential divided between six reversible-pump turbines. Using a reversible-pump turbine is widely regarded as the most cost effective solution, but there are also other technical arrangements such as the combinations Francis turbine/pump or Pelton turbine/pump. The world highest lifting height for a single stage RPT is 779 meters, Ikeda [3], but with multiple stages, such as in Grand Mason, Henry [4], the lifting height can be much higher. Many new pumped storage power plants are recently initiated in central Europe where the need for stabilizing is high.

Fast and reliable start-up in turbine mode is an absolute requirement for pump turbines. This is in many cases, such as f.ex. Bhira [5], COO II [6] and Bajina Basta [7], not

achieved because of instability caused by the pump turbine characteristics. These characteristics are curves relating the non-dimensional flow rate (Q_{ed}) to non-dimensional speed (N_{ed}), and non-dimensional torque (T_{ed}) to N_{ed} at constant guide vane opening. Mechanical arrangements can solve the stability problems but are not desired because of cost and reliability. Some new power plants have installed variable speed generators. The associated turbines can operate with high efficiency over a wide range of power outputs and stability during start-up may be solved if turbine and generator can be synchronized at a speed lower than nominal speed. The variable speed has an initial cost and also a cost of extra electrical losses. Therefore it will always be the best to solve the root cause of the instabilities which is to be found in the runner hydraulic behaviour.

The stability problems to be solved in turbine mode apply to three different situations:

- Synchronization of turbine and generator during start-up
- Instability during load-rejection with governor failure
- Instability during extreme low head operation

1.2 Objectives

One objective of this research is to understand the underlying physical mechanism of turbine-mode instability of reversible-pump turbines. Herein lay the description of flow features and stability mechanisms of hydraulic systems. A second objective is to investigate the relation between runner inlet geometry and the instability in order to make suggestions for design improvements.

1.3 Hypothesis

The type of instability investigated in this work is mostly connected to high head and low specific speed number reversible-pump turbines and not so much to Francis turbines. The fact that the distributor and draft tube can be very similar for those two types of machines leads to the assumption that the instability problem has its source in the runner flow. Furthermore it follows that the stability can be solved by runner geometry alterations. These alterations should however not be performed on the cost of pump-mode stability or efficiency in best operation point.

Pump turbines in pump mode work against a higher head than the available head for a Francis turbine in the same hydro power plant due to friction forces in the waterways. To get this extra lift, pump turbines have larger diameters than comparable Francis turbines. This prolongation is essentially two dimensional and since the inlet blade angle normally is small, it constitutes a large portion of the blade. Research performed by Staubli [15] concludes that the instability is related to vortices that form at the inlet part of the runner. Since the inlet part of the runner essentially is two dimensional, and is shown to be important for stability, two dimensional analyses can be performed to investigate the source of the instability.

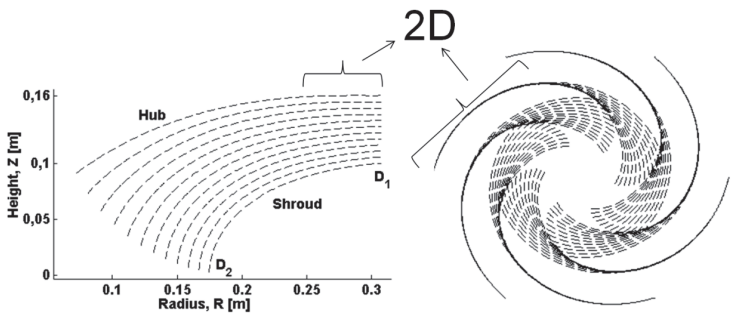

Figure 2 Two dimensional inlet of the pump turbine

Two dimensional analyses have multiple benefits that are valuable in this work. A first aspect is that flow patterns cannot spread into three-dimensional space and therefore appear more distinct in two-dimensional analysis. A second aspect is that comparisons between geometries become easy to interpret. One simple geometry change can be analysed without any three-dimensional coupling of pressure contours and streamlines. Even though two dimensional investigations will provide valuable insight into the instability phenomenon, complete analyses will have to incorporate three dimensional effects.

The hypotheses that form the basis of this work can be summarized in three points:

1. The s-shape of the characteristics is connected to the behaviour of the flow field inside the runner, primarily at the inlet.
2. The s-shape instability can be solved by modifications on the runner inlet geometry.
3. The s-shape instability can be investigated as a two dimensional problem.

1.4 Delimitations

The flow field of a reversible-pump turbine at off design condition is very complex. Flow features such as separation and recirculation occurs heavily in an unsteady manner. Different structures occur along the characteristics where the flow rate ranges from negative in reverse pump mode to positive in turbine mode. At off design conditions neither the distributor nor the draft tube works properly and give awkward boundary conditions to the runner. In addition there is a strong interaction between the runner and these parts. However, in this thesis, emphasise is given to the runner flow field alone, since it is believed to be the source of instability. Furthermore, studies of the inlet part of the runner have been prioritized. This priority is argued for under chapter 1.3, but one further argument is that the inlet geometry compared to the outlet geometry is less sensitive for the design point performance. Any inlet geometry

alterations are therefore more easily implemented by pump turbine manufactures than alterations on the outlet geometry. It is recognized that inlet geometry alterations change the pump performance, but it is not a part of this work to optimize the runner geometry for both pump and turbine operation. The work is limited to high head and low specific speed reversible pump turbines.

1.5 General Conclusions

In this chapter some main conclusions are presented. These are based on the material presented in chapter 2 and in the papers.

The three hypotheses that formed the basis for this work are confirmed by results in this thesis. 1) Vortices are formed towards the inlet at the pressure side of the runner channels. These obstruct the through flow and make the characteristics s-shaped. 2) Measurements on different leading edge profiles showed significant changes of the characteristics with only minor changes to best operation point performance. 3) The two dimensional analysis was a useful tool to investigate flow features in the s-shaped region. It can also be used to analyze inlet geometry and showed great accuracy for small changes in the inlet blade angle. Nevertheless, two dimensional analyses are not a complete method and should be complemented by three dimensional analyses.

Curves of Q_{ed}-N_{ed} and T_{ed}-N_{ed} are real characteristics in the sense that similarity of flows normally is sufficiently described by these variables having equal values. However, measurements on different pressure levels revealed a Reynolds number dependency in high speed operation points.

Stability depends on the slope of the characteristics at the operation point in question. The criterion is found in the eigenvalues of the equation matrix that describes the power plant hydraulic- and mechanical system. These are for simple systems algebraic terms that in addition to the characteristics hold parameters such as friction, and inertia of the water and the rotating masses. Positive values of the real part of the eigenvalue represent instability. With constant speed of rotation the criterion require the slope of the turbine head-flow curve to be steeper than the slope of available head (reservoir head minus waterway head losses). With free-varying speed of rotation the criterion for instability sets limitations to the slope of T_{ed}-N_{ed} characteristics.

The pump turbine characteristics (Q_{ed}-N_{ed} or T_{ed}-N_{ed}) have a so called s-shape which can be measured if the system fulfills the static stability criterion for all operation points. All these stable operation points have a unique set of boundary conditions, i.e. turbine head and speed of rotation. If the system is unstable, three or two different operation points are possible for a given set of boundary conditions. Which one of these three operation points that actually occurs depends on the history of the turbine flow. This is a hysteresis behavior which is inherent in the s-shape of the characteristics.

The s-shape of the characteristics is a result of high energy dissipation in part load, turbine brake mode and reverse pump mode. Secondary flow structures and especially an inlet vortex is the cause to the dissipation. The inlet vortex starts to build up at the pressure side of the runner channel close to the leading edge of the adjacent blade. It builds up to cover most of the channel in turbine brake mode.

Changing the leading edge profiles of the runner blades alters the characteristics around runaway. This can improve stability and will alter the maximum speed and pressure during a load rejection with governor failure. More rounded off profiles give better stability, higher runaway speed and lower runaway head. The inlet blade angle can be decreased to improve stability. Decreased values of the inlet diameter or nominal speed also alter the shape of the characteristics and improve stability. Shortening the blade by increasing the internal blade angles makes the pump turbine less stable.

1.6 Further work

This work has focused on finding the characteristics and their connection to the geometry of the runner inlet. These tasks have the purpose to improve stability and therewith operation capabilities of the pump turbines. Further work is possible in this direction and some suggestions are listed here.

1) This project has focused on the geometry on the runner inlet. The geometry investigations can be expanded to include other parts of the turbine. Further optimizations can also be performed on the inlet profile. Pump performance and efficiency should then be included in the investigation. These factors are especially important for turbine manufacturer.

2) Accuracy of CFD modelling can be improved. Special care should be given to rotational effects in turbulence models, wall-boundary treatment, influence of inlet- and outlet boundary conditions and transient effects. A simplified potential flow approach can be conducted for fast analysis and can be useful during the runner design process.

3) The measurements technique called torque input method (ref. Paper II) can be improved. This method solved the static stability problem but was flawed by a fluctuating speed of rotation. The fluctuations can possibly be solved by a counteracting torque governing algorithm. A benefit of this method is the constant head for all operation points on the characteristics curves.

4) The effect of compressibility can be further investigated. Such an investigation can for example lead to limiting values of T_w/T_a and T_e/T_a to show when compressibility can be neglected.

2 Theory and Supplementary Analysis

This chapter consists of three sections which together with the papers make up the technical achievements in this thesis. First a fundamental description of the non-dimensional number is given. In section two, the stability is thoroughly explained through theory and examples. Section three describes how the unstable characteristics are formed through irregular flow patterns and high dissipation rates.

2.1 Non-dimensional numbers and similarity

The non-dimensional variables Q_{ed}, N_{ed} and T_{ed}, eq.(1), are widely used in this thesis and are introduced here.

$$Q_{ed} \equiv \frac{Q}{D_2^2\sqrt{gH}}, \quad N_{ed} \equiv \frac{nD_2}{\sqrt{gH}}, \quad T_{ed} \equiv \frac{T}{\rho g H D_2^3}, \quad [-] \quad (1)$$

Q_{ed}, N_{ed} and T_{ed} are non-dimensional variables whose construction is based on similarity analysis. Two fully similar flows, e.g. model and prototype, must be geometric-, kinematic- and dynamic similar. The dynamic similarity of flows is achieved if the forces exerted on a fluid element are proportional everywhere inside the turbine. This can be derived from the Navier-Stokes equation, which in eq. (2) is written on non-dimensional form. The similarity is evident if the non-dimensional numbers, eq. (3), have the same value for both the model and the prototype.

$$\text{Strouhal}\frac{dc}{dt} = \frac{1}{Froude}g + \text{Euler}\nabla p + \frac{1}{\text{Reynolds}}\nabla^2 c \quad [-] \qquad (2)$$

$$\begin{aligned}
\text{Strouhal} &= \frac{L/T}{C} = \frac{\text{Unsteady}}{\text{Inertia}} \quad [-] \\
\text{Froude} &= \frac{C^2}{gL} = \frac{\text{Inertia}}{\text{Gravity}} \quad [-] \\
\text{Euler} &= \frac{P}{\rho C^2} = \frac{\text{Pressure}}{\text{Inertia}} \quad [-] \\
\text{Reynold} &= \frac{\rho CL}{\mu} = \frac{\text{Inertia}}{\text{Viscouse}} \quad [-]
\end{aligned} \qquad (3)$$

In many settings the effect of the Froude- and Reynolds numbers are neglected. In these cases the similarity is sufficiently described by the Euler- and Strouhal numbers. The Euler number relates the pressure force to the three velocity components for all fluid parcels in the turbine. If the velocity field can be sufficiently described by the averaged meridional speed at the outlet, then the Q_{ed} variable represents the Euler-similarity. This can be shown by squaring Q_{ed} and substitute Q/D^2 with c_m, eq. (4).

$$Q_{ed}^2 \equiv \left(\frac{Q}{D_2^2\sqrt{gH}}\right)^2 \sim \left(\frac{c_m}{\sqrt{gH}}\right)^2 \sim \frac{C^2}{H} \sim \frac{1}{Euler} \qquad (4)$$

In the Strouhal number the reference length can be the diameter and the reference time can be the inverse of the frequency of rotation, 1/n. A substitution of $(gH)^{0.5}$~C in the definition of N_{ed} then reveals the proportionality to the Strouhal number, (5).

$$N_{ed} \equiv \frac{nD_2}{\sqrt{gH}} \sim \frac{nD_2}{C} \sim \text{Strouhal} \qquad (5)$$

The Froude number is mostly relevant for free surface flows and is certainly not relevant for high head hydro turbines. Furthermore, constant values of Q_{ed} and N_{ed}, which are easy to obtain, show the Euler- and Strouhal similarity. The parameter that prevents full similar flows is therefore the Reynolds number. This number is hard to keep constant and will always be much higher for a prototype than for the model. To minimize the discrepancy between model- and prototype performance, the Reynolds number for the model should be as high as possible.

The T_{ed} parameter comes forth by multiplying the efficiency, η, by Q_{ed}/N_{ed} as in eq. (6).

$$T_{ed} = \frac{Tn}{\underbrace{\rho g Q H}_{\eta}} \frac{Q_{ed}}{N_{ed}} = \frac{T}{\rho g H D_2^3} \qquad (6)$$

The constant values of Q_{ed} and N_{ed} (or T_{ed}) is commonly regarded as sufficient for showing similarity of flows and is called kinematic similarity. Consequently plots of Q_{ed} and T_{ed} versus N_{ed} are regarded as real characteristics of the turbine. This is also how they are used in this thesis, but paper II shows that full similarity also requires constant pressure level and therewith constant Reynolds number.

In the derivation of the Strouhal number in eq. (5) the time scale was taken to be the inverse of the frequency. Other timescales may be important during transient operation such as load rejection or start and stop of the turbine. The flows are then similar to the steady state characteristics only if the acceleration forces are negligible. This applies when the mass of water inside the turbine domain is very small compared to the total water mass or the acceleration is very low.

2.2 Stability for Pump Turbines

This chapter describes the influence of pump turbine characteristics on stability. Analytical criteria have been found for three limiting cases of an example power plant system. The whole system is analysed through system dynamic analyses and stability limits are found as Q_{ed} and T_{ed} values. The original blade and a new profile from paper I are compared. The results show different stability limits and different maximum values for speed and head during a load rejection. Compressibility may influence system dynamics but that is not the case for the example power plant as it is.

"Stability can be defined as the quality of being immune to small disturbances" Greitzer[8]. If the added force that comes with a perturbation of the original state drives the system state back to the origin, the system is stable. In the opposite case the perturbation will drive the system away from its initial point and be unstable. Oscillations may occur, but can only exist together with at least two energy storage elements. "The strength of the oscillations grows if the energy input during one cycle of the oscillation is greater than during steady operation Greitzer" [8].

Any linearized system can be described by a set of differential equations on the form in eq. (7). Their solutions are characterized by the eigenvalues, λ, which are found by solving eq. (8). The solutions can be written on the form denoted in eq. (9) and will be oscillatory in the case of complex eigenvalues. In order to obtain stability, the real parts of the eigenvalues must be negative.

$$\dot{\bar{x}} = \bar{\bar{A}} \cdot \bar{x} \quad (7) \qquad \det(\bar{\bar{A}} - \lambda \bar{\bar{I}}) = 0 \quad (8) \qquad \bar{x} = \bar{c} \cdot e^{\lambda t} \quad (9)$$

The instabilities that occur in RPT systems are divided into two categories; static and dynamic instability. If the eigenvalues of the system are real, i.e. $\lambda_{Imaginary}=0$, the system response is static. The solutions in eq. (9) are then asymptotic curves which approach zero if the system is stable. If any of the eigenvalues are complex, the system will undergo oscillations as response to a perturbation. The system is dynamically unstable if these oscillations do not decrease with time.

The pumped hydro storage system in Figure 3 is used as an example to analyse stability. This is described by first order ordinary differential equations for the water masses, the rotating inertia, and the shaft pressure. In the following sections three limiting cases will be discussed. These cases have one or two governing equations and the stability limits can therefore be analytically derived with a reasonable amount of mathematics. At the end of this chapter the full system is analyzed to find its stability limits and dynamic response to a load rejection.

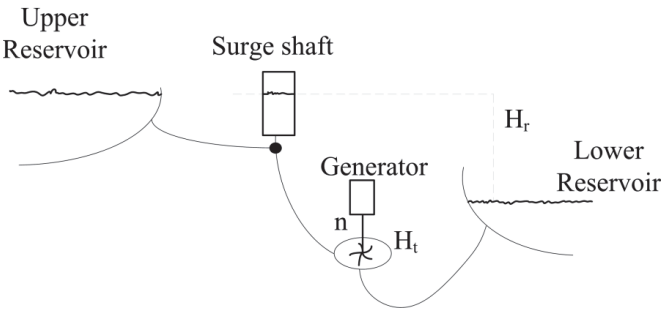

Figure 3 Hydropower System

2.2.1 Case 1: No surge shaft and constant speed of rotation

Limitations: The polar moment of inertia is very high such that the speed of rotation is regarded as a constant. The surge shaft is not taken into account.

This system is described by eq. (10). The left hand side denotes the total mass (LAρ) of the moving water multiplied with the time derivative of the mean velocity, Q/A. The right hand side denotes the pressure force that works on the water, where H_r is the reservoir head, H_f is the friction head loss, H_t is the net turbine head and A is the cross-sectional area of the waterway. The friction head loss is represented as in the Moody diagram, eq. (11).

$$LA\rho\frac{dQ/A}{dt} = (H_r - H_f - H_t)\rho gA \quad [N] \qquad (10)$$

$$H_f = \frac{fL}{D2g}\frac{Q^2}{A^2} \quad [m] \qquad (11)$$

The turbine head is linearized around the steady state value H^0 with constant speed of rotation, eq. (12). The constant a, is the slope of the linearized head curve.

$$H_t = H_t^0 + a(Q - Q^0) \quad [m] \qquad (12)$$

The system equation cannot be solved directly because of the nonlinearity of the friction term. The flow rate is therefore written as the steady state value Q^0 plus the perturbation q. The eq. (10) written out becomes:

$$\frac{L}{Ag}\frac{d(Q^0+q)}{dt} - H_r + \frac{fL((Q^0)^2 + 2Q^0q + q^2)}{DA^2 2g} + H_t^0 + a(Q^0 + q - Q^0) = 0 \quad [m] \qquad (13)$$

The system equation for the steady state flow is subtracted from eq. (13) to get the equation for the flow perturbation. This flow perturbation is the stability variable of interest.

$$\frac{L}{Ag}\frac{dq}{dt}+\frac{fL(2Q^0q+q^2)}{DA^2 2g}+aq=0 \quad [m] \qquad (14)$$

The perturbation is assumed to be small compared to the steady state flow and second order terms of the perturbation can therefore be neglected. Thus the equation to solve becomes:

$$\frac{L}{Ag}\frac{dq}{dt}+\frac{fLQ^0q}{DA^2 g}+aq=0 \quad [m] \qquad (15)$$

Reordering the terms:

$$\frac{dq}{dt}+\frac{fQ^0}{DA}q+\frac{aAg}{L}q=0 \quad [m^3s^{-2}] \qquad (16)$$

This equation is solved by separation of variables.

$$\frac{dq}{q}=-(\frac{fQ^0}{DA}+\frac{aAg}{L})dt \quad [-] \qquad (17)$$

and the result is:

$$q=q^0e^{\lambda t} \quad [m^3s^{-1}], \quad \lambda=-(\frac{fQ^0}{DA}+\frac{aAg}{L}) \qquad (18)$$

The constant q^0 represents the initial flow perturbation at t=0. The flow rate is stable if the eigenvalue, λ, is negative and unstable if λ is positive. With negative λ, the flow perturbation will be zero after some time.

$$\text{Stable if:} \quad \lim(q)_{t\to\infty}=0 \qquad (19)$$

For stability the following static criterion must be fulfilled:

$$a>-\frac{fQ^0}{DA}\frac{L}{Ag} \quad [m^{-2}s] \qquad (20)$$

The two terms encapsulated in the eigenvalue are representing the slopes of the turbine head and friction losses. Thus the criterion can be written as in eq. (21) and its graphical interpretation is showed in Figure 4. If the friction head loss is neglected the criterion is that the turbine slope must be positive. Paper II describes how the criterion can be written in terms of Q_{ed} and N_{ed}.

$$\frac{dH_t}{dQ}+\frac{dH_f}{dQ}>0 \quad [s/m^2] \qquad (21)$$

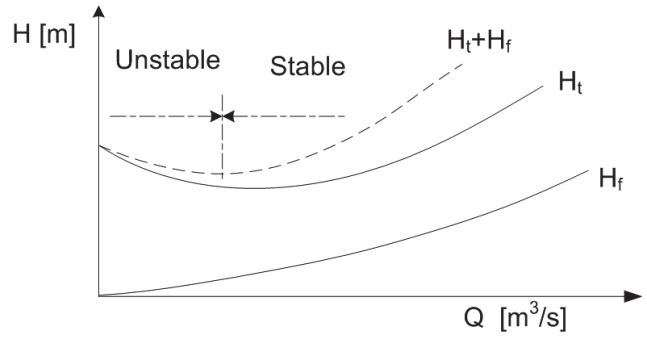

Figure 4 Static "H-Q" stability criterion

2.2.2 Case 2: No surge shaft and variable speed of rotation

Limitations: The surge shaft is not taken into account.

The analysis of this system is based on Martin [9] where a necessary but not sufficient criterion for dynamic instability is derived. Martin's analysis is confirmed through analysis in Martin [10]. A sufficient criterion for dynamic instability is derived in this section together with a static stability criterion. First the method used by Martin is briefly explained.

The water masses is modelled as in eq. (10), with neglected friction losses while the rotating masses are modelled by eq. (22). The left hand side denotes the polar moment of inertia of the rotating parts (J) multiplied with the rate of change in speed of rotation. The right hand side denotes the unbalanced torque which is the hydraulic torque (T_h) minus the generator torque (T_g).

$$J 2\pi \frac{dn}{dt} = T_h - T_g, \quad [\text{Nm}] \qquad (22)$$

The normal characteristics, Q_{ed}-N_{ed} and T_{ed}-N_{ed} have singularity points (infinite slope) along their curves. Therefore the characteristics are represented in terms of the new variables in eq. (23). The new characteristics relate h-v and β-v and are shown in Figure 5.

$$h = \frac{H}{n^2}\frac{(n^*)^2}{H^*}, \quad \beta = \frac{T}{n^2}\frac{(n^*)^2}{T^*}, \quad v = \frac{Q}{n}\frac{n^*}{Q^*} \; [-] \qquad (23)$$

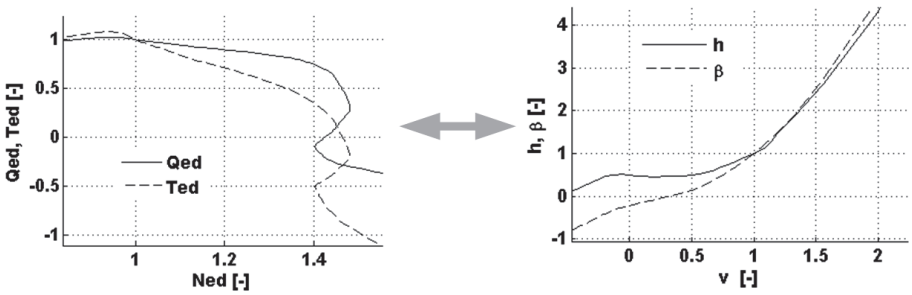

Figure 5 New representation of the characteristics

The characteristics are represented as a Taylor series around the steady operation point and the variables are written as the steady state value plus a perturbation. By reordering the terms, the system is represented as a 2x2 matrix equation. The eigenvalues from this matrix are denoted in eq. (24). The constants a_1 and b_1 are the linear slopes of the h-v and β-v characteristics respectively and steady state values are marked with a 0. The fluid to machine timescale is denoted τ_f and is the fluid timescale, T_w, divided by the machine timescale, T_a, as defined in eq. (25).

$$\lambda_{1,2} = \frac{1}{2}\underbrace{\left(-\frac{a_1 n^0}{n^* \tau_f} - b_1 \frac{Q^0}{Q^*}\right)}_{M} \pm \frac{1}{2}\sqrt{\underbrace{\left(\frac{a_1 n^0}{n^* \tau_f} + b_1 \frac{Q^0}{Q^*}\right)^2}_{M} - \underbrace{\frac{8 b_1}{\tau_f}}_{N}} \quad [-] \qquad (24)$$

$$T_w = \frac{Q^* L}{A g H^*}, \quad T_a = \frac{J n^* 2\pi}{T^*} \quad [-] \qquad (25)$$

If the eigenvalues are complex the system will undergo oscillations as a response to a perturbation. These oscillations will be dampened if the term denoted M is negative. Hence the dynamic stability criterion is:

$$-\frac{a_1 n^0}{n^* \tau_f} - b_1 \frac{Q^0}{Q^*} < 0 \qquad (26)$$

Martin [9] showed that the term a_1/b_1 can be rewritten by using the slope of Ted-Ned characteristic. By inserting this into eq. (26) the dynamic stability criteria become:

Stable in turbine- and turbine brake mode if: $\frac{dT_{ed}}{dN_{ed}} > \frac{n^0 2 T_{ed}^* Q^*}{\tau_f n^* N_{ed}^0 \left|Q^0\right|}$ or $\frac{dT_{ed}}{dN_{ed}} < 0$ [–] (27)

Stable in reverse pump mode if: $\frac{dT_{ed}}{dN_{ed}} > -\frac{n^0 2 T_{ed}^* Q^*}{\tau_f n^* N_{ed}^0 \left|Q^0\right|}$ and $\frac{dT_{ed}}{dN_{ed}} < 0$ [–] (28)

By including the friction losses in the analysis, the criteria become slightly different and is for turbine and turbine brake mode as in eq. (29).

$$\frac{dT_{ed}}{dN_{ed}} > \frac{n^0 2T_{ed}^* Q^*}{n^* N_{ed}^0 Q^0} \frac{b_1}{b_1 \tau_f + 2H_f / H^*} \quad [-] \qquad (29)$$

In the case of real eigenvalues the system will not oscillate but can be statically unstable if the term N in the eigenvalues is negative. This corresponds to the criterion in eq. (30). The left hand side is the slope b_1 written in terms of Q_{ed}, N_{ed} and T_{ed} as in Martin [9].

$$\frac{\frac{dT_{ed}}{dN_{ed}} - 2\frac{T_{ed}}{N_{ed}}}{N_{ed}\frac{dQ_{ed}}{dN_{ed}} - Q_{ed}} < 0 \quad [-] \qquad (30)$$

2.2.3 Case 3: Fixed speed of rotation and very long tunnels to upper reservoir

Limitations: The length of the surge shaft is regarded very small such that the respective water masses can be neglected and the head in the node in Figure 3 *is the same as the water level in the surge shaft. The tunnel to the upper reservoir is very long, such that the flow rate in that part can be regarded as constant. The speed of rotation is held constant.*

The system is now described by two equations. The first is eq. (10) where the reservoir head is replaced with the shaft water level. The second equation, eq. (31), describes the surge shaft water level where the flow rate from the upper reservoir is denoted Q_1.

$$\frac{dz_s}{dt} = (Q_1 - Q) / A_s \quad [m/s] \qquad (31)$$

The two equations are solved for the disturbance in flow rate and shaft water level and the equation matrix has the following eigenvalues:

$$\lambda_{1,2} = \frac{1}{2}\underbrace{(-a\frac{Ag}{L} - f\frac{Q^0}{DA})}_{M} \pm \frac{1}{2}\sqrt{\underbrace{(a\frac{Ag}{L} + f\frac{Q^0}{DA})^2}_{M} - 4\underbrace{\frac{gA}{LA_s}}_{N}} \qquad (32)$$

The eigenvalues show that the dynamic stability criterion (M<0) for this system is the same as the static criterion for the system in Case 1. The static stability criterion, N>0, is always fulfilled for this case.

This analysis can be compared to the analysis of U-tube oscillations that leads to the well known Thoma criterion. Unlike here, that criterion put restrictions on the shaft area. The most obvious differences between these two analyses are that for this case the

flow rate from the upper reservoir is held constant while in the Thoma-analysis an ideal governor holds the product of flow rate and head constant.

2.2.4 The Whole System

Limitations: The length of the surge shaft is regarded very small such that the respective water masses can be neglected and the head in the node in Figure 3 i*s the same as the water level in the shaft.*

The system is described by four equations for the primary variables q_1, q_2, z_s and n. These equations are briefly described in Appendix 1 and are represented on matrix form as follows:

$$\begin{bmatrix} \frac{dq_1}{dt} \\ \frac{dq_2}{dt} \\ \frac{dz_s}{dt} \\ \frac{dn}{dt} \end{bmatrix} = \begin{bmatrix} -k_1 2Q^0 \frac{A_1 g}{L_1} & 0 & -\frac{A_1 g}{L_1} & 0 \\ 0 & -k_2 2Q^0 \frac{A_2 g}{L_2} - a_1 N^0 \frac{A_2 g}{L_2} & \frac{A_2 g}{L_2} & a_1 Q^0 \frac{A_2 g}{L_2} - 2\frac{H^0}{N^0}\frac{A_2 g}{L_2} \\ \frac{1}{A_s} & -\frac{1}{A_s} & 0 & 0 \\ 0 & \frac{b_1 N^0}{\pi J} & 0 & -\frac{b_1 Q^0}{\pi J} \end{bmatrix} \begin{bmatrix} q_1 \\ q_2 \\ z_s \\ n \end{bmatrix} \quad (33)$$

The eigenvalue-equation of this matrix has to be solved numerically. To do this an example power plant is used together with the measured characteristics for the pump turbine designed by the author. The power plant dimensions are given in Figure 6.

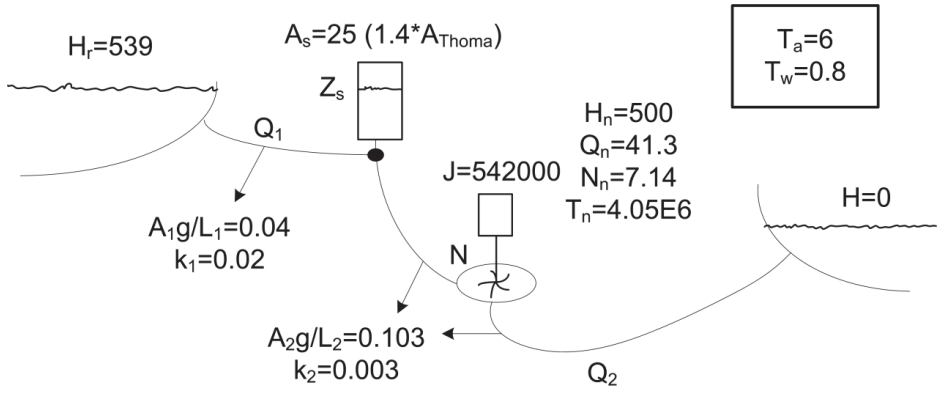

Figure 6 Example system

The eigenvalues are found for 300 operation points along the characteristics and the stability limits are found were the highest damping factor (λ_{Re}) is zero. These limits are

marked with lines on the characteristics in the Figure 7 and Figure 8. For the example system the hydraulic timescale T_w is so small that the stability limit practically is $dT_{ed}/dN_{ed}<0$. Changing the T_w by increasing the length of the penstock (L_2) yields new stability limits. These are shifted towards lower Q_{ed} and T_{ed} values as indicated with dotted lines in the figures. The penstock length (L_1) is multiplied by a factor of five in order to get significant changes on the stability limits. The friction coefficient is increased proportionally with the penstock length to reflect increased losses. Multiplying with a factor of two instead of five gave no changes in the stability limits. The sensitivity of the stability limits to the penstock length can therefore be considered small.

By giving the surge shaft area (A_s) and the tunnel length (L_1) infinite high values the system reduces to the limited Case 2. A comparison of the simulated results reveals that the stability limits are governed by the two equations in Case 2 alone.

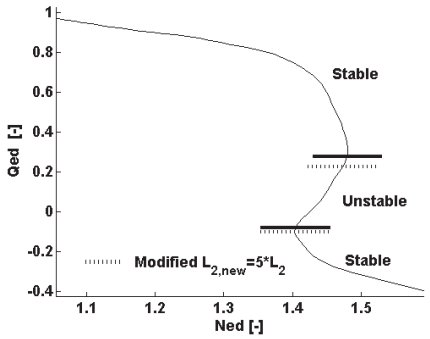

Figure 7 Stability limits for Q_{ed}

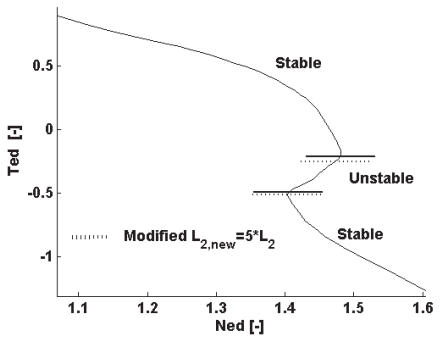

Figure 8 Stability limits for T_{ed}

A dynamic simulation is performed to show the system response to a load rejection. The equations solved are not linearized, but are otherwise the same as those in eq. (33). A Runge-Kutta method is used to resolve the time derivatives and the simulations start at nominal speed of rotation and flow rate. Values for the head and torque are interpolated from the characteristics. The time evolution of the four primary variables is shown in Figure 9. As can be seen, in the beginning the dynamic behaviour is dominated by the turbine flow rate, Q_2, and the speed of rotation. The maximum speed of rotation and head are 1.53 and 1.10 times their respective nominal values. The U-tube oscillations have a time period of 160 seconds while the turbine flow rate has a time period ranging from 6 to 20 seconds. These periods are taken from the eigenvalues of eq. (33), and seems reasonable compared with the transient results in Figure 9.

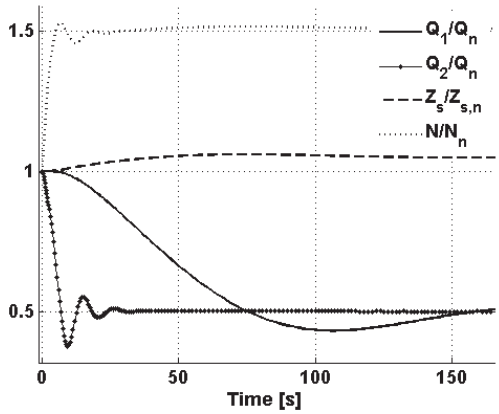

Figure 9 Load rejection with governor failure

2.2.5 Comparisons of profiles from paper I

The different characteristics presented in paper I are all equally stable at the runaway curve. However, the maximum speed and head during a load rejection are different. The dynamic simulation in Figure 9 was performed using the characteristics for the runner called original. A second simulation using the characteristics for profile C yields new maximum values for head and speed of rotation. Those were $1.09*H_n$ and $1.55*N_n$ respectively, which are slightly lower and higher than for the original profile. The characteristics for the two different profiles are shown in Figure 10.

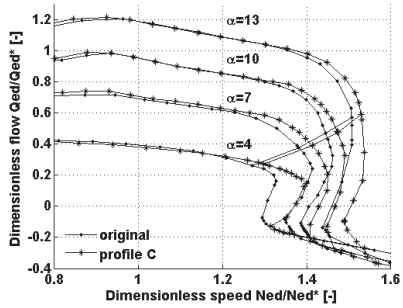

Figure 10 Characteristics for original and profile C.

If the runaway curve had been placed differently on the characteristics the difference between the original and profile C with respect to stability could have been large. To visualize this, the runaway curves have been altered by subtracting eight percent of the nominal torque from the torque-speed characteristics. Then the dynamic simulation of a

load rejection shows that the original profile has sustained oscillations whereas profile C is stable, Figure 11.

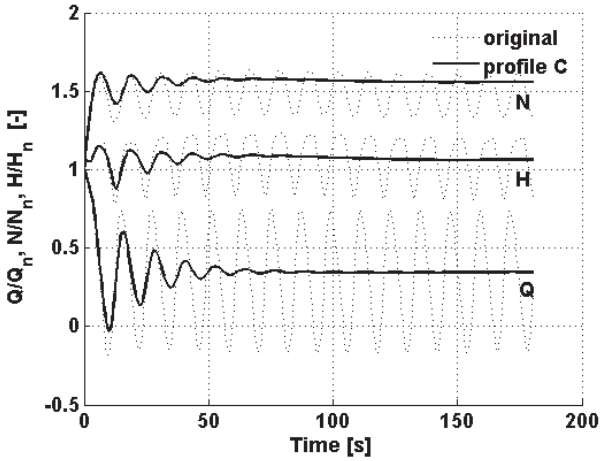

Figure 11 Dynamic comparison of original and profile C

2.2.6 Effect of compressibility

Water is regarded as incompressible in this thesis, except from this chapter were the effect of compressibility on stability is briefly discussed.

An analysis that includes water elasticity (compressibility) has been performed on the example system. A short description of the method used is described in the section below. The example system has the elastic timescale T_e=1.3(=2L/a) and the ratio of hydraulic to elastic timescales is T_w/T_e=0.62. The results of the load rejection case, now with elastic equations, show an equal time history as that of the inelastic simulation in Figure 9. Therefore the compressibility has no influence on the stability during a load rejection for the example system. However, it has been shown by Martin [9] that the elasticity may have an effect. In one of Martin's simulation the turbine entered reverse pump mode with the elastic analysis while it stayed in turbine brake mode with inelastic analysis. Elastic stability analyses on pump turbines at runaway are also conducted in Nicolet [11] and [12]. Simulations of the two-unit power plant showed generally lower damping factors when elasticity was taken into account. For some configurations there was a switch from rigid column mode to elastic column mode oscillations after a certain time of the transient simulations.

The elastic analysis evaluates the compatibility equations along characteristics lines as described in Wylie [26] and is commonly known as method of characteristics (MOC). The turbine is placed at the end of the penstock and is directly connected to the lower

reservoir. The flow rate, head, speed of rotation and torque are found by interpolation in the characteristics and by solving one compatibility equation together with the rotational momentum equation, eq. (22). The time integration in the rotational momentum equation is solved by an improved Euler integration with second order accuracy. At the surge shaft the water level is found by integrating the shaft level equation, eq. (31) by the improved Euler method.

2.3 Flow in Reversible-Pump Turbine Runners

The flow field at part load has a disorderly character and is the cause of the s-shape of the characteristics. It is complex, highly dissipative and contains a variation of secondary flow structures. This chapter presents flow analyses with the purpose of showing the connection between the flow field and the characteristics. Chapter 2.3.1 discusses the role of ideal characteristics and energy dissipation while chapter 2.3.2 link the cause of dissipation to part load flow structures. These structures are discussed by analytical velocity diagrams and two- and three-dimensional CFD analysis. In chapter 2.3.3 simulated characteristics are compared to measurements. Some technical information of the CFD simulations is presented in the appendix together with a short general text about CFD.

2.3.1 The role of "ideal" characteristics and dissipation

The efficiency along the characteristics falls to low and negative values as the flow rate approach to zero. We shall now see how the head loss, due to low efficiency, alters the characteristics. To do that, characteristics obtained from CFD simulations are compared to characteristics with "ideal" head (no losses). This "ideal" head is found by using the Euler formula, eq. (34) in which the term u_1c_{u1}-u_2c_{u2} is found through integration of the flow velocities over the entrance and exit area of the runner. The "ideal" head is used together with the flow rate and speed of rotation from the CFD simulations to find new Q_{ed} and N_{ed} values. Figure 12 shows the "ideal" characteristic together with the real characteristic. The "ideal" characteristic is asymptotic towards the N_{ed}-axis in both turbine and pump mode while the real characteristic has its usual s-shape. In between the curves there is an area that represents the impact of the losses.

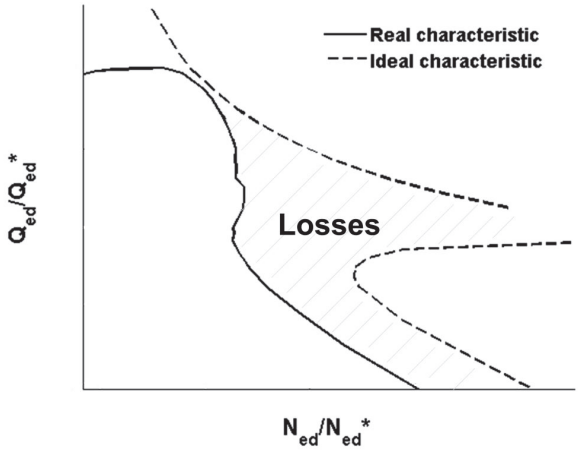

Figure 12 The difference between real and "ideal" characteristics shows the influence of losses.

$$H = \frac{1}{g}(u_1 c_{u1} - u_2 c_{u2}) \quad [m], \text{ with } \eta=1 \qquad (34)$$

The head loss is caused by viscous dissipation in the flow. This is in the Navier-Stokes equations represented by the dissipation function, which in naive terms is a bunch of velocity gradients. The next section discusses the flow field with emphasis on the dissipation part of the characteristics. All flow features presented are increasing the dissipation through steep velocity gradients and therewith contributes in the destabilization of the characteristics.

2.3.2 Secondary flow structures and dissipation

Theoretic velocity diagrams at both sides of the vaneless gap

Velocity diagrams for the runner entrance and the guide vane exit are made by assuming that the flow follows the geometry exactly. When moving from BEP towards higher speeds the velocity diagrams on the guide vane exit and runner entrance get more and more different. In reverse pump mode they always mismatch and this mode is therefore always subjected to very high losses. Particularly one conclusion may be drawn from these diagrams, namely that in the short distance of the vaneless gap the absolute velocity(c) is deflected and strongly accelerated.

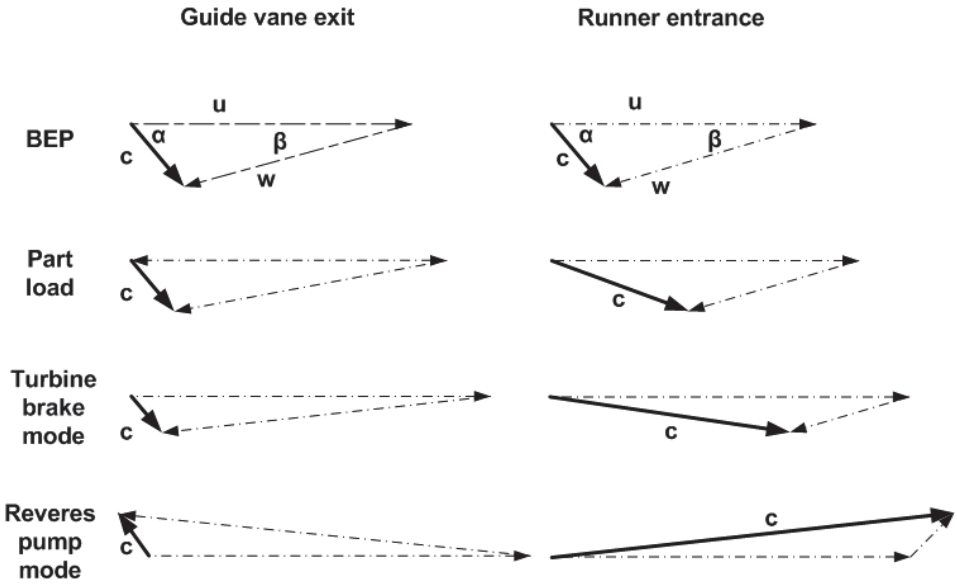

Figure 13 Theoretical velocity diagrams at both sides of the vaneless gap

Two-Dimensional Steady Simulations of one Channel and Four Guide Vanes

Two-dimensional analyses can be used to analyze the flow at the inlet of the runner due to the two-dimensionality of the geometry, see paper IV and V. There are two reasons why those analyses are especially descriptive: 1) the secondary flow structures are bound to form in only one plane which makes them more distinct, 2) the whole flow field can be represented in one picture with no unrevealed flow structures.

The relative velocities at three sampling lines are shown in the following figures for five operation points distributed between nominal and zero flow rates. These operation points are shown in terms of Q_{ed} -N_{ed} characteristics. It can be seen that the velocity profile inside the channel gets more and more skewed as the flow rate goes down. At low flow rate it flows outwards at the pressure side (convex side) of the runner channels and inwards at the suction side.

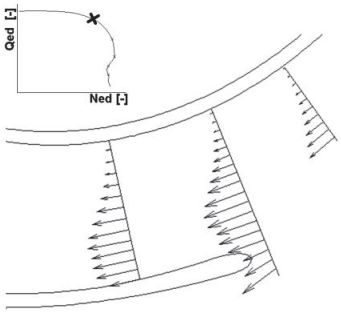

Figure 14 Velocity at Q/Q*=1

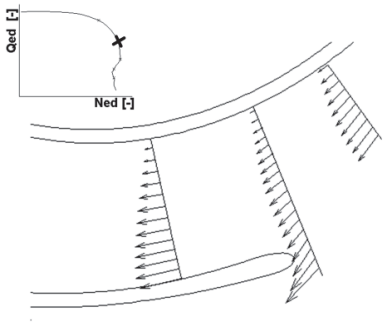

Figure 15 Velocity at Q/Q*=0.66

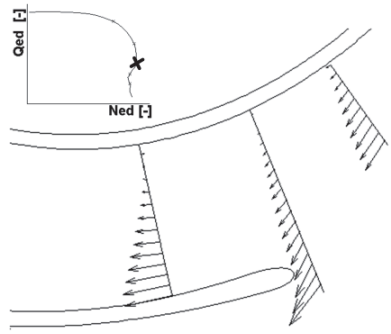

Figure 16 Velocity at Q/Q*=0.33

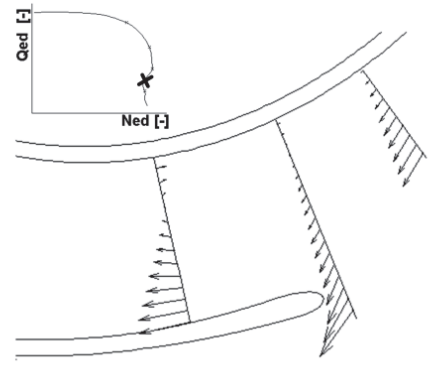

Figure 17 Velocity at Q/Q*=0.16

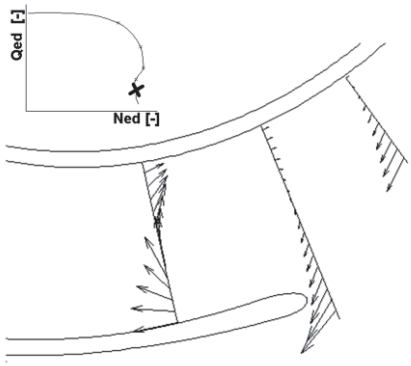

Figure 18 Velocity at Q/Q*=0

Three-Dimensional Simulations of 360 Degree Runner and Guide Vanes

The distribution of the flow rate in the runner channels is investigated at a rotation surface with slightly smaller radius than the runner blade leading edge. Comparing the flow rate through this surface for each of the six channels reveals that the flow rate may not be evenly distributed between the channels, Figure 19. At certain operation points one channel have negative flow rate while the flow rate is positive in the other channels. Figure 20 shows that the flow rate divides unevenly on the upper and lower half of the runner channels at the same surface. At very low flow rates the lower part is pumping water while the upper part is turbining. The flow rates plotted are relative to the total flow rate in the respective operation point, such that the sum of the flow rates at two corresponding points is always equal to one. In Figure 21 it can be seen that at part load the flow rate is strongest at the pressure side of the channel. The flow rates are also here relative to the total flow rates and the pressure and suction sides are divided on the geometric middle line between them.

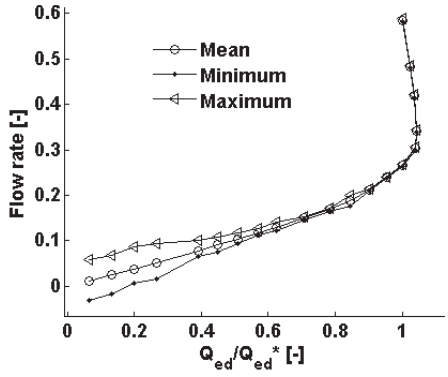

Figure 19 Showing that the total flow rate is unevenly distributed on the six runner channels at part load and in turbine brake mode

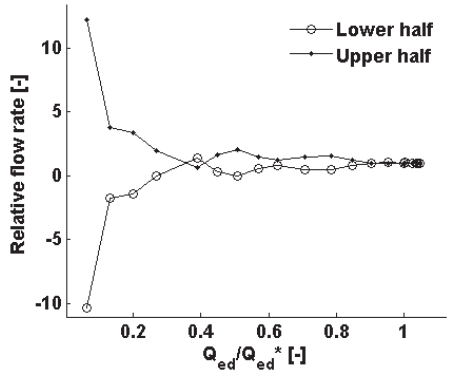

Figure 20 In turbine brake mode the flow rate in the upper part of the runner channels is much higher than in the lower part

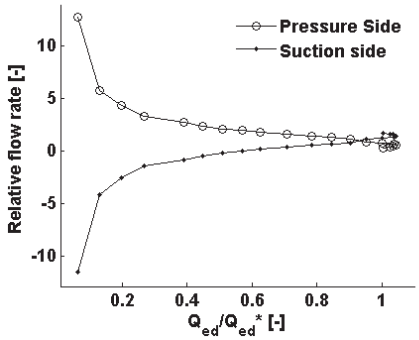

Figure 21 At low total flow rates the flow rate is much higher at the pressure side of the channels than at the suction side

The next four figures show representative instantaneous pictures of the flow in the runner at meridional- and constant-span-planes. In the meridional view, Figure 22, a large vortex can be seen at the inlet, which covers most of the channel at this operation point in turbine brake mode. At the outlet water is flowing upwards from the draft tube at low radii and downwards at larger radii. The upward flow is stopped just inside the runner leading to a strong cross flow in this area. Figure 23 shows streamlines at a plane at 15 percent span from the hub. Two vortices can be seen in each channel. These vortices gradually diminish towards the shroud. The same views are showed for a part load operation point with ten percent efficiency. Here the inlet vortex in the meridional view, Figure 24, is smaller and the streamlines in Figure 25 do not show any vortices at all. In other fields of fluid mechanics various vortex identification methods are used to identify the vortices. These methods are not used here since they generally perform poorly on turbomachinery runner flows, Roth [13].

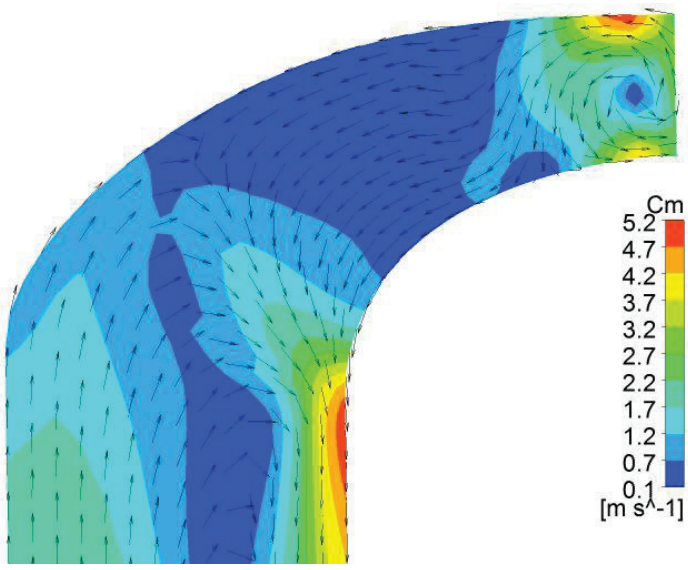

Figure 22 Averaged c_m velocity vectors at the meridional plane from a unsteady simulation in CFX in turbine brake mode at Q_{ed}/Q_{ed}*=0.22

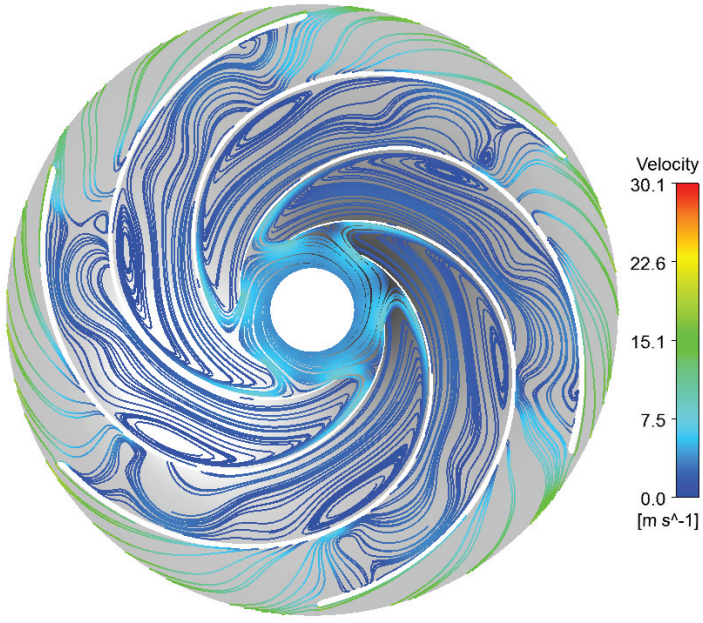

Figure 23 Streamlines at a plane close to the hub from a unsteady simulation in CFX in turbine brake mode at Q_{ed}/Q_{ed}*=0.22

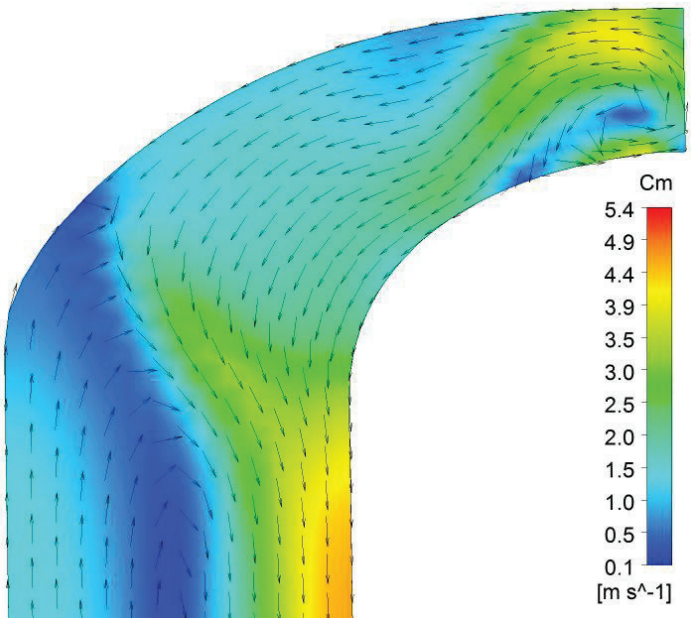

Figure 24 Averaged c_m velocity vectors at the meridional plane from a unsteady simulation in CFX in turbine part load at Q_{ed}/Q_{ed}*=0.72

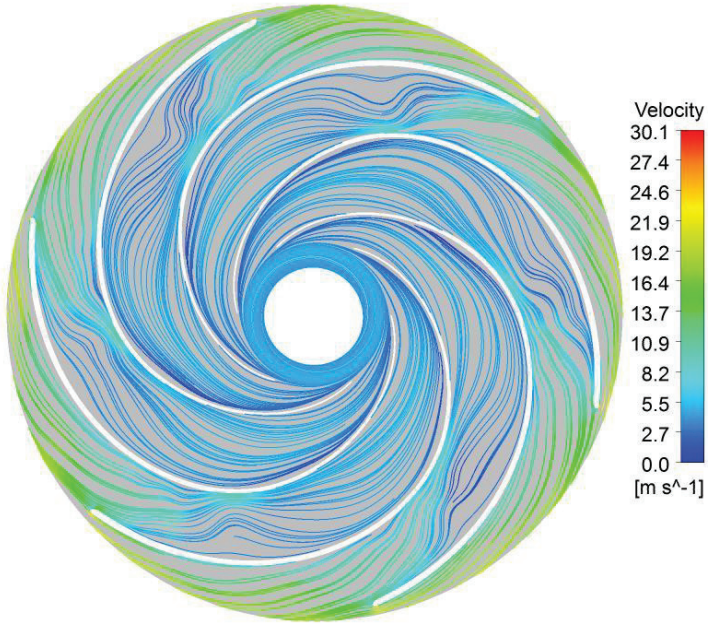

Figure 25 Streamlines at a plane close to the hub from a unsteady simulation in CFX in turbine part load at Q_{ed}/Q_{ed}*=0.72

Flow structures in the literature

The flow structure at part load behaviour of pump turbines has become an international research topic due to its importance for stability. An early study was performed in 1987 by Senoo [14], who visualized a vortex forming at the inlet in operation at zero flow rate. A vortex at the same position has been detected by Staubli [15], Wang [16] and Casartelli [17]. Staubli concluded that this vortex is the origin of unsteady out- and inflow in the vaneless gap. Uneven mass-flow-distribution between upper and lower half of the runner channel is reported by Børresen [18]. At most operation points the flow rates through the upper and lower halves are equal but for large speed they diverge as the lower half starts pumping water outwards in radial direction. A no-load operation point was studied numerically by Liang [19]. Pressure plots along the blades showed that the inlet part has negative load and thus work as pump while the outlet part has positive load and work as turbine. Rotating stall has been found by Hasmatuchi [20] and by Widmer [21]. This stall cell may cover a large portion of the inlet of the turbine and rotates with a geometry dependent frequency, at typically 0.6-0.7 times the rotor frequency. The vortices, stationary or moving, are blocking a part of the flow area, leading to higher pressure. This pressure increase pushes the characteristics into an s-shape.

2.3.3 Comparison with measurements

The simulated characteristic is compared to measurements. Unfortunately there is no measured characteristic for twelve degree guide vane opening. However it is possible to see that the simulated and measured curves do not fit very well at low Q_{ed} values. At least it should not cross the measured 10-degree-characteristics. The simulations are therefore not used to predict absolute values. Nevertheless their phenomenological information of flow structures is considered valuable.

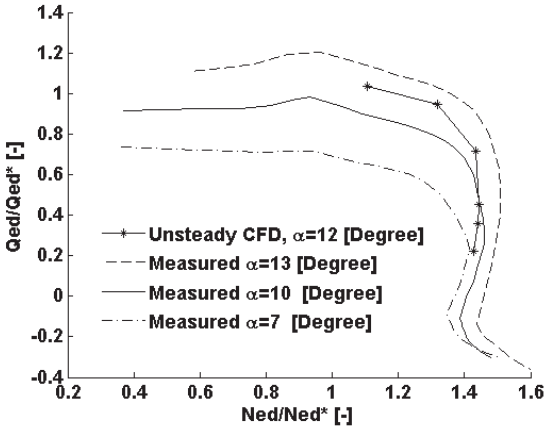

Figure 26 Comparison of measurements and unsteady CFD simulations

3 Bibliography

1 Norges vassdrags- og energidirektorat(NVE), *Pumpekraft i Noreg: Kostnader og utsikter til potensial*, Rapport nr 22, 2011

2 First Hydro Company, Available at: < http://www.fhc.co.uk/dinorwig.htm> [Accesssed 1 May 2012]

3 Ikeda, K., Inagaki, M., *Development of 700m-400MW Class Ultrahigh Head Pump Turbine,* Hitachi Review, Vol. 49 (2000), No. 2

4 Henry, P., *Turbomachinery hydrauliques*, Presses polytechniques et universitaires Romand. 1992

5 Dörfler, P.K., Engineer, A.J., Pendse, R.N., Huvet, P., Brahme, M.V., *Stable operation achieved on a single -stage reversible pump-turbine showing instability at no-load*, in Proceeding of the 19th Symposium on Hydraulic Machinery and Systems. 1998. Singapore.

6 Klemm, D., *Stabilisierung der Kennlinien einer Pumpenturbine im Bereich zwischen Turbinen-Teillast und Rückwärtspumpenbetrieb*. Voith Forschung und Konstruktion, 1982. Heft 28, Aufsatz 2.

7 Pejovic S., Jemcov R., Crnkovic P., *Unstable Operation of High-Head Reversible Pump-Turbines*, in 8th IAHR Symposium 1976, Leningrad.

8 Greitzer E. M., The Stability of Pumping Systems –The 1980 Freeman Scholar Lecture, Journal of Fluids Engineering, 1981, 103(June 1981)

9 Martin, C.S. *Stability of pump-turbines during transient operations*, 5th International conference on pressure surges, 1986, Hannover, Germany.

10 Martin, C.S. *Instability of pump-turbines with s-shaped characteristics*. in *In Proceedings of the 20th IAHR Symposium on Hydraulic Machinery and Systems*. 2000, Charlotte, USA.

11 Nicolet, C., Alligne, S., Kawkabani, B., Simond, J.J., Avellan, F., *Unstable Operation of Francis Pump-Turbine at Runaway: Rigid and Elastic Water Column Oscillation Modes,* 24th Symposium on Hydraulic Machinery and Systems, October 27-31, 2008, Foz Do Iguassu

12 Nicolet, C., Alligne, S., Kawkabani, B., Koutnik, J., Simond, J.J., Avellan, F., *Stability Study of Francis Pump-Turbine at Runaway*, 3rd IAHR International Meeting of the Workgroup on Cavitation and Dynamic Problems in Hydraulic Machinery and Systems, October 14-16, 2009, Brno, Czech Republic

13 Roth, M., Peikert, R., *Flow Visualization for Turbomachinery Design,* Proceedings of the 7th conference on Visualization, 1996

14 Senoo, Y., Yamaguchi, M., *A Study on Unstable S-Shaped Characteristic Curves of Pump Turbines and No-Flow*, Journal of Turbomachinery, 1987. 109/77

15 Staubli, T., Senn, F., Sallaberger, M., *Instability of pump-turbines during start - up in the turbine mode*, Hydro 2008, Ljubljana.
16 Wang, L., Yin, J., Jiao, L., Wu, D., Qin, D., *Numerical investigation on the "S" characteristics of a reduced pump-turbine model*, Science China, 2011, 54(May 2011)
17 Casartelli, E., Widmer, C., Lederberger, N., *Simplified CFD model for flow field investigations at no load conditions,* Proceedings of Hydro 2010, September 27-29, 2010, Lisboa, Portugal
18 Børresen B., Dahl Knutsen S., *Numerical Computation of the Pump-Turbine Characteristics,* Proceedings of the Hydraulic Machinery and System 21st IAHR Symposium, September 9-12, 2002, Lausanne
19 Liang, Q., Keller, M., Sick, M., *Rotor Stator Interaction During no Load Operation of Pump-Turbines,* Hydro 2009, Lyon, France 2009
20 Hasmatuchi, V., Farhat, M., Roth, S., Botero, F., Avellan, F., *Experimental Evidence of Rotating Stall in a Pump-Turbine at Off-Design Conditions in Generating Mode,* Journal of Fluids Engineering, 2011. 133(May 2011).
21 Widmer C., Staubli T., Ledergerber N., *Unstable Characteristics and Rotating Stall in Turbine Brake Operation of Pump-Turbines*. Journal of Fluids Engineering, 2011. 133(April 2011).
22 Petit, O., Page, M., Beaudoin M., Nilsson H., *The ERCOFTAC centrifugal pump OpenFOAM case study,* 3rd IAHR International meeting of the Workgroup on Cavitation and Dynamic Problems in Hydraulic Machinery and Systems, October 14-16, 2009, Brno, Czhec Republic
23 Pope S.B., *Turbulent Flows*, Cambridge University press, 10. aug. 2000.
24 Versteeg H.K., Malalasekera W., *An Introduction to Computational Fluid Dynamics,* Pearson Eductaion Limited, Second edition 2007.
25 Alidoosti, H.K., *Hydrodynamics of non-circular bluff bodies,* Doctoral theses at NTNU, 2011:302
26 Wylie, E.B., Streeter, L.V., *Fluid Transients in Systems*, Prentice Hall, 1993

4 Appendices

4.1 Appendix I Equations for hydro power plant system

Developing the equation matrix for the hydro power plant system in chapter 2.2.4.

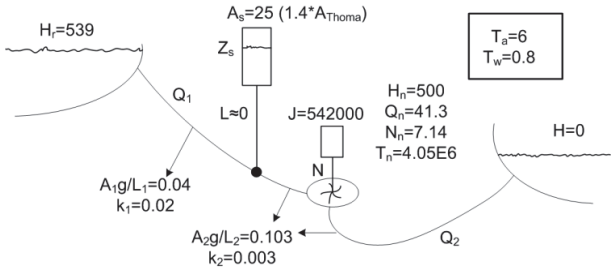

Figure 27 Example system (duplication of Figure 6)

The system has four primary variables, Q_1 (Flow from the reservoir), Q_2 (Flow in the turbine), Z_s (Surge shaft level) and N (turbine speed of rotation), governed by four quasi linear differential equations. These four equations are successively described in the following where the variables are divided into a mean flow value and a perturbation. Throughout this thesis the turbine characteristics has most commonly been expressed as Q_{ed}=f (N_{ed}, α). However, given the definitions of Q_{ed} and N_{ed} one can also express these as H/N^2=f (Q/N, α). The turbine characteristics are represented on the form H/N^2 –Q/N and T/N^2-Q/N as described in "Case 2" in the chapter "Stability of Pump Turbines". Their curves are linearized around the operation point in question as follows:

$$\frac{H}{N^2} = \frac{H^0}{(N^0)^2} + a_1\left(\frac{Q}{N} - \frac{Q^0}{N^0}\right) \quad [s^2 m] \qquad (35)$$

$$\frac{T}{N^2} = \frac{T^0}{(N^0)^2} + b_1\left(\frac{Q}{N} - \frac{Q^0}{N^0}\right) \quad [m^2 kg] \qquad (36)$$

Equation for Q_1:

The flow in the hydro power plant system is modelled using the rigid water column model. This implies a non-deformable pipe line and an incompressible liquid.

$$L_1 A_1 \rho \frac{dQ_1 / A_1}{dt} = (H_r - k_1 Q_1^2 - Z_s)\rho g A_1 \quad [N] \qquad (37)$$

By linearizing around the flow rate Q^0 and subtracting the mean flow, as in the procedure in "Stability of Pump Turbines", eq. (37) becomes:

$$\frac{L_1}{A_1 g}\frac{dq_1}{dt} = -k_1 2Q^0 q_1 - z_s \quad [m] \qquad (38)$$

Equation for Q_2:

Likewise, the equation for Q_2 can be written as

$$L_2 A_2 \rho \frac{dQ_2 / A_2}{dt} = (Z_s - k_2 Q_2^2 - H_t)\rho g A_2 \quad [N] \qquad (39)$$

Around the operation point in question the slope of the turbine head is linearly described by eq. (35). The perturbation of the head caused by perturbations in flow rate and speed of rotation becomes:

$$\begin{aligned} H_t &= N^2 \frac{H^0}{(N^0)^2} + a_1(Q_2 N - \frac{Q^0 N^2}{N^0}) \quad [m] \\ &= [(N^0)^2 + 2nN^0]\frac{H^0}{(N^0)^2} + a_1[(Q^0 + q)(N^0 + n) - \frac{Q^0}{N^0}((N^0)^2 + 2N^0 n)] \quad [m] \\ &= H^0 + 2n\frac{H^0}{N^0} + a_1[Q^0 n + qN^0 + Q^0 N^0 - Q^0 N^0 - Q^0 n2] \quad [m] \\ h_t &= H_t - H^0 = 2n\frac{H^0}{N^0} + a_1[qN^0 - Q^0 n] \quad [m] \end{aligned} \qquad (40)$$

By inserting this into eq. (39) and linearizing the friction term the new equation becomes:

$$\frac{L_2}{gA_2}\frac{dq_2}{dt} = z_s - k_2 2Q^0 q_2 - a_1(\mathrm{q_2 N^0 \text{-} Q^0 n}) \text{-} 2\frac{H^0}{N^0}\mathrm{n} \quad [m] \qquad (41)$$

Equation for Z_S:

The equation for the shaft water level is a continuity equation and takes the following form:

$$\frac{dZ_s}{dt} = \frac{Q_1 - Q_2}{A_s} \quad [m/s] \qquad (42)$$

Or with perturbation variables:

$$\frac{dz_s}{dt} = \frac{q_1 - q_2}{A_s} \quad [m/s] \qquad (43)$$

Equation for N:

The rate of change of the rotational speed depends on the unbalance torque and the rotating inertia.

$$J2\pi\frac{dN}{dt} = T\ [Nm] \qquad (44)$$

An unbalance in the torque, T, is caused by perturbation in flow rate and speed of rotation. It is described by the slope of the characteristics as in eq. (36) and the expression for it becomes:

$$\begin{aligned} T' &= N^2 b_1\left(\frac{Q_2}{N} - \frac{Q^0}{N^0}\right) \quad [Nm] \\ &= 2N^0 N b_1\left(\frac{Q_2}{N} - \frac{Q^0}{N^0}\right) \quad [Nm] \\ &= 2b_1(Q_2 N^0 - Q^0 N) \quad [Nm] \\ &= 2b_1(q_2 N^0 - Q^0 n) \quad [Nm] \end{aligned} \qquad (45)$$

Equation (44) becomes:

$$J2\pi\frac{dn}{dt} = 2b_1(q_2 N^0 - Q^0 n) \quad [Nm] \qquad (46)$$

4.2 Appendix II Computational Fluid Dynamics in Hydro Turbines

This appendix is written with three purposes. First the setup for the simulations that are analysed in chapter 2.3 is documented. Then there are some practical comments to the simulations and uncertainties, and a short text about CFD simulations in general.

Two programs were used for the CDF analysis, namely OpenFOAM and ANSYS CFX. The computational domain contained the runner, part of the draft tube and guide vanes for all 3-D simulations. The 2-D simulations were performed with only one runner channel and four guide vanes using periodic boundary conditions. The steady simulations performed with OpenFOAM were compared to CFX simulations and gave equal results.

OpenFOAM: Boundary conditions were set as in table 1. At the interface between rotating and stationary domain a GGI surface was used without any averaging. The simulations performed with OpenFOAM were steady state. Transient simulations gave too high pressure-oscillations arising from numerical instability. The case setup was similar to the reference case ERCOFTAC Centrifugal Pump by Petit [22].

Table 1 Boundary conditions in OpenFOAM

Boundary	**Velocity**	**Pressure**	**Turbulence, k and ε**
Inlet	C=[C_r, C_u, C_z]	zeroGradient	values corresponding to 7% turbulence intensity
Outlet	zeroGradient	meanValue=0	zeroGradient
Walls	W=[0, 0, 0]	zeroGradient	zeroGradient

The 2D case included only one runner channel and had "cyclicGgi" boundary conditions at the periodic surface.

ANSYS CFX: CFX were used for transient analysis. The interface between rotating and stationary domain was set to "Transient rotor stator". Boundary conditions were set as in table 2, and the numerical schemes were set to "higher resolution" for advection terms and first order for turbulence numerics. Time steps were set to 0.00015 second which corresponds to 0.7 degree rotation per time step.

Table 2 Boundary conditions in CFX

Boundary	**Condition**
Inlet	Mass flow rate and direction, medium turbulence intensity
Outlet	Opening , reference pressure
Walls	no slip, smooth wall

Practical comments to the simulations in chapter 2.3:

The flow did not always converge to a constant state. Therefore the main output from the simulations, which is the head, was averaged over a number of iterations. This was done for both steady and unsteady simulations.

Grid convergence test were performed, but this only applies to the mean-flow since the boundary layer is modelled by a logarithmic law of the wall. With appropriate wall distance, i.e. y^+=30-100, all simulations with more than 70.000 cells in one channel gave equal results.

The two turbulence models K-epsilon and K-omega SST were tested in this work, showing no significant difference in the resulting mean flow.

Uncertainty and errors: Widely accepted definitions of uncertainties and errors have been listed in Versteeg [24]. Some elements of that list are presented here together with comments that apply to the simulations performed in this thesis.

- Iterative convergence errors:
  - *i.* Steady simulations: *For some operation points the flow was not steady-state and the solution did therefore not converge to a steady state.*

ii. Transient simulations: *Time-steps were set to a value corresponding to approximately one degree of rotation which is a widely used time-step size in the literature. However, it might be too high to capture details of transient flow structures.*

- Uncertainty due to approximate representation of geometry: *The guide vanes opening was not exactly the same in the simulations as in the measurements*
- Uncertainty due to boundary conditions: *The inlet was placed at the guide vane entrance and the outlet just a small distance down in the draft tube.*
- Physical model uncertainty: *The turbulence models used do not capture effects of rotation and curvature.*

About CFD

The CFD simulations solve the Navier-Stokes equations for incompressible flow. This flow is then uncoupled from the energy equation and the pressure has a pure elliptic behaviour. A direct simulation, DNS, of the flow is not possible due to the requirement of spatial and temporal resolution which grows with the Reynolds number to the power of 9/4. The smallest scales in the flow are therefore modelled by turbulence models in order to have a feasible amount of equations to solve. When a Reynolds averaging is performed on the Navier-Stokes equation, turbulent quantities called Reynolds stresses comes forth. These are modelled by the Boussinesq assumption, eq. (47), that links them to the turbulent viscosity, μ_t, and turbulent kinetic energy, k. The turbulent viscosity is a function of the two turbulent quantities modelled and represents an analogy between the physical processes of turbulent and molecular movements. The molecular movements exchange momentum regardless of the mean-flow direction and turbulence does the same but have a larger length scale.

$$\tau_{ij} = \mu_t\left(\frac{\partial C_i}{\partial x_j} + \frac{\partial C_j}{\partial x_i}\right) - \frac{2}{3}\rho k \delta_{ij} \ [N/m^2] \qquad (47)$$

The last term in eq. (47) is a normal stress that can be absorbed into a modified pressure in the CFD simulations, Pope [23]. The flow needs not to be resolved into the walls if a wall-law is applied. Such a wall-law can be used in the log-law layer were y^+ takes values between 30 and 500, Versteeg [24], where y^+ is the normalized wall distance eq. (48). However it is beneficial to have y^+ in the lower part of that range. During simulation of characteristics the flow rate ranges from nominal flow rate and down to zero. Since the wall distance depends on the velocity through u_t, it is impossible to have "correct" y^+ value for all simulations. Resolving the boundary layer is an option but requires $y^+=1$ close to the wall, which for the model turbine in this thesis corresponds to a wall distance of approximately y=0.005mm. This, together with the growth factors for grid cells at maximum 1.2, results in a very high number of cells. The boundary

condition for the turbulent quantity epsilon is also an issue. Unlike the turbulent kinetic energy whose value is zero at the wall, the value and gradient of epsilon at the wall is unknown.

$$y^+ = \frac{\rho y u_t}{\mu} \quad [-] \qquad (48)$$

In the incompressible Navier-Stokes equation there is no description of the time evolution of the pressure. The pressure is therefore coupled to the flow field through various algorithms, e.g. SIMPLE and PISO, Versteeg [24]. These velocity-pressure couplings generally modify the continuity equation to solve for the pressure. The time-step is normally restricted by the CFL condition. By using the SIMPLE algorithm the time-step can be enlarged disregarding the CFL condition.

For the flow in the rotating part of the turbine a decomposition of the acceleration is performed, eq. (49), and the equations can be solved for the relative velocity instead of the absolute velocity. The last term represents the centrifugal acceleration, which can also be absorbed into a modified pressure, Alidoosti [25].

$$a_{abs} = a_{rel} + 2w \times \omega + \frac{\omega^2}{r} \; [m/s^2] \qquad (49)$$

5 Papers

5.1 Short Summary of papers

This chapter summarizes the papers I-VI.

5.1.1 Paper I: Dependency on Runner Geometry for Reversible-Pump Turbine Characteristics in Turbine Mode of Operation

This paper investigates how the runner leading edge profile influences the characteristics. Four different profiles were made in a composite material and glued on to the pump turbine model. Characteristics in all modes of operation were then measured for all profiles. In part load and towards runaway the flow meets the blade with a too small angle which makes separation likely to occur at the pressure side of the blade. Two profiles were therefore made to test whether a larger radius of curvature on the pressure side of the leading edge could remedy this problem. Other profiles were created to test for the inlet blade angle. Both larger radius of curvature and smaller blade angle improves the stability of the turbines. CFD simulations revealed further connections between geometry and characteristics.

5.1.2 Paper II: Stability Limits of Reversible-Pump Turbines in Turbine Mode of Operation and Measurements of Unstable Characteristics

Two types of stability criteria apply to pump turbines, static and dynamic stability. The term static is used when the energy only takes one form and the dynamic term is used when the energy alternate between two forms and create oscillations. With fixed speed of rotation the traditional static H-Q criterion applies, which is rewritten into a criterion for the slope of Q_{ed}-N_{ed} characteristics. When the speed of rotation is free to vary with the unbalanced torque there are two new criterions for static and dynamic stability respectively.

Characteristics measured with speed as input got a hysteresis shape caused by static instability. This instability was solved by two different measurements techniques that permitted measurements of the full s-shaped characteristics. These were the valve-throttling and torque-as-input techniques. Both solved the static stability problem but the valve-throttling reduces the pressure to low values and the torque-as-input technique suffered from some dynamic oscillations. Pressure dependency was tested with measurements on three different pressure levels. Towards runaway the absolute pressure level influence the characteristics such that high pressure gives the steepest characteristics. The Reynolds number increases with the pressure level and the pressure dependency can therefore be identified as an effect of the Reynolds number.

5.1.3 Paper III: Design of a Reversible Pump-Turbine – with purpose to Investigate Stability

This paper describes the design process of the pump turbine runner. This was designed to fit into an existing Francis distributor and draft tube. U_1 was chosen based on empirical data and the other main parameters were given values that fulfilled the Euler equation and the dimensions of the original Francis turbine. An uc_u distribution along the blade was chosen to give small load on the blades close to the inlet and outlet. The geometry was adjusted in an iteration process with CFD simulations. Mainly two methods were used to change the blade, namely shortening or lengthening of the blade and adjustments of the outlet blade angle. Characteristics were simulated on the final blade and showed to have an s-shape for all opening degrees.

Remark: The parameters listed in tables 1-3 are based on Euler-equations and are modified later in the design process. Final parameters values are listed in paper IV and V.

5.1.4 Paper IV: A Two-Dimensional Model for Pump-Turbine Instability Investigations

A two-dimensional model was created for stability investigations. This model was created by means of conformal mapping of the pump turbine described in paper III. The outlet was adjusted to get homologous velocity diagrams and the diameters were held constant. The idea of doing two-dimensional analysis was formed from the observations that the inlet of pump turbines essentially has a two-dimensional shape and that a vortex forming in the inlet zone is one of the main flow structures leading to the s-shape of the characteristics. Simulations of the flow field along the characteristics showed that a vortex starts to build up at the pressure side of the blade close to the leading edge of the adjacent blade. This vortex grows to cover the whole channel in turbine brake mode. The simulations also showed that the flow is not periodic between the runner channels.

5.1.5 Paper V: Geometry Impact on Pump-Turbine Characteristics

Runners with different designs were simulated with the two-dimensional model presented in paper IV and with the analytical model presented in Paper VI. Diameters and speed were analyzed with the analytical model for geometries with equal Euler-conditions. Both parameters give steeper characteristics when their values are increased. This is linked to the radial force, which is the sum of the centrifugal force and the radial component of the coriolis force. CFD simulations showed that smaller inlet blade angle give less steep characteristics. The cause is found in the channel vortex that has increased head loss when the blade angle is large.

5.1.6 Paper VI: Dynamic Behaviour of Reversible Pump-Turbines in Turbine Mode of Operation

A one-dimensional model was developed by Prof. Torbjørn Nielsen which estimates the characteristics by an algebraic equation developed from the Euler turbine equation. This is a second degree equation, eq. (50), for the flow rate which is solved at operation points along the characteristics using constant head.

$$gH = gH_n\left(\frac{Q}{\kappa Q_n}\right)^2 + s(\omega^2 - \omega_n{}^2) - (\omega - 1)R_q(Q - Q_c) \quad [m^2/s^2] \quad (50)$$

Pump turbines normally have prolonged blades compared to a Francis turbine. The effect of this prolongation is accounted for by a term denoted pumping effect (R_q). With this term included, the characteristics get steeper and compares well to the measured characteristics for the pump turbine.

5.2 Papers

Paper I

Olimstad, G., Nielsen, T.,K., Børresen, B., 2012, “Dependency on Runner Geometry for Reversible-Pump Turbine Characteristics in Turbine Mode of Operation”, ASME J. Fluids Eng., Accepted for publishing

Dependency on Runner Geometry for Reversible-Pump Turbine Characteristics in Turbine Mode of Operation

Grunde Olimstad[1], Torbjørn Nielsen[1] and Bjarne Børresen[2]

[1]Department of Energy and Process Engineering, Norwegian University of Science and Technology

Alfred Getz Vei 4, 7491, Trondheim, grunde.olimstad@ntnu.no, torbjorn.nielsen@ntnu.no

[2]Energi Norge, Næringslivets Hus, Middelthunsgate 27, Oslo, bbo@energinorge.no

Abstract

Characteristics of a reversible-pump turbine have been measured with five different leading edge profiles in turbine mode. These profiles varied the inlet blade angle and the radius of curvature. Further geometry parameters have been investigated through numerical simulations. The pump turbine tested has much steeper flow-speed characteristics than a comparable Francis turbine. The most obvious geometry difference is the inlet part of the runner blades, where the blade angle for the pump turbine is much smaller than for the Francis turbine. Two different blade angles have been tested on a physical model and CFD simulations have been performed on four different angles. Both methods show that a smaller blade angle gives less steep characteristics in turbine mode, whereas the measured s-shape in turbine brake- and turbine pumping mode gets more exaggerated. Long-radius leading edges result in less steep characteristics. The unstable pump turbine characteristics are in the literature shown to be a result of vortex formation in the runner and guide vane channels. A leading edge with longer curvature radius moves the formation of vortices towards higher speed of rotation.

Keywords: reversible-pump turbines, stability, characteristics, geometry, inlet profile, measurement, numerical simulation

Introduction

Many pumped storage hydropower plants with reversible-pump turbines (RPTs) suffer from stability problems during start-up in turbine mode, during load rejection or at low head operation. Three examples of this are described in Pejovic [1], Dörfler [2] and Klemm [3]. In the start-up, the turbine speed is synchronized with the grid frequency before the generator is loaded. At the time of synchronizing, the turbine runs in idle mode, and the opening of the guide vanes is small. At these conditions many pump turbines are dynamic unstable, and undergo oscillations in speed, torque, head and flow rate. Francis turbines at the same operation point are commonly stable. Therefore the starting point of this paper is that the stability depends on the turbine design and more specifically on the geometry of the runner inlet. It should be noted that the shape of pump turbine runners have more similarity to a pump than to a Francis turbine. Reverse running pumps have been utilized as generating turbines, as for example in water supply systems, Apfelbacher [14].

The criterion for stability of the pump turbine is called dynamic when the shaft is disconnected from the generator and the speed of rotation varies with the unbalanced torque. In this situation the energy in the system may oscillate between rotating energy of the turbine shaft and kinetic energy in the water masses. The system is unstable if these oscillations are not dampened and a necessary but not sufficient criterion for the instability was derived by Martin [4]. This criterion demands the slope of the torque-speed (T_{ed}-N_{ed}) characteristics to be positive. In fact the slope can be slightly positive and still stable depending on the fluid- and machine time scales and the slope of the flow-speed (Q_{ed}-N_{ed}) characteristic. Friction losses and possibly water elasticity also influence the stability limits. The dimensionless variables Q_{ed}, T_{ed} and N_{ed} are defined in eq. (1). When the pump turbine is connected to the generator with a frequency proportional to the electric grid frequency a static stability

criterion applies. The system is then unstable if the slope of the pump turbine head-flow curve is positive and the magnitude greater than for the slope of the system head loss curve. At such an unstable operation point the system cannot withstand the smallest perturbation and the perturbation will grow exponentially towards some system limits.

This paper presents a parameter study on the pump turbine leading edge. This is performed on a physical model and characteristics are measured in the laboratory. Other parameters are studied by means of CFD simulations. The purpose of this work is to find out which geometry parameters that influence the characteristics and how significant they are. It is intended to keep the parameter alteration within a range that is relevant for manufactures.

$$Q_{ed} = \frac{Q}{D^2\sqrt{gH}},\ N_{ed} = \frac{nD}{\sqrt{gH}},\ T_{ed} = \frac{T}{D^3\rho gH} \quad [-] \tag{1}$$

At the Waterpower laboratory in Trondheim two runners, one high head Francis and an RPT, have been tested. The runners have many similarities. Diameters of inlet and outlet and the inlet height are the same for both runners and the flow rate and head at best efficiency point (BEP) are close to each other. Both runners use the same distributor and draft tube. Despite many similarities the measured characteristics of the two runners are very different. As can be seen in Figure 1, the Francis characteristics of dimensionless flow rate versus dimensionless speed are shifted towards lower speed compared to the RPT characteristics. The Francis characteristics are also very steep in a small area around the runaway curve but they are not s-shaped as the RPT characteristics are. It should be noticed that the flow rate through the RPT depends very little on the speed of rotation in the major part of the chart, but at high speed the flow rate changes very rapidly.

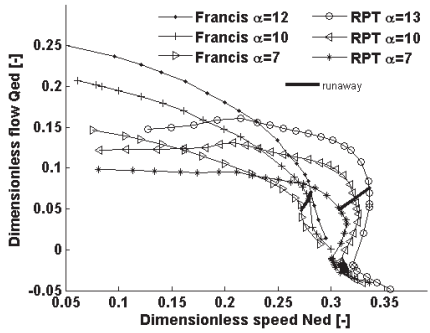

Figure 1 RPT versus Francis characteristics

D_1	D_2	B_1
0.63 [m]	0.35 [m]	0.06 [m]
	Q_{ed}*	N_{ed}*
Francis	0.159 [-]	0.179 [-]
RPT	0.133 [-]	0.223 [-]

Table 1 Common dimensions and best operation point

The runners are also different and the most significant differences are the speed of rotation at BEP, blade angles and the number of blades. The blade angles at the inlet are twelve and sixty eight degrees for the RPT and the Francis respectively and the number of blades is six for the RPT and 24 for the Francis runner. The geometry of the RPT is shown in Figure 2 together with the blade angle distribution. Because of the small blade angles towards the inlet of the RPT the blades are stretching circumferentially 180 degrees.

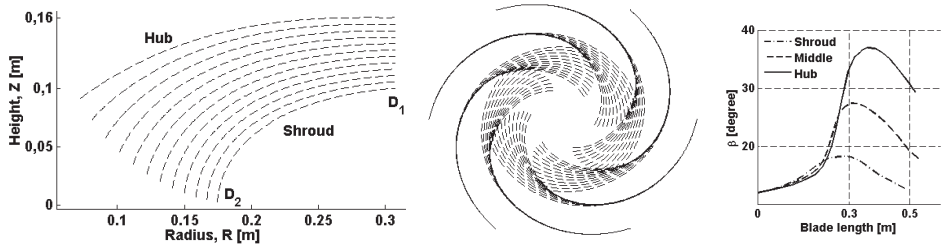

Figure 2 Pump turbine runner geometry

Little is found in the literature on the runner geometry impact on characteristics but Olimstad [5] and Nielsen [6] have presented some studies. From the model by Nielsen it can be seen that the diameter and speed of rotation both have great impact on the steepness of characteristics. Higher values give in both instances steeper characteristics. In Olimstad [5] the inlet blade angle is investigated by means of a two dimensional model and the characteristics became steeper with higher inlet blade angle. Olimstad also found that tiny geometry changes, as small as 0.1 degree in the blade angle, could be analyzed by the CFD model.

Parameter study on the physical model

The leading edge of the runner was investigated by four different profile alterations. Small plastic parts were manufactured with a strong composite material to fit onto the outer part of the blade inlet. They were glued on to the model runner vanes and removed after testing. Four different profiles were made and tested. The main purpose of these profiles was to test different radius of curvature on the pressure side of the leading edge and the inlet blade angle. The profiles A and B both enlarge the radius of curvature on the pressure side, but in two different ways. The profile C also enlarges the radius of curvature, but is much more pronounced than the profiles A and B. The profile D is the same as profile C except that it is moved slightly toward lower radius and consequently has a smaller blade angle.

Profile A: This is an extension on the pressure side of the blade which increases the radius of curvature on that side, Figure 3. The thickness of the blade is slightly increased.

Profile B: This profile moves the leading edge towards lower radius and therewith makes the radius of curvature larger on the pressure side, Figure 4. The blade is slightly prolonged.

Profile C: The blade inlet is altered on both pressure and suction side and the radius of curvature is considerably larger on the pressure side, Figure 5. The thickness of the blade is increased and the blade is slightly prolonged.

Profile D: This profile is equal to profile C except that the leading edge is moved towards lower radius, Figure 6. The new radius is 0.16 percent shorter and the blade angle is 1.5 degree smaller. The main difference between the profiles “C” and “D” is the blade angle. This can be concluded after evaluation of impact on the head in the Euler turbine equation. Assuming that the relative flow angle equals the blade angle and omitting the outlet, since it remains unchanged, the Euler equation becomes eq. (2). The blade angle as a single parameter will theoretically increase the head by 13.5 percent while the diameter will increase the head by only 0.5 percent.

$$H = \frac{\omega}{g}\frac{D_1}{2}\left(\omega\frac{D_1}{2} - \frac{Q}{\pi D_1 B_1 \tan(\beta_1)}\right) \tag{2}$$

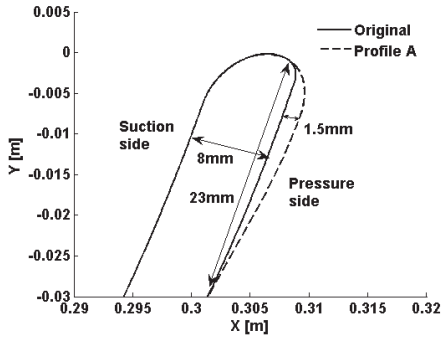

Figure 3 Profile A

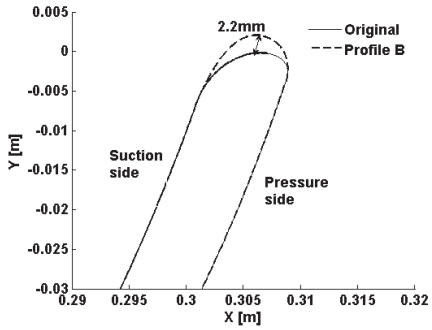

Figure 4 Profile B

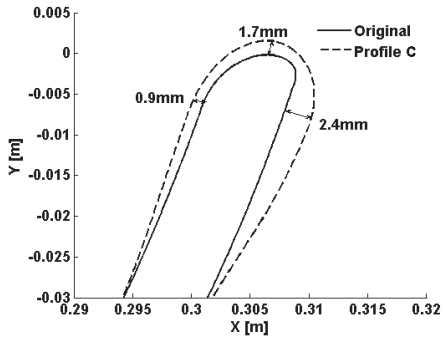

Figure 5 Profile C

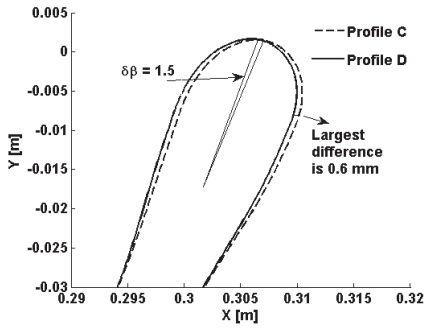

Figure 6 Profile C and D

The test-rig, Figure 7, is a closed loop system where the water is driven by a pump. This delivers water through pipes to a pressurised tank. The water flows through a flowmeter before it enters the turbine. From the turbine it continues through an outlet-tank before it returns to the pump. A generator which can also work as a motor is mounted on the turbine shaft. This generator floats freely and is held back from rotating by a level arm connected to a force-cell which measures the force. The torque is obtained by multiplying this force with the length of the level arm. There is a perforated disk mounted on the shaft that is used by an optical device to measures the speed and three meters up-front of the turbine inlet there is an electro-magnetic flowmeter. The pressure difference over the turbine is measured by a pressure transducer which gets one pressure signal from each side of the turbine. These are taken at four different angular positions on the pipes. The random errors in the measurements were found in BEP by eleven repeated measurements at the same operation point. The sampling period for each measurements was thirty seconds and the sampling rate was 1.4 hertz or higher. The standard deviations of the repeated measurements were, in percent of BEP values, 0.16 for efficiency, 0.07 for N_{ed}, 0.27 for Q_{ed} and 0.28 for T_{ed}. Repetition of a whole curve, such as that in Figure 8, shows no significant deviation in any part of the curve. To stabilise operation points in the s-region two valves were partly closed to elevate the head-flow curve and therefore fulfil the static stability criterion. The measurements were generally performed with twenty meter head, but the throttling valves decreased the head for some operation points. The absolute uncertainties of the measurements are considered to be of little importance since all results are comparisons of two measured curves. However the accuracies for the test rig are, 0.2% for the efficiency, 0.1% for the flow rate, 0.15% for the torque and 0.16% for the pressure difference.

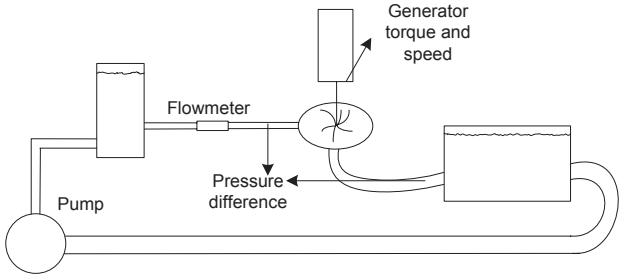

Figure 7 The test rig

Results from measurements

Two terms need to be defined before starting this section. The first term is the slope of the characteristics. This is generally the derivative of the flow-speed (Q_{ed}-N_{ed}) characteristics which takes different values along the curves. In this text it is taken to be the change in Q_{ed} divided through the change in N_{ed} between the runaway curve and twenty percent over-speed. The latter is where N_{ed}/N_{ed}* is equal to 1.2. The second term is the s-shape region which is defined as the region below the runaway curve that forms an s-shape. Additional notations are the turbine brake mode, which is the region between the runaway curve and zero flow rates and the reverse pump mode which is the region below zero flow rates.

Profile A: Characteristics of flow rate versus speed and torque versus speed are shown in the Figure 8 and Figure 9. The profile A increased the flow rate at high speed of rotation and positive flow rate. This effect is strongest just below the runaway curve and before the curve turns in the upper part of the s-shape. The s-shape is however exaggerated since the curves from the original blade and profile A meet at flow rates below zero. The numeric value for the slope at ten degree guide vane opening is seven percent lower than for the original profile which means that the margin to the stability limit is increased. At four degree guide vane opening the s-shape was so much exaggerated that it could not be stabilised by the valves. No measurements were therefore done in this part of the curve. With profile A the runaway curve moved a little towards higher speed of rotation. At best efficiency point the efficiency was degenerated by 0.2 percent, Figure 10. The BEP did not change operation point. In pump mode the difference in the head-flow curve was very small, Figure 11.

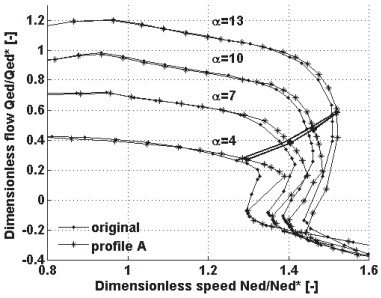

Figure 8 Flow-speed characteristics of profile A

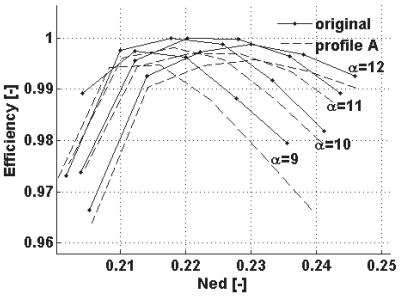

Figure 10 Turbine efficiency for profile A

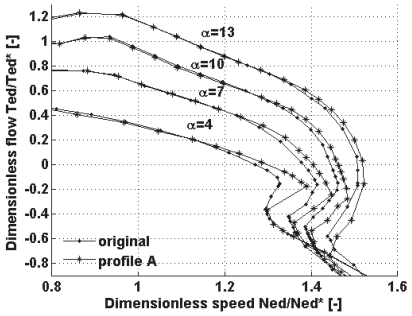

Figure 9 Torque-speed characteristics of profile A

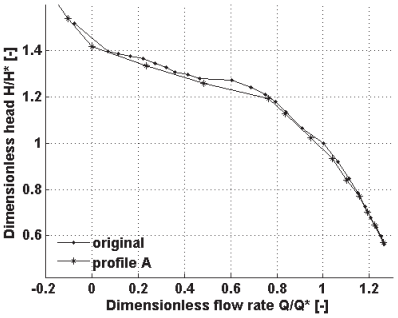

Figure 11 Head-flow characteristics in pump mode

Profile B

This profile also lifted the characteristics in the upper part of the s-region, Figure 12 and 13. Towards the best efficiency point and in reverse pump-mode the characteristics are very similar for profile B and the original profile. This gives a more distinctive s-shape. In BEP the efficiency is 0.5 percent lower for profile B. The pump curve is here shown as a head-flow curve. Profile B has a slightly lower pump capacity than the original profile, Figure 14, but the efficiency curves in pump mode are very similar, Figure 15. The characteristics in turbine mode differ at speeds just below nominal speed, and the curves forms an enveloped area. The profile B has higher head at these operation points. It comes from disadvantageous flow associated with the sharper leading edge at the suction side of the blade.

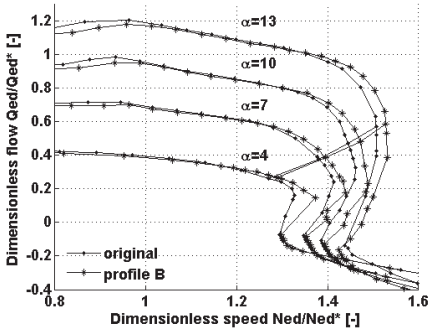

Figure 12 Flow-speed characteristics of profile B

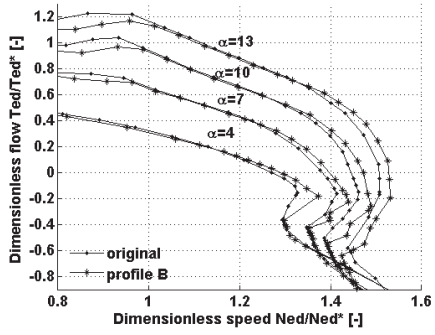

Figure 13 Torque-speed characteristics of profile B

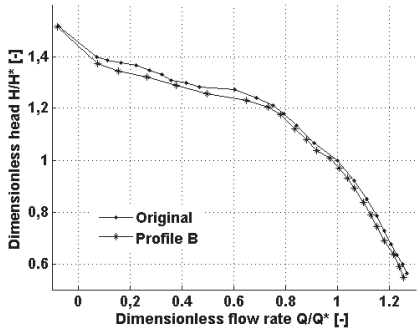

Figure 14 Head flow curve for profile B in pump mode

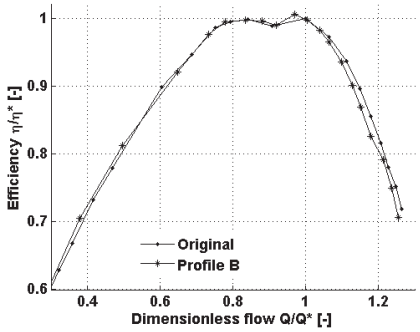

Figure 15 Efficiency for profile B in pump mode

Profile B compared to A: The profiles A and B have a conspicuous difference. This is they compare different depending on the guide vane angle. For ten and thirteen degree guide vane openings the characteristics for profile B have higher flow rate than profile A. For the two lowest guide vane openings the relation is the opposite, Figure 16. It should be noticed that the differences are small.

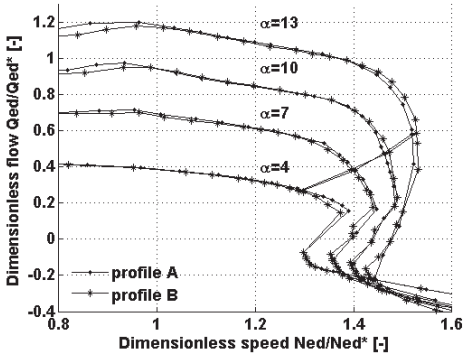

Figure 16 Flow-speed characteristics of profile A and B

Profile C and D: These two profiles have almost the same effect on the characteristics compared to the original profile. Figure 17 shows the comparison of the original and profile C and Figure 18 shows the comparison between profile C and D. The dimensionless flow rate versus speed characteristics are stretched towards higher speeds. Their slopes for the flow-speed characteristics at ten degree guide vane opening are twelve percent less elevated than the slope of the original profile. They have a less distinctive s-shape than the original profile and the zero efficiency line has moved towards higher speed. The top efficiency is 0.5 and 0.4 percent lower for profile C and D respectively. However the efficiency curves for profile C and D are broader than for the original profile, Figure 19. The difference between profile C and D is small, but at high speeds the profile D gave slightly higher flow rates, but it also has slightly more distinctive s-shape. The profile C gave the steepest characteristics between best efficiency point and the runaway curve. In pump mode of operation there are small differences between the original profile and profile C and D. The original and profile D are distinguished only at low flow rates where the original profile gave slightly higher pumping head, Figure 20. Compared to profile D, the profile C has a slightly higher pumping head over the whole range of flow rates, Figure 21. The efficiencies in pump mode are equal for the two profiles C and D and the original blade, Figure 22.

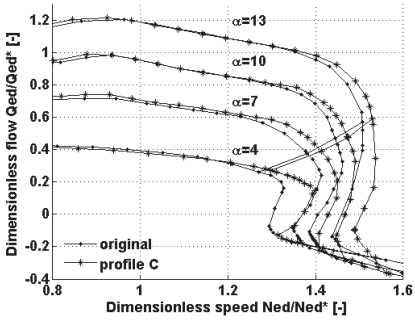

Figure 17 Comparison of original and profile C in turbine mode

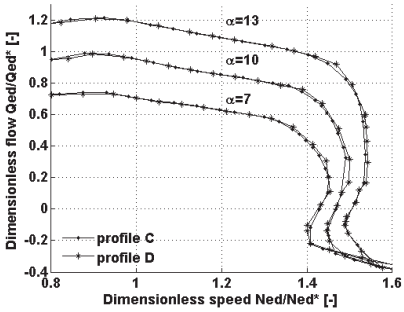

Figure 18 Comparison of profiles C and D in turbine mode

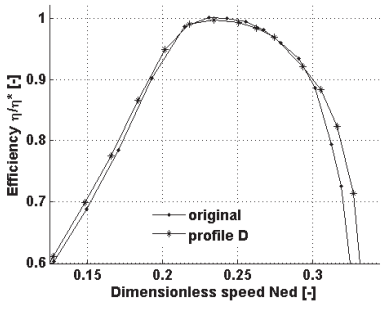

Figure 19 Efficiency in turbine mode

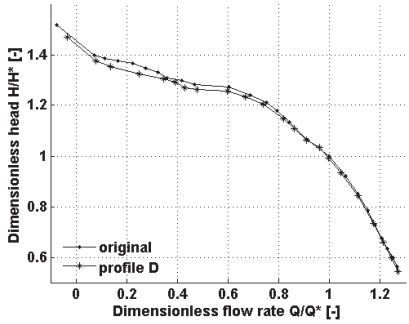

Figure 20 Comparison of original blade versus profile D in pump mode

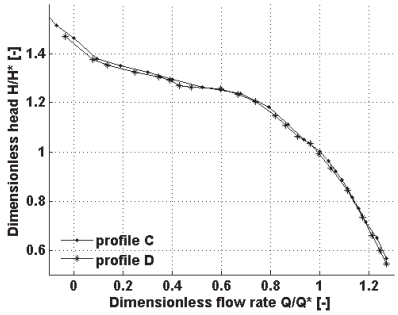

Figure 21 Comparison of profile C and D in pump mode

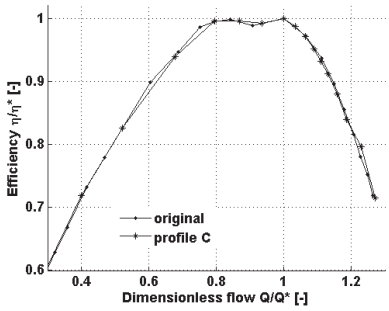

Figure 22 Efficiency in pump mode

Parameter study by CFD

Even though recent scientific papers, Widmer [12] and Hasmatuchi [13] document rotating stall in reversible pump turbines this is not proven to be the root cause of the s-shaped characteristics. In fact the characteristics for low guide vane openings in Widmer [12] are s-shaped but have neither rotating stall cells nor unsteady vortices. Since the flow phenomena leading to s-shaped characteristics at low guide vane openings seem to be stationary, a stationary approach for the CFD is regarded as sufficient for the geometry comparisons analysed here. Stationary CFD, both two- and three dimensional, have proven to detect the effect of the inlet blade angle correctly. In Olimstad [6] blade angle differences, as small as 0.1 degree, were correctly simulated by CFD. A transient sliding mesh simulation for one characteristic curve has been conducted for accuracy assessment. This simulation included a 360 degree runner and guide vane cascade. The time step was given a value which

corresponds to one degree runner rotation per time step and five full rotations were simulated for each operation point. Figure 23 compares the characteristics from the transient and a steady state simulation with the measured characteristics. Both the steady state and the unsteady simulation fail to predict the characteristic in the s-shape region.

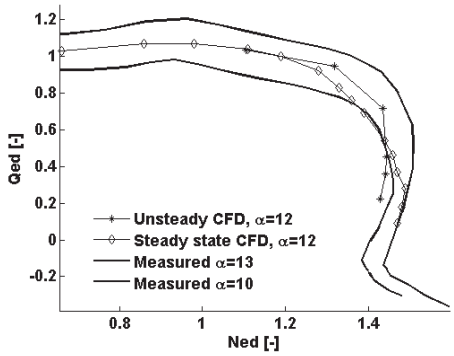

Figure 23 Measured verus simulated characteristics

The OpenFOAM CFD analysis was performed using one channel of the runner together with five guide vanes in stationary analysis using the frozen rotor approach. The blade leading edge had the same position relative to the guide vanes in all compared cases. As boundary conditions, velocity vectors were prescribed at the inlet with the same angle as the guide vanes. At the outlet the pressure was set to a fixed mean value and the velocity was restricted by a zero gradient condition on velocity normal to the boundary. The k-epsilon model was used for modelling turbulence and inlet values reflecting seven percent turbulence intensity was prescribed. Hexahedral is the only cell shape used and their amount was 185.000 for all simulations. The same mesh was used for all operational points on the respective geometry leading to a certain variation in the average values of the non-dimensional wall distance, y+. Second order schemes were used for both convection and diffusion terms. The series of simulations that build up the characteristics were performed with constant speed and varying inlet flow rate. To calculate the head, the total pressure difference between inlet and outlet was found by integration on the boundaries and the energy in the draft tube swirl was included. When the new geometries were made, a set of (x,y,z) coordinates were computed based on a set of radii(r), heights(z), and blade angles(β). A blending function (F) with a smooth shape and values from zero to one was applied on the new and the original blade, such that: $XYZ_{used}=XYZ_{original}*F+XYZ_{new}*(F-1)$. This was done to secure fixed outlet regions when changes were made on the inlet. All blades in this article have a straight and vertical leading edge and by retaining this shape without the blending function, any change on blade angle is deemed to affect the outlet geometry. Geometry changes are by intention made small to avoid dominating secondary effects, but are made large enough to have significant impact on the characteristics.

The first compared parameters are blade angle and the inlet diameter. The blade angle is altered in two different ways, first directly on the leading edge angle and second on blade angles internally between inlet and outlet. The internal blade angle change is shown in Figure 30. At the inlet and outlet the angles are kept as original whereas the angles are given higher values in between. To quantify the change an integration of the blade angle curves are performed and the relative change in integral-area is denoted in the figures. The blade angles determine the length of the blades and consequently the position of the inlet. Higher blade angles give shorter blades and vice versa. The influence of the number of blades was investigated by simulation of characteristics with 3, 6 and 10 blades. Ten blades give the steepest slope of the characteristics and three blades give the least steep characteristic. Figures 24-29 and 31 show horizontal cuts of the different geometries and the resulting characteristics. The internal blade angle distributions are shown in Figure 30.

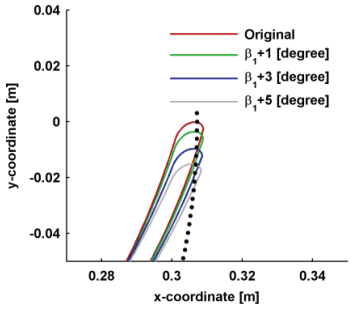

Figure 24 Inlet blade angles

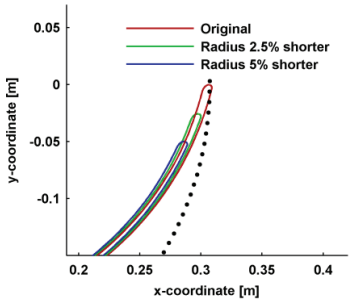

Figure 25 Shorter radii

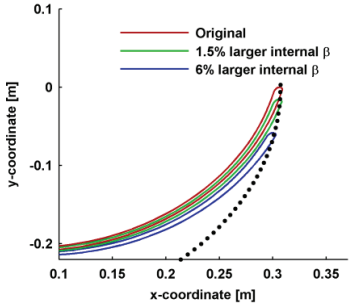

Figure 26 Different internal blade angles

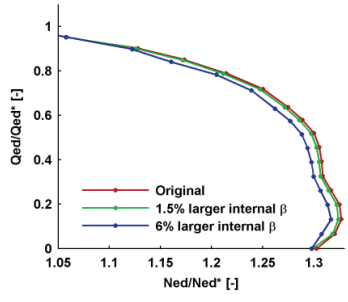

Figure 27 Characteristics for different internal blade angle

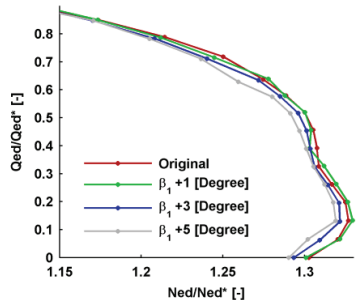

Figure 28 Characteristics for different inlet blade angles

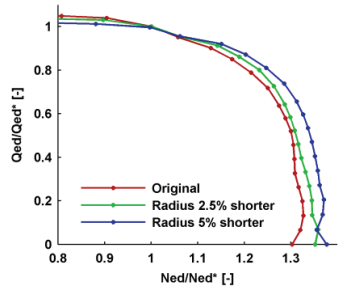

Figure 29 Characteristics for different radii

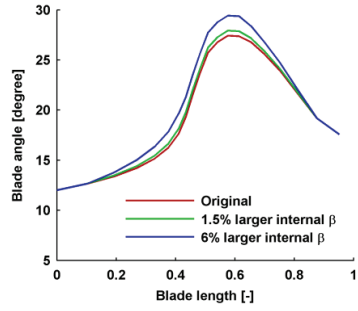

Figure 30 Internal blade angle distribution from inlet (0) to outlet (1)

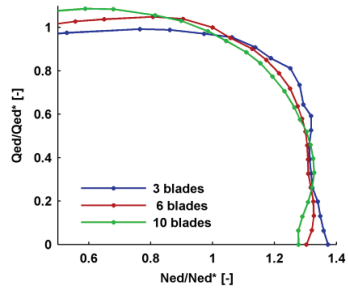

Figure 31 Different number of blades

Conclusions

The geometry changes performed in this article are by intention made small enough not to influence the BEP performance in turbine mode. This is confirmed by the measurements showing equal characteristics around BEP for all profiles. The geometry changes on the physical model were very small, with the smallest difference between profile “C” and profile “D”. The largest distance between these two profiles is 0.6mm, Figure 6. From the standard IEC 60193[7] there is a geometric accuracy required of 0.1 percent of the outlet diameter, which for this turbine is 0.34mm. Thus the difference between the two profiles is less than two times the demanded accuracy requirement from the IEC standard. An important conclusion is therefore that the characteristics can be altered by very small changes on the inlet blade profile without affecting the characteristics around best operation point.

Compared to the original profile, all four profiles had higher radius of curvature at the pressure side of the leading edge. Since the characteristics from all profiles were consequently less steep this clear relation is established. Both Staubli [7] and Olimstad [8] reported that a vortex formed in the entrance part of the runner channels is a cause of steeper characteristics. This vortex may be influenced from separation or turbulent eddies created by a too sharp a leading edge. Both profile “A” and “B” had a larger radius of curvature on the pressure side of the blade leading edge. While the profile A increased the thickness of the blade, the profile B slightly prolonged the blade. The effect on the characteristics was almost equal with less steep characteristics and a more distinctive “s-shape”. A peculiar observation was made in the comparison between these two profiles, which was dependent on the guide vane opening. The profile “B” had steepest characteristics for small guide vane angles and profile “A” steepest for high guide vane angles.

The profile “C” and “D” had a more pronounced/thicker shape than profile “A” and “B”. Consequently their characteristics were even less steep. Their s-shapes were slightly less exaggerated and the efficiency curve had a lower top but preserved the efficiency better at off design operation points. The comparison of profile “C” and “D” shows that higher inlet blade angle gives steeper characteristics, but the effect is small. In pump mode the higher blade angle gave a slightly higher pumping head. The relation between the blade angle and characteristics is partly seen in measurements by Yamabe[10] and in CDF simulations on a two-dimensional model by Olimstad [6].

Generally the influence by the profiles were very small or none at all both in ordinary pumping mode and reverse pumping. The profiles had significant effect on the characteristics around the runaway curve. The profiles A and B were approximately seven percent less steep and the profiles C and D were 12 percent less steep.

Simulations on the model further expanded the parameter study. The capability to capture the effect of the geometry changes showed to be good even though some flow features are not captured. These features are for example moving vortices Senoo [11] and rotating stall which occur in pump turbines, Staubli [12] and Hasmatuchi [13]. These are not captured here since the simulations were steady state. The blade angle variation confirmed the finding in the measurement that the characteristics get steeper with increased blade angle. The internal blade angle has the same effect. Simulations with decreased radii showed that decreasing the radius give less steep characteristics while comparison of 5, 6 and 10 runner blades showed that more blades give steeper characteristics. The radius is also a parameter in the model in Nielsen [5], where the effect of decreasing the radius is the same as here.

To make a pump turbine more stable it is recommended to: increase radius of curvature on the pressure side of the leading edge in turbine mode, decrease the inlet radius, increase inlet blade angle, or increase the length of the blade.

Acknowledgments

This work is financed by Norwegian power companies, consultants and equipment suppliers through Energy Norway.

List of Symbols

B_1	Inlet Height	[m]
D_1	Inlet diameter	[m]
D_2	Outlet diameter	[m]
g	Gravitational acceleration	[m/s^2]
H	Head	[m]
k	Turbulent kinetic energy	[m^2/s^2]
n	speed	[1/s]
N_{ed}	Dimensionless speed	[-]
Q	Flow rate	[m^3/s]
Q_{ed}	Dimensionless Flow	[-]
R	Radius	[m]
T_{ed}	Dimensionless torque	[-]
X,Y,Z	Dimensional coordinates	[m]
α	Guide vane angle	[Degree]
β	Blade angle	[Degree]
ε	Turbulent dissipation	[m^2/s^3]
ω	Rotational speed	[1/s]

Sub- and superscripts

1 Inlet

2 Outlet

* Best operation point

References

[1] Pejovic, S., Krsmanovic, L., Jemcov, R., Crnkovic, P., *Unstable Operation of High-Head Reversible Pump-Turbines*, in 8th IAHR Symposium, 1976, Leningrad.

[2] Dörfler, P.K., Engineer, A.J., Pendse, R.N., Huvet, P., Brahme, M.V.. *Stable operation acvhieved on a single -stage reversible pump-turbine showing instability at no-load*. Proceeding of the 19th Symposium on Hydraulic Machinery and Systems. 1998. Singapore.

[3] Klemm, D., *Stabilisierung der Kennlinien einer Pumpenturbine im Bereich zwischen Turbinen-Teillast und Rückwärtspumpenbetrieb*. Voith Forschung und Konstruktion, 1982. Heft 28, Aufsatz 2.

[4] Martin, C.S., *Stability of pump-turbines during transient operations.* 5th International conference on pressure surges, 1986, Hannover, Germany.

[5] Nielsen, T.K, Olimstad, G., *Dynamic Behaviour of Reversible Pump-Turbines in Turbine Mode of Operation*, in International Symposium on Transport Phenomena and Dynamics of Rotating Machine, 2010, Honolulu.

[6] Olimstad, G., Børresen, B., Nielsen, T.K., *Geometry Impact on Pump-Turbine Characteristics*, in 14th International Symposium on Transport Phenomena and Dynamics of Rotating Machine. 2012 Honolulu.

[7] International Electrotechnical Comission, *IEC 60193 Hydraulic turbines, storage pumps and pump-turbines - Model acceptance tests*, in *Dimensional check of model and prototype*. 1999.

[8] Staubli, T., Senn, F., Sallaberger, M., *Instability of pump-turbines during start -up in the turbine mode*. Hydro 2008, Ljubljana.

[9] Olimstad, G., Børresen, B., Nielsen, T.K., *A Two Dimensional Model for Pump-Turbine Instability Investigation*, in 14th International Symposium on Transport Phenomena and Dynamics of Rotating Machine, 2011, Honolulu.

[10] Yamabe, M., "I*mprovement of Hysteresis Characteristics of Francis Pump-Turbines When operated as Turbine",* Journal of Basic Engineering, 1972. September 1972.

[11] Senoo, Y., Yamaguchi, M., *A Study on Unstable S-Shaped Characteristic Curves of Pump Turbines and No-Flow*, Journal of Turbomachinery, 1987. **109**(77)

[12] Widmer, C., Staubli, T., Ledergerber, N., *Unstable Characteristics and Rotating Stall in Turbine Brake Operation of Pump-Turbines.* J Fluids Eng- Trans ASME, 2011. **133**(April 2011).

[13] Hasmatuchi, V., Farhat, M., Roth, S., Botero, F., Avellan, F., *Experimental Evidence of Rotating Stall in a Pump-Turbine at Off-Design Conditions in Generating Mode.* J Fluids Eng- Trans ASME, 2011. **133**(May 2011).

[14] Apfelbacher, R., Etzold, F., *Energy-Saving, Shock-Free Throttling With the Aid of a Reverse Running Centrifugal Pump,* KSB Technische Berichte, Frankenthal, 1988, 24e, 33-41,68

Paper II

Olimstad, G., Nielsen, T.,K., Børresen, B., 2012, “Stability Limits of Reversible–Pump Turbines in Turbine Mode of Operation and Measurements of Unstable Characteristics”, ASME J. Fluids Eng., Accepted for publishing

Stability Limits of Reversible–Pump Turbines in Turbine Mode of Operation and Measurements of Unstable Characteristics

Grunde Olimstad[1], Torbjørn Nielsen[1] and Bjarne Børresen[2]

[1]Department of Energy and Process Engineering, NTNU University in Trondheim
Alfred Getz vei 4, Trondheim, 7491, Norway, grunde.olimstad@ntnu.no, torbjorn.nielsen@ntnu.no
[2]Energi Norge,
Næringslivets Hus, Middelthunsgate 27, Oslo, Norway, bbo@energinorge.no

Abstract

Measurements have been performed on a reversible-pump turbine model installed in a closed loop conduit system. The characteristics of the unstable pump turbine in turbine mode show a hysteresis pattern. Hence the output of the system is dependent on the previous state of the flow and not only the input variables. The hysteresis pattern is a characteristic of the whole system, but is caused by the unstable pump turbine. The unstable part of the characteristics was measured by three different methods: 1) By transient sampling of data during the transition between operation modes 2) By throttling valves that steepens the friction-loss curve 3) By switching the causality in the system such that the torque becomes an input parameter and the speed of rotation becomes an output parameter.

In the valve throttling measurements a pressure dependency was seen for the characteristics at high non-dimensional speeds. This was further investigated by additional measurements of the characteristics at three different pressure levels.

A rigid-water-column stability analysis has been conducted. The classic H-Q criterion describes static stability for a pump turbine with constant speed of rotation. With the speed of rotation as a variable, there is a new static stability criterion in addition to the dynamic stability criterion.

Keywords: pump turbine, characteristics, instability, measurements, similarity,

1. Introduction

Pumped storage hydropower plants are increasingly important for stabilizing the electricity system. They utilize excess power from wind, solar or thermal energy by storing water with high energy potential. The grid can therewith be stabilized and high frequency peaks prevented. Traditionally most pumped storage plants have been used on a seasonal basis. In today's energy market the time scale of pump and turbine regimes are much lower and a fast and reliable start-up in both modes is then necessary. Many pumped storage hydropower plants have reversible-pump turbines, RPTs, which are cost effective, compared to a system of separate pump and turbine. One drawback with RPTs with high head and low speed number are their tendency to instable behavior during start-up and at low load operation points. Examples of these are the power plants in Bajina Basta, Birna and COO2 in Belgium reported by Pejovic [1], Dörfler [2] and Klemm [3] respectively. The two latter were stabilized by extra mechanical arrangements. A more recent trend is to extend operation area such that the turbine can be used with a wide range of operational head. This broadening of the operation band tends to give even more unstable machines. The reason for the instability is related to complex flow patterns, not yet fully understood. Staubli [4] correlates the unstable characteristics with vortices forming in the runner channel close to the leading edge. An inlet vortex was also visualized by Senoo [5] at zero flow rate for a simplified pump turbine model. Widmer [6] and Hasmatuchi [7] proved the existence of rotating stall and correlated it with the s-shape of the characteristics. This paper investigates instability of pump turbines and their theoretical stability limits. Furthermore a new technique to measure the unstable s-shaped characteristics is investigated and compared to two other methods.

2. On Stability

There are two types of instability that may occur in RPT power plants and they are static and dynamic instability. In a static unstable operation point the system will simply jump to another operation point that is stable. The dynamic instability is associated with hydraulic- and mechanical oscillations with growing amplitudes. Mathematically the two types are described by the eigenvalues of the governing system of linear equations. For dynamic instability there are at least two complex conjugated eigenvalues with positive real part and for static instability the eigenvalues are real positive numbers. The concept of static and dynamic instability is thoroughly described in Greitzer [8].

For a simple system with fixed speed of rotation as depicted in Fig. 1, the static criterion is described by the slope of the head-flow curves alone, see appendix. The system has unstable operation points if the slope of the turbine head-flow curve plus the slope of the head-loss curve is negative. This criteria is derived from Newton's second law applied to the system, eq. (1), and is denoted as in eq. (2). In eq. (1) the left hand side denotes the total mass ($LA\rho$) of the moving water times the time derivative of the mean velocity, Q/A. The right hand side denotes the pressure force that works on the water, where H_r is the reservoir head, H_f is the friction head loss, H_t is the net turbine head and A is the cross-sectional area of the waterway.

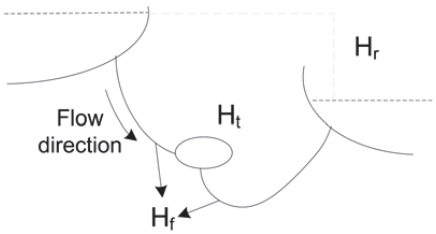

Figure 1 Simple power plant system with indicated upper and lower reservoir, water conduits and turbine

$$LA\rho\frac{dQ/A}{dt} = (H_r - H_f - H_t)\rho gA \quad [N] \tag{1}$$

$$\frac{dH_t}{dQ} > -\frac{dH_f}{dQ} \quad [m^{-2}s] \tag{2}$$

A common way to represent the turbine characteristics is by the dimensionless variable Q_{ed}, N_{ed} and T_{ed} defined in eq (3). It is therefore beneficial to convert the static stability criterion to these variables. By expanding the derivatives of Q_{ed} on N_{ed}, eq. (4), an expression for the gradient of the turbine head-flow curve can be found, eq. (5). This expression is inserted into eq. 2 which then forms the new stability limit. By reordering the terms the final stability limit based on the dimensionless variables becomes as in eq. (6). In the limit of zero head losses this equation describes a vertical line in the Q_{ed}-N_{ed} characteristic diagram. When the head loss grows larger, the slope representing the stability limit is gradually less steep and it is rotated in clockwise direction around the applicable operation point, Fig. 2. The turbine head is the constant reservoir head minus the friction loss in the waterways such that with zero friction loss the turbine head is equal the reservoir head. Under this constant turbine head the limiting slope is infinite steep and an s-shaped characteristic can therefore not be stable. With a constant head the non dimensional flow rate and speed of rotation convert to real flow rate and speed of rotation. The vertical line is therefore the stability limit for the flow-speed characteristics, eq. (7).

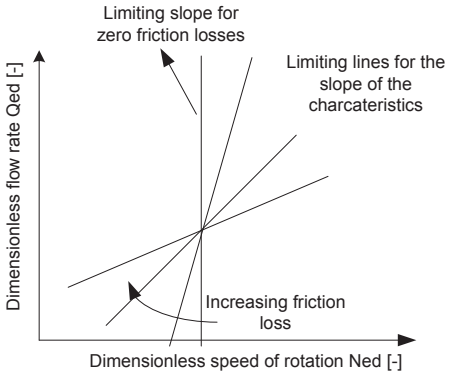

Figure 2 Limiting lines for the slope of the characteristics in turbine mode

$$Q_{ed} = \frac{Q}{D^2\sqrt{gH_t}}, \quad N_{ed} = \frac{nD}{\sqrt{gH_t}}, \quad T_{ed} = \frac{T}{D^3 g\rho H_t}, \quad [-] \tag{3}$$

$$\frac{dQ_{ed}}{dN_{ed}} \equiv \frac{d(\frac{Q}{D^2\sqrt{gH_t}})}{d(\frac{nD}{\sqrt{gH_t}})} = \frac{(\frac{1}{D^2\sqrt{gH_t}})dQ + (\frac{Q}{D^2\sqrt{g}})d(\frac{1}{\sqrt{H_t}})}{\frac{nD}{\sqrt{g}}d(\frac{1}{\sqrt{H_t}})} \tag{4}$$

$$\frac{dH_t}{dQ} = (\frac{Q}{2H_t} - \frac{D^3 n}{2H_t}\frac{dQ_{ed}}{dN_{ed}})^{-1} \quad [m^2 s] \tag{5}$$

$$\frac{dQ_{ed}}{dN_{ed}} = \frac{Q_{ed}}{N_{ed}}(1 + \frac{H_t}{H_f}) \quad [-] \tag{6}$$

$$\frac{dQ}{dn} = \infty \text{ , constant head} \quad [m^3 s^{-2}] \tag{7}$$

When the rotational speed is variable, the system becomes slightly more complex and dynamic oscillations may occur. The system is now described by two equations, one for the speed of rotation, eq. (8), and one for hydraulic flow, eq. (1). In eq. (8) the left hand side denotes the polar moment of inertia of the rotating parts, J, multiplied with the rate of change in speed of rotation. The right hand side denotes the unbalanced torque which is the hydraulic torque, T_h, minus the generator torque, T_g. Martin [9] derived a dynamic stability criterion for such a system, where he neglected friction losses. This criterion relates stability limit to the slope of the T_{ed}-N_{ed} characteristic. When the slope has a too low positive value, any system oscillation will grow in amplitude and be unstable. From Martin's analysis, it is also possible to extract a static stability limit. That comes forth when the system equations have two real eigenvalues and their values are identical equal to zero. To express this stability limit the characteristic of the machine is expressed by two new variables. Those are torque divided through the speed of rotation to the power of two, T/n^2, and flow rate divided through the speed of rotation, Q/n. The stability is correlated by the magnitude of the slope of the torque-flow characteristics. A negative value corresponds to a static unstable operation point. By employing the definition of Q_{ed}, N_{ed} and T_{ed} a transformation of the stability limit can be made, eq. (9). It should be noticed that the static stability no longer relates only to the slope of Q_{ed}-N_{ed} characteristic, but is now dependent on the slopes of both Q_{ed}-N_{ed} and T_{ed}-N_{ed} characteristics.

$$J2\pi\frac{dn}{dt} = T_h - T_g, \quad \text{[Nm]} \tag{8}$$

$$\frac{dT/n^2}{dQ/n} = \rho D^2 \frac{\frac{dT_{ed}}{dN_{ed}} - 2\frac{T_{ed}}{N_{ed}}}{N_{ed}\frac{dQ_{ed}}{dN_{ed}} - Q_{ed}} = 0 \quad [kg/m] \tag{9}$$

The consequence of the stability criteria is applied and discussed in section 4, “Measured characteristics”.

3. The pump turbine and the laboratory

The test-rig, Fig. 3, is a closed loop system were one or two pumps deliver the hydraulic energy. A generator which can also work as a motor is mounted on the turbine shaft. This generator floats freely and is held back from rotating by a level arm connected to a force-cell which measures the force. The torque is obtained by multiplying this force with the length of the level arm. There is a perforated disk mounted on the shaft that is used by an optical device to measure the speed. Three meters up-front of the turbine inlet there is an electro-magnetic flowmeter, ALTO SC 100 AS, from Krohne. The pressure difference over the turbine is measured by the pressure transducer, Fuji Electronics FHCW 36 Ackay.

Normally the rig is used for testing turbines with head in the range of 20 to 40 meter. The normal nominal flow rate is 0.2 to 0.3 m^3s^{-1} and the maximum flow rate is 1.0 m^3s^{-1}. The laboratory has calibrating equipment for all measuring devices and operates with uncertainty associated with systematic errors in according to the IEC standard [10]. Calculation of the random uncertainties was performed based on eleven measurements with a sampling period of thirty seconds and sampling rate of 1.4 hertz. The standard deviations of the results were, in percent of BEP-values, 0.16 for efficiency, 0.07 for N_{ed}, 0.27 for Q_{ed} and 0.28 for T_{ed}.

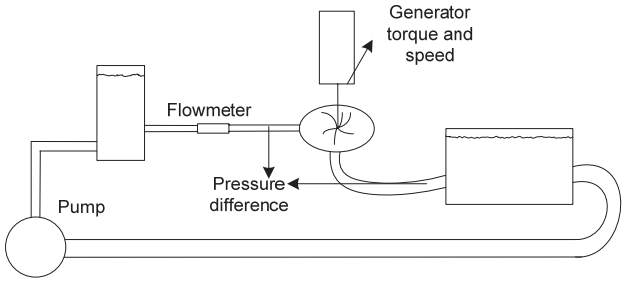

Figure 3 The test rig

The pump turbine runner used in the measurements was designed to fit into an already existing Francis turbine. It has a distributor and draft tube originally designed for a high head and low specific speed Francis turbine. This has twenty eight guide vanes and fourteen stay vanes. Different data for the pump turbine used in this paper are tabulated in Table 1. A geometry description is given through the radial view, Fig. 4 and the axial view, Fig. 5, of the runner. The performance diagram is showed in, Fig. 6. It depicts the efficiency in turbine mode of operation as a function of dimensionless flow rate, Q_{ed} and speed of rotation, N_{ed}. The top efficiency is slightly above 90.5 percent.

Table 1

Parameter	Value	Parameter	Value	Parameter	Value	Parameter	Value
D_1	0.631 [m]	n^*	10.8 [1/s]	Q_{ed}^*	0.133 [-]	β_1	12.0 [degree]
D_2	0.349 [m]	Q^*	0.275 [m^3/s]	N_{ed}^*	0.223 [-]	β_2	12.8 [degree]
B_1	0.059 [m]	H^*	29.3 [m]	n_q	27.1 [rpm $m^{3/4}s^{-1/2}$]	α_1^*	10.0 [degree]

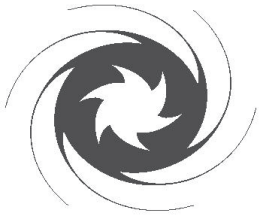

Figure 4 Radial view of the runner blade surface

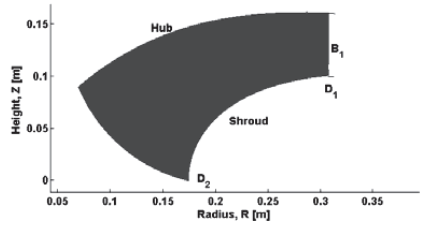

Figure 5 Meridional view of the runner blade surface

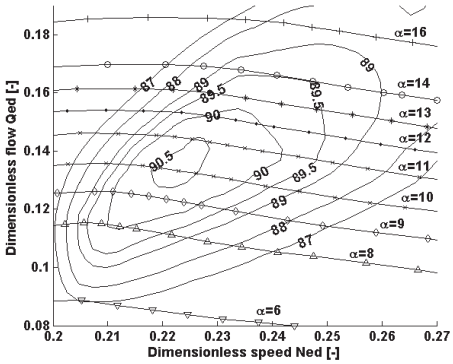

Figure 6 Performance diagram with labeled efficiency contours

4. Measured characteristics

The characteristics of the pump turbine are measured with about twenty meter head and with a speed of rotation in the range between 60 and 1000 rpm. The pump speed of rotation which regulates the total Head in the system is kept constant for all operation points at the characteristics. This restricts the flow rate to vary only due to pump- and turbine characteristics, and pipe head losses. The starting point was at about seventy rpm and the speed was stepwise increased with steps in the range of two to sixty revolutions per minute (rpm). Figure 8 shows how the flow rate varies with the speed of rotation in turbine mode of operation. The flow rate varies only slightly with the speed of rotation for speed of rotations up to nominal speed of rotation at 530 rpm. At higher than nominal speed of rotation the flow rates sink gradually until a certain speed of rotation where the turbine jumps from turbine mode of operation to reverse pump mode with only a step of two rpm. The operation points were measured a second time, this time by starting at a high speed of rotation and stepping the speed of rotation towards lower values. At a certain speed of rotation the operation mode shifts from reverse pump mode to turbine mode within a step of two rpm. This shift in operation mode occurs at a lower speed of rotation than the shift from turbine to reverse pump mode and the two curves together form a hysteresis shape. Figure 9 shows the Q_{ed}-N_{ed} characteristics were the slopes in the hysteresis zone is slightly positive. The slope difference between Fig. 8 and Fig. 9 is explained by the fact that the net turbine head vary slightly with the flow rate due to friction head losses.

By creating a control volume around the whole system in Fig. 3 the input and output variables can be structured as in Fig. 7. The inputs are the pump and turbine speeds of rotation, and the guide vane opening while the outputs are the flow rate, and the turbine head and torque. The hysteresis curves show that for a given set of input variables there are two sets of output variables. Which set of output variables that occurs, depends on the previous operation point, when the pump turbine is operated in the hysteresis area.

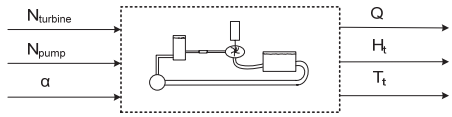

Figure 7 Inputs to- and outputs from the system

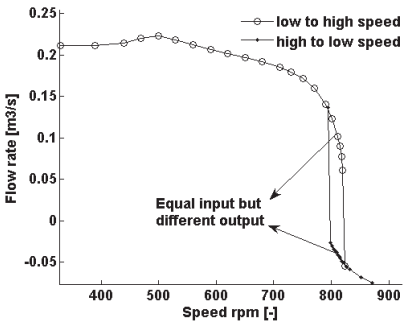

Figure 8 Hysteresis flow-speed curves with 10 degree guide vane opening

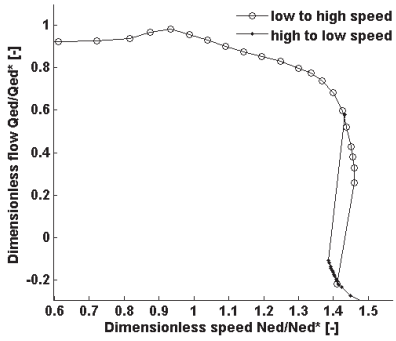

Figure 9 Hysteresis Q_{ed}-N_{ed} characteristics with 10 degree guide vane opening

Operation points within the hysteresis area exist, but are not statically stable according to the limit in eq. (6) and could therefore not be measured. Three different ways of measuring the unstable zone are presented in the next paragraphs.

4.1 Transient measurement

The flow was measured during transition from turbine mode to reverse pump mode. The sequence was started in turbine mode and initiated by a step in turbine speed of rotation of five rpm. Each transient point in the characteristics showed in Fig. 10 is averaged over 0.7 seconds and the duration of each of the transition sequences is 40 to 50 seconds. The resulting characteristics have realistic shapes but do not exactly match the stable operation points in reverse pump mode. This can be caused by dynamic effects in the laboratory where the water within the turbine has a significant mass compared to the water masses in the pipe system.

Pros: The common way to measure in the industry and in accordance with the IEC standards requirement for constant head
Cons: Depends on dynamic behavior of the system

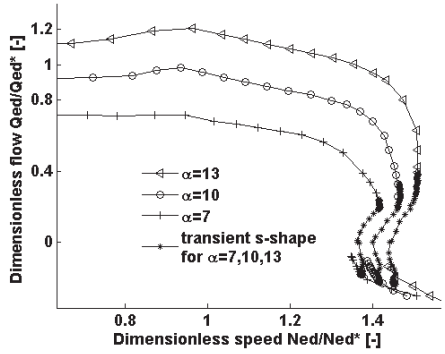

Figure 10Transient measured characteristics for three different guide vane openings (α)

4.2 Throttling valves

The static instability was resolved through throttling of the pipe flow, a method first introduced by Dörfler [2]. The resulting characteristic can be seen in Fig. 11. The throttled characteristic fits well to the characteristic without throttling in the unstable zone. In the area were the curves overlap there is a variation which is due to very low pressure at these operation points. The characteristic in general has a pressure level of approximately 20 m but for these operation points the pressure is as low as 4-10 meter.

Pros: Resolve the hydraulic instability
Cons: Pressure is very low when the flow rate is non-zero

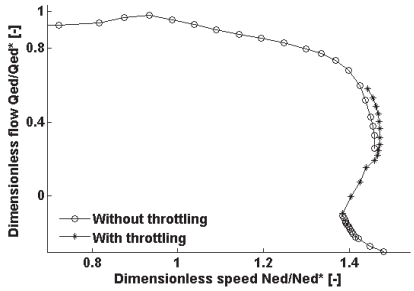

Figure 11 Stabilizing through valve throttling

4.3 Torque as input

To measure the unstable zone, torque was used as input. The causality of the system is then reversed such that the speed of rotation becomes an output variable from the system. Figure 12 shows the characteristic measured with torque as input for operation points in the unstable zone. There were some oscillations in speed during these measurements. The standard deviation of N_{ed} and Q_{ed} were therefore calculated to quantify the unsteadiness in the flow. These standard deviations were compared with the standard deviations from the valve-throttling-measurements. For each operation point, 43 readings were taken over a time period of 30 seconds. Figure 13 shows the standard deviations, eq. (10), and it can be seen that the torque-input method has two operation points with high standard deviations for N_{ed}. This is caused by significant oscillations in speed of rotation. The valve throttling measurements also has two operation points with high standard deviations, but the unsteadiness now comes from variation in the flow rate. The results from the measurements of the s-shape with torque as input show that the method solved the static instability, now described by the limit in eq. (9). However two of the measured operation points violated the dynamic stability criterion, and were not stabilized. With the torque as input method the head is constant along the whole characteristic, which the IEC standard recommends.

Pros: Resolves the static instability and is in accordance with the IEC standard standards requirement for constant head
Cons: Two dynamically unstable points with large oscillations in speed of rotation

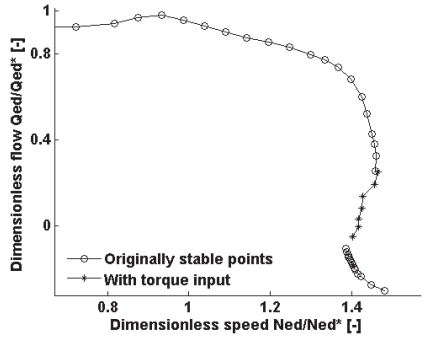

Figure 12 Characteristic with torque as input

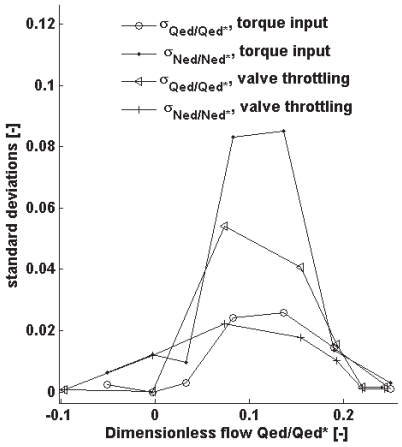

$$\sigma_{N_{ed}} = \sqrt{\frac{\sum (N_{ed,i} - \overline{N_{ed}})^2}{n}}, \quad [-] \tag{10}$$

Figure 13 Standard deviations in the unstable zone

4.4 Final characteristics

A comparison of the results from the three measurement techniques is shown in Fig 14.To create the final characteristics of the pump turbine the two stable characteristic fractions in turbine mode and reverse pump mode were used. To connect the two parts, either of the two measurement technique, valve throttling of torque input, can be used with no significant deviation. The torque input method has high standard deviations of N_{ed}. By using the valve throttling technique one should carefully use only those points with head in the otherwise used level, which here was H=20m. Operation points around zero flow rates have little head losses and therefore have the wanted pressure level. The final characteristics were created by the valve-throttling technique and plots of Q_{ed} versus N_{ed} and T_{ed} versus N_{ed} are shown in the figures 15 and 16. The curves are s-shaped which means that for certain speeds of rotation there are three possible outputs of the same system input.

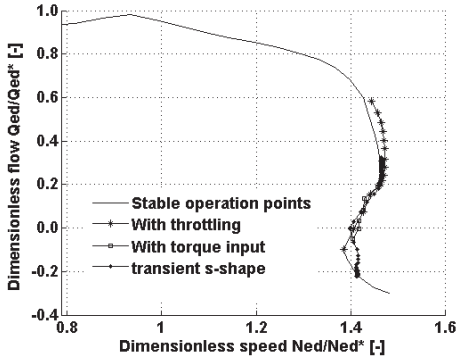

Figure 14 Comparison of the three measurement techniques

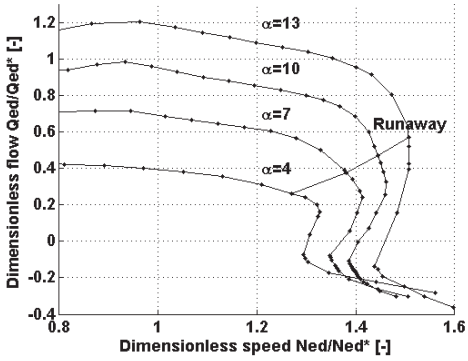

Figure 15 Final Q_{ed}-N_{ed} characteristics

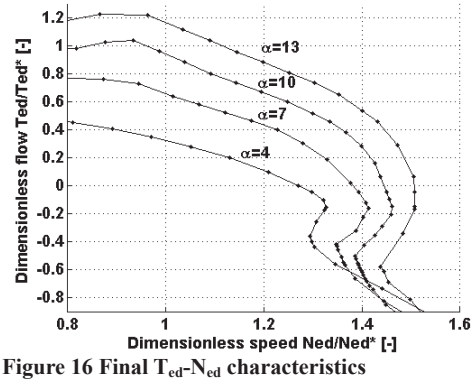

Figure 16 Final T_{ed}-N_{ed} characteristics

5. Pressure dependency

In the valve throttling measurements a certain pressure dependency was observed. To verify this, three additional characteristics were measured with different pressure level. The pump speed of rotation was now set to 400, 600 and 800 rpm which gave net heads for the turbine of approximately 9, 20 and 36 meter respectively. The Reynolds numbers based on the outlet peripheral speed and the outlet diameter vary and are for these cases Re=2.2E6, Re=3.35E6 and Re=4.4E6. In the unstable zone the valve throttling technique was used. The resulting characteristics are equal around BEP but different at N_{ed} values of 1.35 and higher, Fig. 17. At these N_{ed} values the Q_{ed} value is highest for the 9m head and smallest for 36m head. Hence the high head characteristic seem to be subjected to relatively higher flow resistance than the low head characteristic. In Fig. 18 the markers are rectangles with sides corresponding to plus/minus three standard deviations of the measured mean values. This shows that the curves are significantly different.

The use of the non-dimensional numbers, Q_{ed} and N_{ed}, are based on similarity analysis. The similarity of flows is achieved if geometric, kinematic and dynamic similarities are preserved and the characteristics in terms of Q_{ed} versus N_{ed} are then unique. In fact the Q_{ed} and N_{ed} variables represent the non-dimensional meridional and circumferential speeds at the runner outlet and, by definition, describe kinematic similarity. The dynamic similarity requires equality of ratios of forces as described by the non-dimensional Navier-Stokes equation, eq. (11). Strouhal-, Euler- and Reynolds number shall formally be the same in model and prototype. In fact this only applies for the Euler and Strouhal numbers.

$$\text{Strouhal}\frac{Dv}{Dt} = \text{Euler}\nabla p + \frac{1}{\text{Reynolds}}\nabla^2 v \quad [-]$$

$$\text{or equivalent} \qquad (11)$$

$$N_{ed}\frac{Dv}{Dt} = \frac{1}{Q_{ed}^2}\nabla p + \frac{1}{\text{Reynolds}}\nabla^2 v \quad [-]$$

Previous studies of pump characteristics have shown that the part load behavior is neither sensitive to rotational speed (Strouhal number) nor to Reynolds number, Gülich [11]. A conclusion from Gülich is that "the *partload behavior is not sensitive to the Reynolds number or to boundary layer effects*". The measurements here however, show that the effect of these similitude numbers is not negligible for pump turbine characteristics at high N_{ed} values.

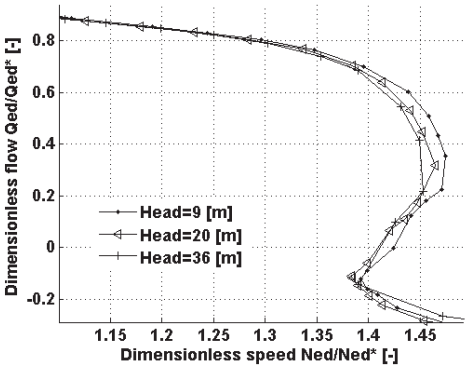

Figure 17 Pressure dependant characteristics

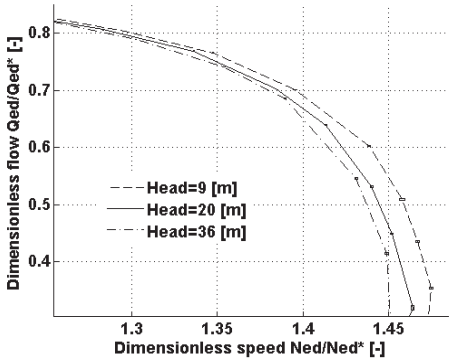

Figure 18 Marker sizes correspond to plus/minus three standard deviations

6. Conclusion

The expressions for the Q_{ed} versus N_{ed} is mathematically expanded and substituted into the normal static stability criterion. This forms a new criterion in terms of Q_{ed} and N_{ed} in which also the system friction loss is included. In case of zero friction losses the limiting line is vertical in the Q_{ed}-N_{ed} diagram and it rotates clockwise as more friction loss is introduced.

The measured characteristics of the unstable pump turbine show a hysteresis pattern. Hence the output of the system is dependent on the previous state of the flow and not only the input variables. In the measurements, the pump turbine speed of rotation is moved stepwise to create the characteristics. At a certain point, a very small step in the rotational speed cause the pump turbine to jump from turbine- to reverse-pump mode of operation. The pump turbine then traverses through its unstable area and finds a stable operation point in reverse pump mode. The hysteresis curve is an interpretation of the s-shaped characteristics for an unstable system.

The whole continuous characteristics curve of the pump turbine was measured by three different methods. One method is transient sampling of data during a transition between operation modes. This only gives an idea of how the characteristics look like since the results depend on the importance of dynamic effects. The two other methods resolve the static instability such that the results could be averaged over time. The first method is the previously established method of throttling valves while the second method switches the causality in the system such that the torque becomes an input parameter and the speed of rotation becomes an output. Both methods enabled measurements of the full characteristics and the resulting s-shaped characteristics are

similar. However the method of torque as input gave large standard deviation of the non-dimensional speed at two operation points. These were dynamically unstable. The throttling valve method should be used only for low flow rates since the head otherwise is drastically lowered.

That the pressure level influences the characteristics is shown by measurement of the characteristics for three different pressure levels. These measurements show that the characteristics are pressure dependent for high non-dimensional speeds.

Acknowledgments

This work is financed by Norwegian power companies, consultants and equipment suppliers through Energy Norway.

Nomenclature

Q_{ed}	Non-dimensional flow rate [-]	β	Blade angle [Degree]
N_{ed}	Non-dimensional speed of rotation [-]	σ	Standard deviation
T_{ed}	Non-dimensional torque [-]	n	Number of points
Re	Reynolds number [-]	ρ	Density [kg/m^3]
H	Head [m]	t	Time [s]
n	Speed of rotation [1/s]	J	Rotating inertia [m^{2}kg]
D	Diameter [m]	α	Guide vane angle [Degree]
g	Gravitational acceleration [m^2/s]	BEP	Best operation point
T	Torque [Nm]	B	Runner inlet height [m]
Q	Flow rate [m^3/s]	L	Length [m]
n_q	Speed number [rpm m$^{3/4}$s$^{-1/2}$]	A	Area [m^2]
v	Fluid velocity [m/s]		

Sub- and superscript

1	Inlet of runner	*r*	Reservoir
2	Outlet of runner	*f*	Friction
*	Best operation point	*t*	Turbine
-	Averaged value	*h*	Hydraulic
		g	Generator

References

[1] Pejovic, S., Krsmanovic, L., Jemcov, R., Crnkovic P., "Unstable Operation of High-Head Reversible Pump-Turbines", in 8th IAHR Symposium, 1976, Leningrad.

[2] Dörfler, P.K., Engineer, A.J., Pendse, R.N., Huvet, P., Brahme, M.V.. "Stable operation acvhieved on a single -stage reversible pump-turbine showing instability at no-load". Proceeding of the 19th Symposium on Hydraulic Machinery and Systems. 1998. Singapore.

[3] Klemm, D., "Stabilisierung der Kennlinien einer Pumpenturbine im Bereich zwischen Turbinen-Teillast und Rückwärtspumpenbetrieb". Voith Forschung und Konstruktion, 1982. Heft 28, Aufsatz 2.

[4] Staubli, T., Senn, F. and Sallaberger, M., "Instability of Pump-Turbines During Start-up in the Turbine Mode" in Hydro 2008, Ljubljana, Slovenia, October 6-8, 2008, Paper No. 9.6.

[5] Senoo, Y., Yamaguchi, M. "A Study on Unstable S-Shape Characteristic Curves of Pump-Turbines at No-Flow", Journal of Turbomachinery, January 1987, **109**(77)

[6] Widmer, C., Staubli,T., Ledergerber, N. "Unstable Characteristics and Rotating Stall in Turbine Brake Operation of Pump-Turbines", Journal of Fluids Engineering, **133**(April 2011)

[7] Hasmatuchi, V., Farhat, M., Roth, S., Botero, F., Avellan, F., "Experimental Evidence of Rotating Stall in a Pump-Turbine at Off-Design Conditions in Generating Mode", J Fluids Eng- Trans ASME, **133**(May 2011)

[8] Greitzer, E. M., The Stability of Pumping Systems –The 1980 Freeman Scholar Lecture, J Fluids Eng- Trans ASME, 1981, **103**(June 1981)

[9] Martin, C.S. "Stability of pump-turbines during transient operations". 5th International conference on pressure surges, 1986, Hannover, Germany.

[10] International Electrotechnical Comission, *IEC 60193 Hydraulic turbines, storage pumps and pump-turbines - Model acceptance tests*, in *Dimensional check of model and prototype*. 1999.

[11] Gülich, J. F., Centrifugal Pumps, Springer-Verlag, 2010, Berlin, pp 192

Appendix
Derivation of H-Q Stability

The system is described by eq. (12) or eq. (1) described in the paper and the friction losses are modelled by Moody's friction factor, denoted f.

$$LA\rho\frac{dQ/A}{dt} = (H_r - H_f - H_t)\rho gA \quad [N], \text{ where } H_f = \frac{fL}{D}\frac{(Q/A)^2}{2g} \quad (12)$$

The turbine head is replaced by the linear expression in eq. (13). Furthermore is the flow rate, Q, divided into a mean flow, Q^0, and a disturbance, q. The result of these two operations yields eq. (14).

$$H_t = H_t^0 + a(Q - Q^0) \quad [m] \, (13)$$

$$\frac{L}{Ag}\frac{d(Q^0+q)}{dt} - H_r + \frac{fL((Q^0)^2 + 2Q^0q + q^2)}{DA^2 2g} + H_t^0 + a(Q^0 + q - Q^0) = 0 \quad [m] \, (14)$$

By subtracting from eq. (14) the corresponding mean flow equation, it becomes:

$$\frac{L}{Ag}\frac{d(q)}{dt} + \frac{fL(2Q^0q + q^2)}{DA^2 2g} + a(q) = 0 \quad [m] \, (15)$$

The flow disturbance is considered much smaller than the mean flow, such that the term q^2 can be neglected. Reordering the terms yields the following equation:

$$\frac{dq}{dt} + \frac{fQ^0}{DA}q + \frac{aAg}{L}q = 0 \quad [m^3 s^{-2}] \, (16)$$

The variable q is separated, eq. (17), to obtain the analytical result eq. (18).

$$\frac{dq}{q} = -(\frac{fQ^0}{DA} + \frac{aAg}{L})dt \quad [-] \, (17)$$

$$q = Ce^{\lambda t} \quad [m^3 s^{-1}], \quad \lambda = -(\frac{fQ^0}{DA} + \frac{aAg}{L}) \, (18)$$

The constant C represents the initial flow disturbance at t=0. The flow rate is stable if the eigenvalue, λ, is negative and unstable if λ is positive. With negative λ, the flow perturbation will be zero after long time.

$$\text{Stabil if:} \quad \lim(q)_{t\to\infty} = 0 \, (19)$$

The two terms encapsulated in λ represent the slopes of the turbine head and friction losses. For λ to be negative the following relation must hold true:

$$a > -\frac{fQ^0}{DA}\frac{L}{Ag} \quad [m^{-2}s] \quad (20)$$

Which also can be written as in eq. (2).

Paper III

Olimstad, G., Nielsen, T., K., Børresen, B., 2011, “Design of a Reversible Pump-Turbine - with Purpose to Investigate Stability”, 4th International Meeting on Cavitation and Dynamic Problems in Hydraulic Machinery and Systems, October, 26-28, Belgrade, Serbia

4-th International Meeting on
Cavitation and Dynamic Problems in Hydraulic Machinery and Systems,
October, 26-28, 2011, Belgrade, Serbia

Design of a Reversible Pump-Turbine -with Purpose to Investigate Stability

Grunde Olimstad[1], Bjarne Børresen[2] and Torbjørn Nielsen[1]

[1]Department of Energy and Process Engineering, Norwegian University of Science and Technology
Alfred Getz Vei 4, 7491, Trondheim, grunde.olimstad@ntnu.no, torbjorn.nielsen@ntnu.no
[2]Energi Norge
Næringslivets Hus, Middelthunsgate 27, Oslo, bbo@energinorge.no

Abstract

This paper describes both the design and simulated characteristics of a reversible pump-turbine (RPT) that is made for research purposes at the Waterpower Laboratory in Trondheim. The main subject for this research is stability of RPTs. Many RPTs show unstable behavior during start up in turbine mode or during operation at low load. What happens to the water flow through the RPT in these situations needs further investigation. A runner has been designed to fit in an existing distributor and draft tube. The inlet and outlet diameters in addition to the inlet height were therefore given in advance. The speed number was decided to be 0.36 and the inlet to outlet diameter ratio is two. The design process consists of two main parts. The first part is an analytical design procedure which ends up in an initial geometry of the RPT runner. All blade angles were calculated from an uc_u distribution, which were drawn from the philosophy that the loading should be small at both inlet and outlet of the blade. The second part of the design process is an optimization procedure involving iteration between geometry design and CFD analysis. The blades were adjusted as to get streamlines following the blade curvature and to get an evenly distributed flow, c_m versus radius, in the draft tube entry. The performance of the RPT is simulated and will later be measured in the laboratory. The performance is presented as first quadrant characteristics and Hill-diagram. The characteristics of the turbine are deliberately made very steep and some of the constant wicket gate characteristics even have positive slope at speed no load.

Keywords: pump-turbine, stability, characteristics, design, geometry

1. Introduction

Pumped storage power plants play an important role in modern energy systems. The increased electricity production from renewable energy sources produces large amounts of unregulated power. Pumped storage is probably the best way to compensate for the gap between produced and consumed power. In a liberalized power market the prizes follow the fluctuation in production and consumption. This represents a trading opportunity for market participants and makes pumped storage profitable for power producers. Most often a reversible pump-turbine (RPT) is preferred in the pumped storage power plant instead of separate pump and turbine units. This preference is mainly a result of cost considerations. Many low specific speed and high head RPTs shows instable behavior at part and no load. The instability is connected to the characteristics which relate dimensionless flow (Qed) and torque (Ted) to dimensionless speed (Ned). With very steep or even s-shaped characteristics an RPT becomes instable. Martin [1] deduced a absolute stability criteria based on equations for invicid flow. The criterion states that the stability limit is where the curve of the Ted versus Ned is vertical. Whereas the pump-turbine will be unstable if the slope is positive. The stability is also dependent on boundary conditions that are different between model and prototype. These can be rotating or hydraulic inertia time constants or hydraulic losses in the water system. Klemm [2] concludes for a pump-turbine in a Belgian power station that "In a model test, any desired operating point can be run with complete stability and an so called S-shaped curve cannot be considered from the beginning as being unstable".

Some examples of unstable pump-turbines are reported from Bhira by Dörfler [3] and Belgium COO II by Klemm [2]. At these pumped storage power plants the flow rate, speed and head oscillated with large amplitudes at part and no load. Such a situation leads to intolerable vibrations in operation and difficulties with synchronization at start up in turbine mode. In the two cases reported by Dörfler and Klemm the instability at start up had to be fixed by additional mechanical arrangement. At Bhira the system characteristic, relation of head versus flow, was lifted to a positive slope by partly closing the inlet valve. A positive slope of the head versus flow curve is another minimum criterion for stability. In Belgium the state of the flow in start-up was altered by preopening two guide vanes to a high opening degree. Both methods worked to fix their stability problems, but made

the turbines more complex, more expensive and more vulnerable to damaged. Pejovic [4] reported from Bajina Basta about an unstable pump-turbine. This RPT have s-shaped unstable characteristics and Pejovic simulated transient operations which showed oscillating and unstable behavior. These cases are only three examples out of many pump-turbines with stability problems.

Fast start-up or change of operation mode from pump to turbine is a necessity in today's power market. It requires that nominal speed is achieved fast and without oscillations. The RPT's where stability is the most problematic are the high head and low specific speed pump-turbines. From Nielsen [5] the relation between inlet and outlet diameter is showed to be one parameter making the characteristics steep and therewith the pump-turbine unstable. This diameter relation is high for typical high head pump-turbines.

This paper describes the design of an RPT which is manufactured and installed in the Waterpower Laboratory in Trondheim. The aim of this model turbine is to create a model suitable for stability investigations. Two important questions for these investigations are which runner geometry leads to steep characteristics and instability and which flow features are associated with the unstable flow. In this context the efficiency is a less important parameter. Nevertheless efficiency became a part target of the design because good efficiency secures reasonable good and realistic flow conditions at best operation point. Since the pump-turbine is subjected to stability studies and never will be commissioned, some instability at part/no load are actually favorable.

2. Main Dimensions

An important restriction for the design is connected to the laboratory test rig's limitations. In addition, the runner shall fit in an existing a distributor and draft tube originally designed for a high head and low specific speed Francis turbine. This restricts the inlet and outlet diameters and the height at the inlet of the runner to be the same as for the Francis turbine. The measurements apparatus also restricts other quantities such as maximum torque, flow, head and speed, connected to measurement ranges and torque tolerability. The restrictions are tabulated below.

Tab. 1 Restrictions

Max. Flow	1.0 [m^3/s]	Max. Head	50 [m]	D_{11}	0.6305	B_1	0.0587[m]
Max. Speed	1000 [rpm]	Max. Torque	2300 [Nm]	D_{21}	0.349		

The main dimensions of the runner consist of six variables. With D_{11}, D_{21} and B_1 given, there are three free parameters left to be decided for the main design, namely α_1, β_1, β_2.These parameters have to be chosen consistently with the Euler turbine equation. The Euler peak efficiency is chosen to be 0.965. Further choices are done for the flow rate (Q), net Head (H) and peripheral velocity at the inlet (u1). The laboratory restricts the magnitude of flow, head, power and generator torque. Therefore H is chosen to be 30 [m] and the design flow rate Q = 0.3 [m^3/s]. These choices results in an acceptable value for the hydraulic power.

For the stability of the pump-turbine in pump mode the steepness of the H-Q characteristics is very important. Steep H-Q characteristics also lead to a broad possible variation in pump hydraulic head. The latter is important when using the RPT for power regulation. The relation between H and Q, eq. (1), can be deduced from the Euler equation in best operation point, eq. (2).

$$gH = \omega R_1(\omega R_1 - \frac{Q}{A_1 \tan(\beta_1)}) \quad [m^2/s^2] \tag{1}$$

$$\eta = \frac{1}{gH}(u_1 c_{u1} - u_2 c_{u2}(=0)) \quad [-] \tag{2}$$

The smaller β at the inlet is the steeper characteristics. With β larger than 90 degrees the slope will be positive. When the value of u_1 is increased the inlet angle β_1 gets smaller which is preferable considering pump characteristics. Acceleration through the runner is undesired since it turns into deceleration when shifting operation mode. A decelerated flow is more vulnerable to secondary flow effects and separation. The aim was then to get a small difference between the magnitudes of relative velocity at the inlet and the outlet. When increasing u_1 and keeping all other free parameters constant, the relative speed at the inlet increases. The relative speed at the inlet was initially lower than at the outlet so a higher value was a favorable change. Data for seven different RPTs are collected by Henry [6] and u_1 can be calculated from the data given there. Plotting the reduced value of u_1 against speed number shows that all RPTs in the statistics have u_1 reduced in the area around $\underline{u}_1=1$.

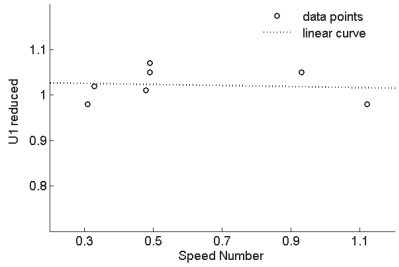

Fig. 1 U_1 versus speed number

Brekke [7] states that u_{1red} should be set higher than 0.95 which is in consistence with the data given by Henry. $\underline{U}_1$ was set to 1.0. This value gives steep pump characteristics and just a small increase of w_1 through the runner channel. The resulting set of main parameters is shown in Table 2 – 4 and the velocity diagrams are shown in Figure 3. The expressions for the different parameters are attached in the right column. The maximum torque does not exceed the limit of the test-rig.

Table 1 Inlet parameters

Parameter	Value	Right Hand Side of Equations
c_{m1} [m/s]	2.68	Q/A_1
$\underline{c}_{u1}$ [-]	0.48	eta/(2*$\underline{u}_1$)
ω [-]	79.32	u_1*2/D_1
α_1 [-]	12.87	atan(c_{m1}/c_{u1})
β_1 [-]	12.02	atan($c_{m1}/(u_1-c_{u1})$)
w_1 [m/s]	12.99	$c_{m1}/\sin(\beta_1)$

Table 2 Outlet parameters

Parameter	Value	Right Hand Side of Equations
c_{m2} [m/s]	3.3	Q/A_2, A_2 is corrected for blade thickness
u_2 [m/s]	13.84	omega*D_2/2
β_2 [-]	13.45	atan(c_{m2}/u_2)
w_2 [m/s]	14.19	$c_{m2}/\sin(\beta_2)$

Table 3 Turbine data

Parameter	Value	Right Hand Side of Equations
Power [W]	8.5E4	Q*H*ρ*g*η
Speed Number [-]	0.36	$\underline{\omega}*(\underline{Q})^{0.5}$
Torque [Nm]	1.07E3	P/ω
Reaction Ratio [-]	0.73	$\eta_h-\underline{c}_{u1}^2$
Efficiency [-]	0.965	$2\underline{c}_{u1}\underline{u}_1$

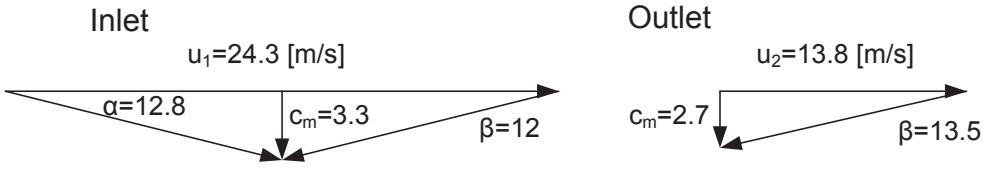

Fig. 2 Velocity diagrams for inlet and outlet

3. Axial View, R, Z Coordinates

After the main dimensions were decided, the geometry in the radial view was designed. Three points where bounded to the distributor and draft tube, namely D_{11}, D_{12}, and D_{21}. The first curve of this view was drawn from D_{11} to D_{21} by means of a fourth order Bezier curve. Calculation of the rest of the radial plane was done numerically by dividing it by twelve streamlines with twenty points on each. Between all streamlines there is an equal flow rate and the meridional velocity, c_m, was set to increase linearly from inlet and outlet. Coordinates for the points on the neighboring streamline were calculated based on equations (3) and(4). These equations origin from the continuity equation and are written to be solved for R and Z.

$$R_2: \quad \frac{Q}{c_m} = 2\pi\left(\frac{R_1 - R_2}{2}\right)\left(\frac{R_1 - R_2}{\sin(\alpha)}\right) \quad \textbf{[m]} \tag{3}$$

$$Z_2: \quad \tan(\alpha) = \frac{R_2 - R_1}{Z_2 - Z_1} \quad \textbf{[m]} \tag{4}$$

4. 3D Coordinates Calculated from Ucu Distribution

The blade surface is defined by the three cylinder coordinates R, θ, Z. R and Z comes from the axial view and the calculation of the θ coordinate is made on the basis of a chosen blade loading on each streamlines. The philosophy is to minimize losses coming from the slip at the blade exit both in turbine and pump mode. The slip-angle can be minimized by reducing the loading of the blade at both ends. The blade loading is through the Euler-equation directly linked to the distribution of uc_u which is shown in Fig. **3.**

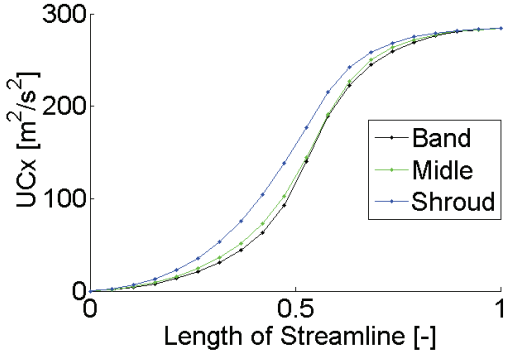

Fig. 3 UCu distribution

From the uc_u distribution the blade angles, β, and peripheral displacement theta can be calculated with the equations (5) and(6).

$$\beta: \quad uc_x = \omega R\left(\omega R - \frac{c_m}{\tan(\beta)}\right) \quad [m^2/s^2] \tag{5}$$

$$\theta: \quad \tan(\beta) = \frac{\sqrt{\delta R^2 + \delta Z^2}}{R\delta\theta} \quad [-] \tag{6}$$

With the choice for the uc_u distribution above, the theta distribution spans over approximately 180 degree. The blade angle distribution and the blade surface are shown in Fig. 44 and Fig. 5.

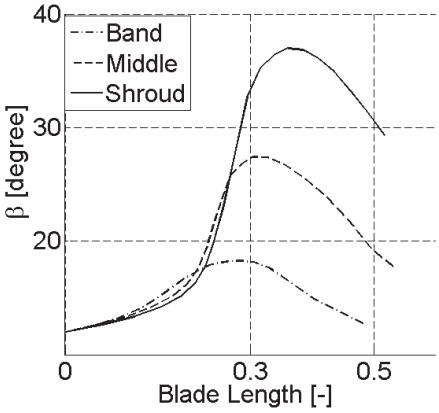

Fig. 4 Blade angles as in final design

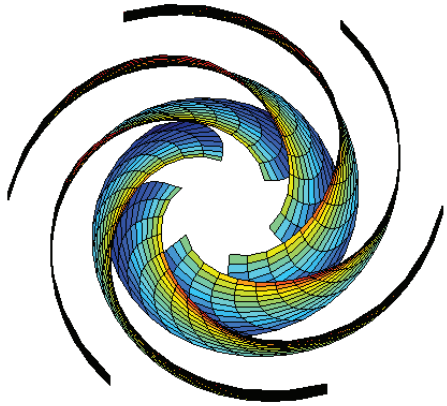

Fig. 5 3D surface of blades as in final design

4.1 Blade Thickness

At the inlet pressure side the profile of the blade is a circular arc with radius, R=3 mm. At the suction side the profile is one fourth of an ellipse with major and minor radius of 8 and 5 mm respectively. At the outlet, the blade is rounded off by a circular arc with a diameter of 2.5 mm. The first half of the blade is 7 mm thick. This is 1mm less than the inlet profile such that the thickness is smoothly decreased by 1 mm at the suction side. On the second half of the blade the thickness is gradually decreased from 7 mm to 2.5 mm at the outlet.

5. Adjusting Geometry with CFD

To obtain a good design an iteration process by use of CFD was performed. The CFD simulations were performed in OpenFOAM, geometry adjusted in Matlab and meshing was done in TurboGrid. For post processing Paraview and Gnuplot were used. As a measure for design quality mainly three plots were used. The first was a vector plot of velocities in a meridional plane, Fig. 10. This plane was taken in the middle between two blades. The second measure was the distribution of c_m at the outlet and the third was rotation at the outlet. Targets for these three design measures where that the velocity vectors in the meridional plane should follow the blade curvature as good as possible, the curve of axial velocity plotted against radius should be as flat as possible and rotation at the outlet should be minimized. The methods to adjust the geometry are shortly explained in the next two paragraphs.

5.1 Shortening and Lengthening the Blade

The blade is build up from twelve theoretical streamlines. They lie between shroud and hub and have equal flow rate between them. Their R and Z coordinate come from the axial view and the blade angle β and θ are connected through equation (6). The length of the blade is found by integration of the theta distribution. An overall decrease or increase of β will change θ in the opposite direction and therefore lengthen or shorten the blade. In figure 6 the blade angles are increased at the shroud side of the blade. The blade then becomes shorter and the water flows with less resistance in this region. A higher flow rate at the shroud side consistently leads to a smaller flow rate at the hub-side. Figure 7 shows the changed flow rate at the runner outlet. Velocity vectors in the meridional plane and outlet circumferential velocity also change but are not shown here.

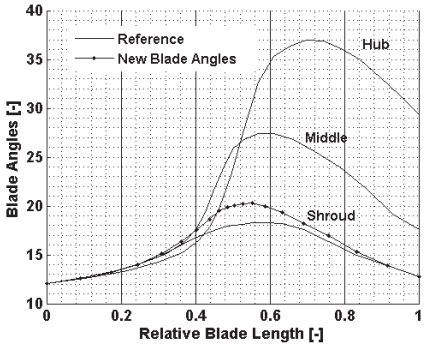

Fig. 6 Blade angles for shortening the blade

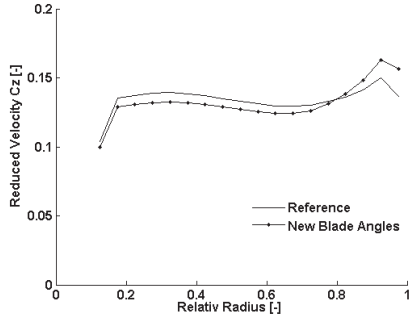

Fig. 7 Velocities at the draft tube inlet

5.2 Adjusting the Outlet Angles

Adjustments were made to the blade close to the trailing edge. An increase in the blade angle at the shroud side will "open" the runner allowing more water to flow here. It will also necessarily change the circumferential velocity to a higher speed. A comparison of two different outlet blade angles is shown in the next two pictures

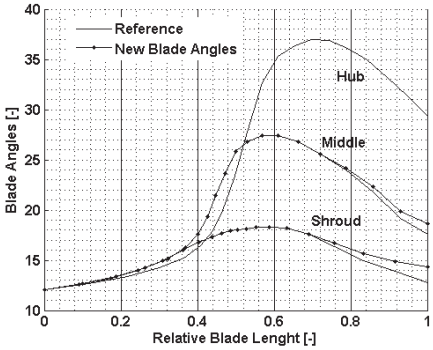

Fig. 8 Blade Angles for changing the Outlet

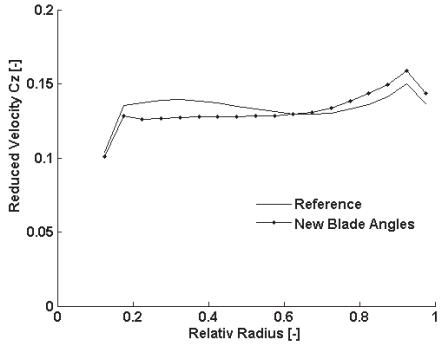

Fig. 9 Velocities at the draft tube inlet

6. Final CFD Results

In this section some results from CFD-simulation of the final design will be presented. Figure 10 shows the velocity in a meridional plane in between two blades at best operation point. Reduced velocities at the outlet are shown in figure.11, with reduced values. Also this at best operation point. The axial velocity is fairly uniform at the outlet section. The c_u-velocity is generally low but builds up to a higher value close to the shroud side.

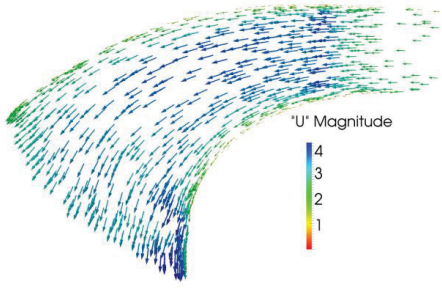

Fig. 10 Velocity in meridional plane

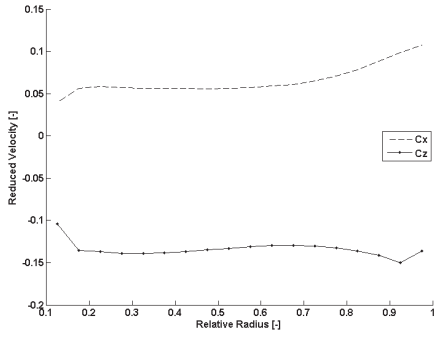

Fig. 11 Velocity at the turbine outlet

The performance of the pump-turbine is here presented as a Hill-diagram. This shows iso-curves of efficiency around best operation point. Diagrams for dimensionless flow and torque versus dimensionless speed are shown in the two subsequent figures. One can observe that the characteristics are s-shaped and thus in principal unstable according to the criteria put forward my Martin. The dimensionless parameters are defined:

$$Qed = \frac{Q}{D^2\sqrt{gH}}, \quad Ned = \frac{nD}{\sqrt{gH}}, \quad Ted = \frac{T}{\rho D^3 gH} \quad [-] \qquad (7)$$

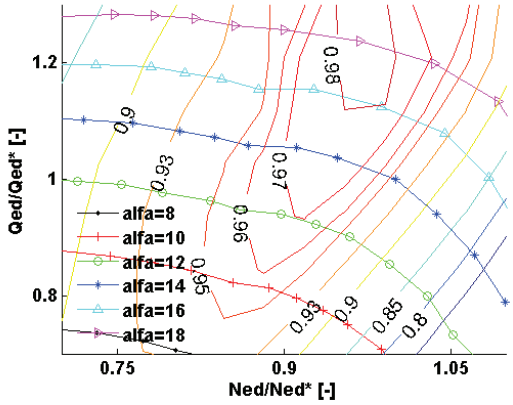

Fig. 12 Hill diagram. Computed points are indicated with symols

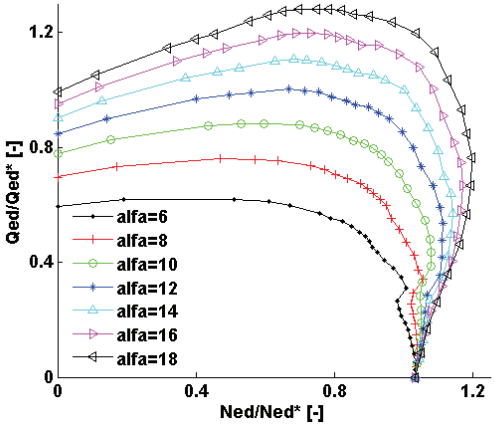

Fig. 13 Flow-speed characteristics

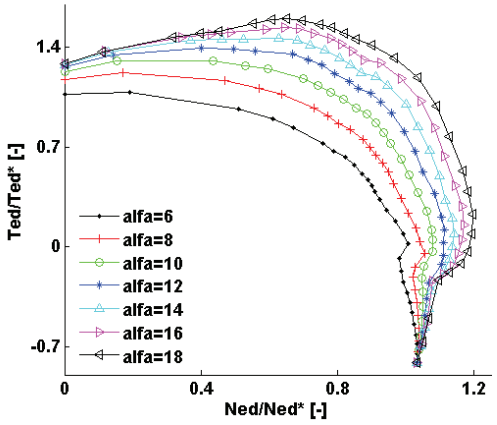

Fig. 14 Torque-speed characteristics

7 Conclusion

A reversible pump-turbine has been designed and produced with the intention of investigating unstable behavior of RPTs in turbine mode of operation. Tests will be performed at The Waterpower Laboratory in Trondheim. It is a high head turbine with speed number 0.36 and high diameter relation of 2. Deliberately, the RPT model is designed with steep characteristics, and as many other RPTs it has S-shaped characteristics, hence it is predicted to become unstable in certain modes of operation and during start up in turbine mode. Despite the simplified design techniques used the runner performance is fairly good with a numerical computed efficiency above 98 percent at BEP.

8 Further Work

The aim for further work is to understand the physics of instability of RPTs by combining CFD simulations and laboratory measurements. Why do they become unstable and which design changes are appropriate for stabilizing the turbine? Some explanations are already in the literature but further understanding is necessary. To be able to see and describe exactly how the flow patterns develop under unsteady operation is an important task. Likewise is the seeking for source of the unsteadiness.

Unsteady CFD simulations will be an important tool, but further development of methods is necessary in order to get accurate results. Especially adverse gradients and circulation zones are hard to capture correctly. Laboratory measurements will be performed to investigate the flow and pressure unsteadiness at off design operation. Measurements of transient operation will be performed to reveal if the stationary characteristics actually describe the transient performance.

Acknowledgments

This work is financed by Norwegian power companies, consultans and equipment suppliers through Energy Norway.Thanks to Ole Gunnar Dahlhaug and Bård Brandåstrø for their work with financing and production of the pump-turbine.

Nomenclature

Nq	Speed number [-]	β	Relative Flow Angle [-]
Qed	Dimensionless Flow [-]	β'	Runner Blade Angle [-]
Ned	Dimensionless Speed [-]	c	Absolute Flow Velocity [m/s]
Ted	Dimensiobless Torque [-]	w	Relative Flow Velocity[m/s]
P	Hydraulic Power [Watt]	u	Tangential Velocity [m/s]
H	Hydraulic Head [m]	ω	Rotational Speed [rad/s]
Q	Flow [m^3/s]	η	Efficiency [-]
R,θ, Z	Cylinder Coordinate	D	Diameter [m]
α	Guide Vane Angle [-]	A	Area [m^2]
δ	Prefix: Difference Between Two Points	B	Inlet Height [m]

Subscripts

u	Peripheral	1	Inlet Turbine Mode
r	Radial	2	Outlet Turbine Mode
z	Axial	11	Inlet Turbine by the Hub
m	Meridional	21	Outlet Turbine by the Hub

References

1. Martin, C.S. *Instability of pump-turbines with s-shaped characteristics*. in *In Proceedings of the 20th IAHR Symposium on Hydraulic Machinery and Systems*. 2000. Charlotte, USA.
2. Klemm, D., *Stabilisierung der Kennlinien einer Pumpenturbine im Bereich zwischen Turbinen-Teillast und Rückwärtspumpenbetrieb.* Voith Forschung und Konstruktion, 1982. Heft 28, Aufsatz 2.
3. P.K. Dörfler, A.J.E., R.N.Pendse, P.Huvet, M.V.Brahme. *Stable operation acvhieved on a single -stage reversible pump-turbine showing instability at no-load*. in *Proceeding of the 19th Symposium on Hydraulic Machinery and Systems*. 1998. Singapore.
4. S.Pejovic, L.K., R.Jemcov, P.Crnkovic, *Unstable Operation of High-Head Reversible Pump-Turbines*, in *8th IAHR Symposium* 1976: Leningrad.
5. T. Nielsen, G.O., *Dynamic Behaviour of Reversible Pump-Turbines inTurbine Mode of Operation*, in *ISROMAC*. 2010: Honolulu.
6. Henry, P., *Turbomachinery hydrauliques*. 1992: Presses polytechniques et universitaires Romand.
7. Brekke, H., *Pumper og Turbiner*. 1999: NTNU, Vannkraftlaboratoriet.

Paper IV

Olimstad, G., Børresen, B., Nielsen, T.K., 2012, “A Two Dimensional Model for Pump-Turbine Instability Investigation”, in 14th International Symposium on Transport Phenomena and Dynamics of Rotating Machine, Honolulu

14th International Symposium on Transport Phenomena and Dynamics of Rotating Machinery, ISROMAC-14
February 27th - March 2nd, 2012, Honolulu, HI, USA

A Two Dimensional Model for Pump-Turbine Instability Investigation

Grunde Olimstad*[1], Bjarne Børresen[2], Torbjørn K. Nielsen[1]

[1]The Waterpower Laboratory, Norwegian University of Science and Technology
Alfred Gets vei 4, Trondheim, 7491, Norway
grunde.olimstad@ntnu.no
torbjorn.nielsen@ntnu.no

[2]Energi Norge
Næringslivets Hus, Middelthunsgate 27, Oslo, Norway
bbo@energinorge.no

Abstract
A two-dimensional model of a reversible pump-turbine has been made. The three-dimensional geometry is projected into two-dimensional space and the outlet is corrected to obtain homologous velocity diagrams. The model is used to investigate stability of the pump-turbine in turbine mode. Towards low flow rates the turbine becomes unstable, which can be concluded from the steep and s-shaped characteristics. At low load operation vortices occur close to the inlet of the runner. These vortices blocks parts of the flow area in one or more runner channels. At some operation points the turbine works both as a turbine and a pump.

Introduction
Reversible pump-turbines (RPTs) are widely used today because of their ability to balance the power production and consumption at a reasonable cost. Intermittent new renewable power sources such as wind power and solar energy are increasingly coming into the market and they have little ability to control when the energy is produced and in what amount. To store the excess energy in a reservoir requires ability to pump water. For this purpose a single stage reversible pump turbine is more cost effective than a pump together with a turbine.

Low specific speed reversible pump-turbines often suffer from hydrodynamic instability at part load. This instability comes forth as fluctuations in speed, pressure and flow rate. This leads to problems during synchronization as well as load rejection. The problems are accentuated at low head operation and may put restrictions on the head variation. Examples of pumped storage power plants with stability problems are reported by Dörfler [1] in Bhira, Klemm [2] in Belgium and Pejovic [3] in Bajina Basta power station. The instable pump-turbine in Belgium was modified with two misaligned guide vanes in order to stabilize the speed in start-up of the RPT in turbine mode. In Bhira the start-up was stabilized by means of a partly closed inlet valve. Even though the solutions worked Dörfler calls the hydraulic stability "the stumbling block" and concludes that "In order to ensure stable operation, the hydraulic instability has to be removed".

The goal of this research is to understand the physical mechanism underlying this so called speed no-load instability. A two dimensional model is created in order to investigate the flow regime close to runaway. Staubli [4] claims that the instability is strongly related to the inlet part of the runner. The inlet region for most high head and low specific speed pump-turbines is almost two dimensional. Figure 1 shows the pump turbine from an axial view, where the two-dimensionality can be seen.

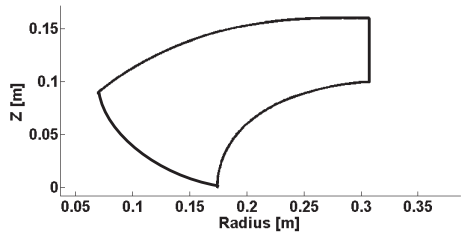

Figure 1 Axial view of the runner

Hypothesis and Scope of the Model

The hypothesis underlying this work is that a two dimensional model is sufficient for describing the main features of the instability problem for pump-turbines with low speed number. Also better understanding between blade geometry and instability is possible since the comparisons get very "clean". Firstly the model avoids three dimensional secondary instabilities. Secondly it is possible to make comparable designs with only few adjustments. The latter is hardly possible in a three-dimensional turbine design due to three dimensional coupling of pressure contours and streamlines.

The model is created to investigate inlet effects on RPT stability. It is not an aim of the model to reconstruct three-dimensional characteristics. A further application of the model is in the design process. The 2d model may be used to design a good inlet profile of the runner blade. The designer can then advance to full 3d design with a good start.

Two-Dimensional Model

The two-dimensional model was created based on the geometry from the NTNU pump-turbine, Olimstad [5]. As methods for projecting the geometry, two approaches were tested; Simple Projection and Conformal Mapping. Simple Projection transforms coordinates (x, y, z) to (X, Y) simply by removing the z-coordinate and letting X=x and Y=y. Conformal mapping, [7], is a method that conserves angles between the blade curvature and the circumference. This is essential since the energy transfer from the flow to the blade is dependent on the blade angle. These are related through Euler turbine equation, (1), here expressed with the blade angle. With equal radius and blade angle the energy transfer is not changed.

$$\omega T = \rho Q[\omega R(\omega R - \frac{Q}{A\tan(\beta)})] \tag{1}$$

The method of conformal mapping performs a transformation of coordinates from equations (2) to equations (3).

$$x = r\cos(\theta),\ y = r\sin(\theta),\ z = f(r) \tag{2}$$

$$X = R(r)\cos(\theta),\ Y = R(r)\sin(\theta),\ Z = 0 \tag{3}$$

The parameters r and θ are used for both original and transformed geometry. New radiuses, R, for transformed points, (X, Y, Z) are calculated through equation (4), where the integral is solved numerically.

$$R = R_0 \exp(-\int \frac{dl}{r}) \qquad dl^2 = dr^2 + dz^2 \tag{4}$$

Two geometries, from simple projection and conformal mapping respectively, are shown in Figure 2. They are almost identical except towards the outlet.

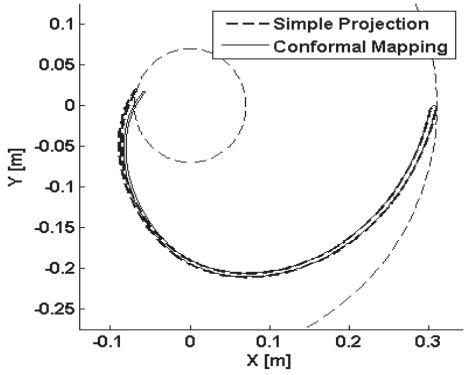

Figure 2 Simple projection versus conformal mapping

The fact that they are equal in most of the blade length confirms that the original blade essentially is two dimensional in that region. Towards the outlet the three dimensional curvature of the original blade makes the two projection different. The finally preferred way to project the 3d geometry followed the three principles;

- Keep the first half of the blade as the projected or conformal.
- Adjust the second half to get homologous velocity diagrams.
- Keep outer diameter constant

The velocity inlet diagram is kept constant. In order to keep the best efficiency point at the same flow rate, the outlet diagram is adjusted, Figure 3. The 2d geometry has a smaller outlet area compared to the 3d geometry and the meridional speed, cm, is therefore higher. The outlet blade angle is adjusted accordingly to avoid rotation. Original outlet blade angel was β_{3d}=30 degree and through equation (5), corrected blade angle became β_{2d}=60 degree.

$$\tan(\beta_{2d}) = \tan(\beta_{3d})\frac{D_{2,3d}^2}{4D_{2,2d}B_1} \tag{5}$$

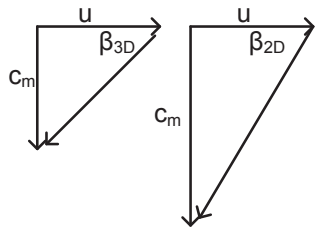

Figure 3 3d and 2d outlet velocity diagrams

Outer diameter is kept constant to avoid additional throttling effects. The two-dimensional geometry used is shown compared to the simple projection in Figure 4.

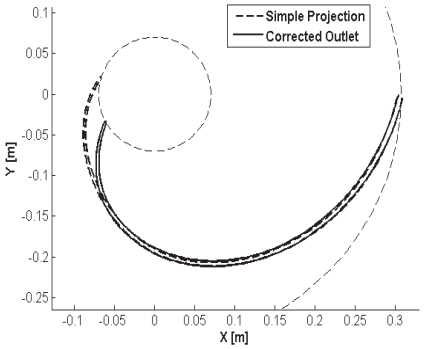

Figure 4 Geometry with corrected outlet

Characteristics

A stability criterion is put forth by Martin [6]. It says that the pump-turbine is unstable if the characteristics have positive slopes at speed no load. The characteristics relates dimensionless flow, Qed, and torque, Ted, to dimensionless speed, Ned.

$$Q_{ed} = \frac{Q}{D_2^2\sqrt{gH}},\ Ted = \frac{T}{\rho D_2^3 gH},\ N_{ed} = \frac{nD}{\sqrt{gH}} \qquad (6)$$

If the characteristics have positive slope they are also "s-shaped". Then two operation points are possible for the same speed of rotation. Therefore the state of operation, i.e. speed, head and flow rate, will fluctuate back and forth in an unstable manner. These fluctuations can be stabilized in laboratory tests and in CFD calculations such that it is possible to acquire the whole s-shaped characteristics. In the CFD calculations both speed and flow rate are given as boundary conditions while the pressure and internal flow field are calculated. The whole turbine is included in the computational domain, such that no periodicity is assumed. The inlet is outside the guide vanes and the outlet at a slightly smaller radius than the runner blade trailing edge. A comparison between the 2d model and the original 3d model from Olimstad [5] is showed in Figure 5. Four different guide vane openings are included. At zero flow rate the 3d characteristics meet in one point. They do so because there are no guide vanes in those simulations.

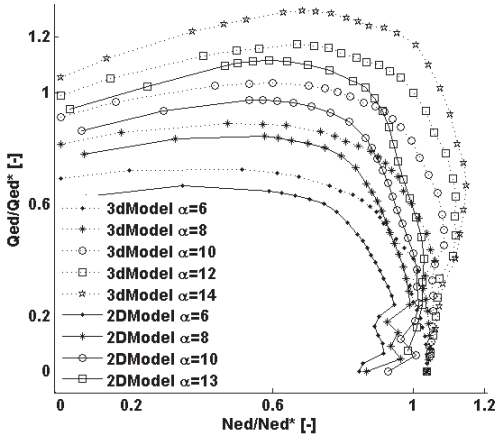

Figure 5 2d versus 3d Comparison

A second 2d model for another pump-turbine was made with the same method. This one compares to measurements as in Figure 6. Both transient and stationary simulated characteristics are included.

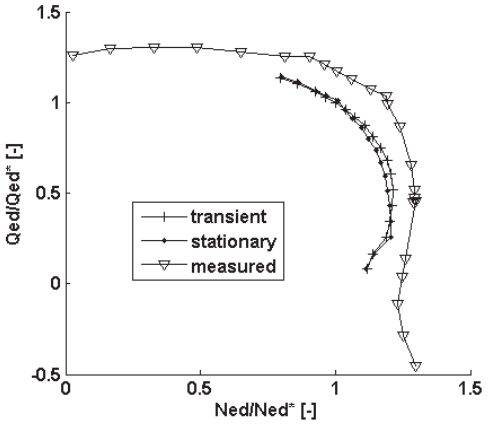

Figure 6 Comparison of measurements and stationary and transient CFD.

To acquire the characteristics, twenty-five operation points have been simulated for each characteristic. To do this a set of flow rates have been chosen and simulated with constant speed, 750 rpm. The two points to the upper left on each of the characteristic curves have been simulated with reduced speed. The flow rates have been adjusted for the different guide vane openings through the valve equation in form of equation (7).

$$Q_\alpha = Q_{\alpha_n} \frac{\sin(\alpha)}{\sin(\alpha_n)} \quad (7)$$

Flow Analysis Results

Sample lines, Figure 7, across each runner channel close to the inlet of the runner are created. Along this line the velocity are sampled at fifty equally distant points. Flow rate per channel and area with backflow is investigated. As nominator in the plots the angle φ=atan(Qed/Ned) is used. This is convenient since the characteristics are s-shaped.

Figure 8 shows that the water flows backwards at some locations at small and high flow rates. The backflow area is a summation of the area where the flow direction is opposite to the bulk flow. Figure 9 shows how the total flow rate varies between the channels. In the figure the value one corresponds to average flow rate per channel at best operation point. For some operation points at low flow the minimum flow rate is negative. These channels then operate as pump instead of turbine.

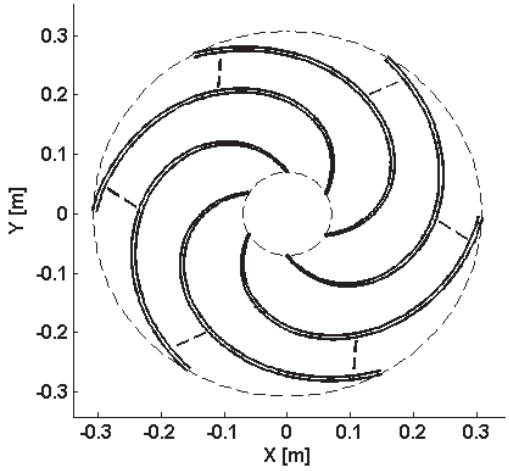

Figure 7 Sample lines

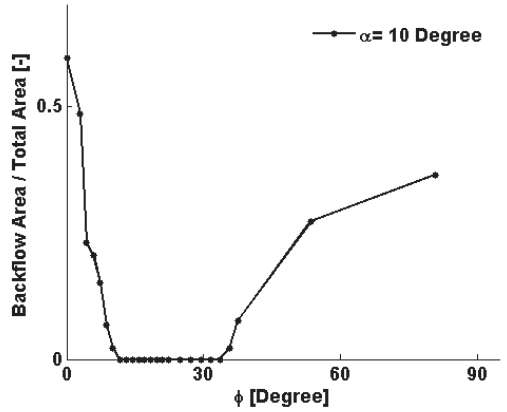

Figure 8 Back-flow Area

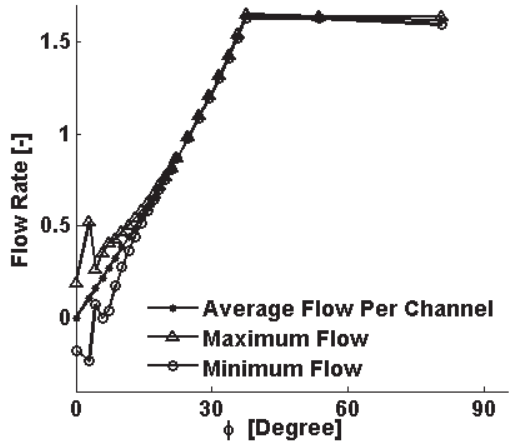

Figure 9 Maximum and minimum flow in channels, normalized through Q*

The flow in the runner channel is shown in the figures 15-19 in appendix. These figures show vector plots of the velocity for four consecutive operation points at low load, Figure 10. A vortex builds up at the pressure side of the runner blade and the position of it is close to the leading edge of the adjacent runner blade. For the last two operation points a vortex covers most of the channel. The water is then blocked from flowing into the runner channel. Consequently it passes the leading edge of the next runner blade and enters the next runner channel.

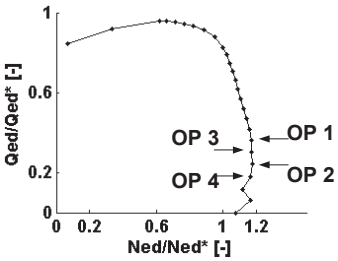

Figure 10 Operation points (OP)

Figure 11 shows a scheme where different characteristic zones are indicated. The operation points with low flow rate are characterized by many vortices and partly pumping.

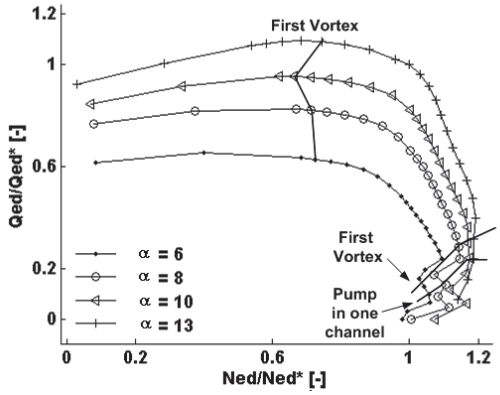

Figure 11 Flow zones

The torque characteristics are shown below. The last three to four points of each characteristic lie at negative torque.

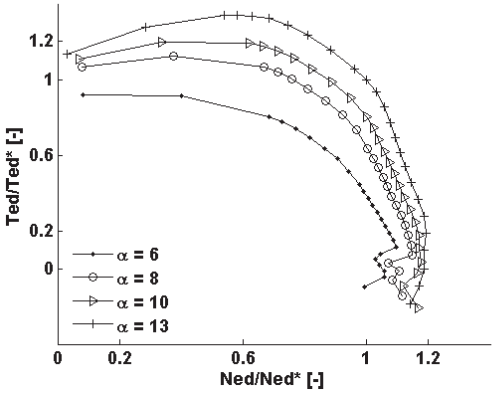

Figure 12 Torque characteristics

Discussion

Vortices form at the inlet and influence the flow. By reducing the flow area the driving pressure force needs to be higher in order to maintain the flow rate. With higher pressure and thus head the operation point, Qed and Ned, are moved to lower values. The characteristics therewith become steeper. Not only vortices, but also low velocity zones, are responsible for this effect. There is a difference between vortices in two- and three-dimensional space. The author believes that vortices that form in two-dimensional space have a greater blocking effect than those forming in three-dimensional space. When a vortex starts to form in two-dimensional space the flow is forced to turn backwards. In three-dimensional space the vortex can form in any possible plane, which may not be parallel to the flow. Since the two-dimensional vortex forms in the parallel plane it occupies a part of the effective flow area. The volute is not a part of the computational domain. Secondary flows, such as vortices, that extend to that area can possibly influence the characteristics but they are nevertheless not taken into account in this work.

When the dimensional variable Qed and Ned have constant values the flow is kinematic similar and the reduced velocity triangles are equal. The performance of the turbine should therefore be equal for all set of flow rate, speed and head that give the same values for these dimensionless variables. In the simulations of the characteristics in this article the speed is set to 757 rpm and the flow rate is set to have suitable values covering the whole 1st quadrant of the characteristic diagram. A new characteristic curve has been simulated to show that the characteristics are independent of the input values. The speed is now set to 1528 rpm and the flow rate is given a new range of suitable values. The Figure 13 compares the two characteristics. The curves are identical, except for the last seven points which show some deviation. These operation points correspond with where vortices dominated the flow.

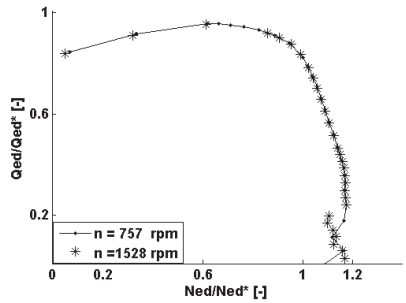

Figure 13 Comparing boundary conditions

Since the runner has six blades and there are 28 guide vanes the geometry is 180 degree periodic. This can be observed in the flow, f.x. by an iso-plot of the relative velocity, Figure 14. The colour plot has an upper threshold of 12 m/s.

Figure 14 Iso-plot of relative velocity in operation point 4

Conclusions

A two-dimensional model has been established for investigation of pump-turbine instability. The model does not reconstruct 3d characteristics perfect but the model can be used to investigate the instability phenomena and its relation to blade geometry. Associated s-shaped characteristics are dependent on vortices forming close to inlet of the RPT. Around speed no-load the flow regime is dominated by such large vortices. The most dominating ones occurs at the pressure side of the blade close to the leading edge of the next blade. At some operation points one or more channels work as pump whereas others work as turbine. The runner and guide vane constellation is 180 degree periodic, which can be observed in the flow pattern. Experimental work on a reduced scale pump-turbine model is ongoing. Unstable characteristics are to be investigated and as also the influence of different inlet blade profiles on the characteristics.

Acknowledgements

This work is financed by Norwegian power companies, consultants and equipment suppliers through Energy Norway.

List of Symbols

A	Area	[m^2]
B_1	Inlet Height	[m]
c_m	Meridional velocity	[m/s]
dl	Small line segment	[m]
$D_{2,2d}$	Outlet diameter for 2d-geometry	[m]
$D_{2,3d}$	Outlet diameter for 3d-geometry	[m]
H	Head	[m]
n	speed	[1/s]
Ned	Dimensionless speed	[-]
OP	Operation point	[-]
Q	Flow rate	[m/s^3]
Qed	Dimensionless Flow	[-]
R	Radius	[m]
T	Torque	[]
Ted	Dimensionless torque	[-]
u	tangential velocity	[m/s]
x,y,z	Original coordinates	[m]
X,Y,Z	Transformed coordinates	[m]
α	Guide vane angle	[Degree]
β	Blade angle	[Degree]
ρ	Density	kg/m^3
φ	Angle in 1st quadrant	[Degree]
θ	Cylinder coordinate	[Degree]
ω	Rotational speed	[1/s]

References

[1] P. K. Dörfler, A. J. Engineer, R. N. Pendse, P. Huvet, M. V. Brahme. “Stable operation acvhieved on a single -stage reversible pump-turbine showing instability at no-load”. Proceeding of the 19th Symposium on Hydraulic Machinery and Systems. 1998. Singapore.

[2] Klemm, D., ”Stabilisierung der Kennlinien einer Pumpenturbine im Bereich zwischen Turbinen-Teillast und Rückwärtspumpenbetrieb”. Voith Forschung und Konstruktion, 1982. Heft 28, Aufsatz 2.

[3] S.Pejovic, L. Krsmanovic, R. Jemcov, P. Crnkovic, “Unstable Operation of High-Head Reversible Pump-Turbines”, in 8th IAHR Symposium 1976: Leningrad.

[4] T.Staubli, F.Senn, M.Sallaberger, “Instability of pump-turbines during start -up in the turbine mode”. Proceedings of Hydro, 6-8 October 2008, Ljubljana.

[5] Olimstad, G., B. Børresen, T. Nielsen “Design of a Reversible Pump-Turbine -with Purpose to Investigate Stability in turbine Mode” 4-th International Meeting on Cavitation and Dynamic Problems in Hydraulic Machinery and Systems. 2011, Belgrade.

[6] Martin, C.S. Stability of pump-turbines during transient operations. 5th International conference on pressure surges, 1986, Hannover, Germany.

[7] Arneberg, J, ”Den beskrivende geometri i kortfattet oversikt”, Bruns vitenskapelige bibliotek bind 4, 1920.

Appendix

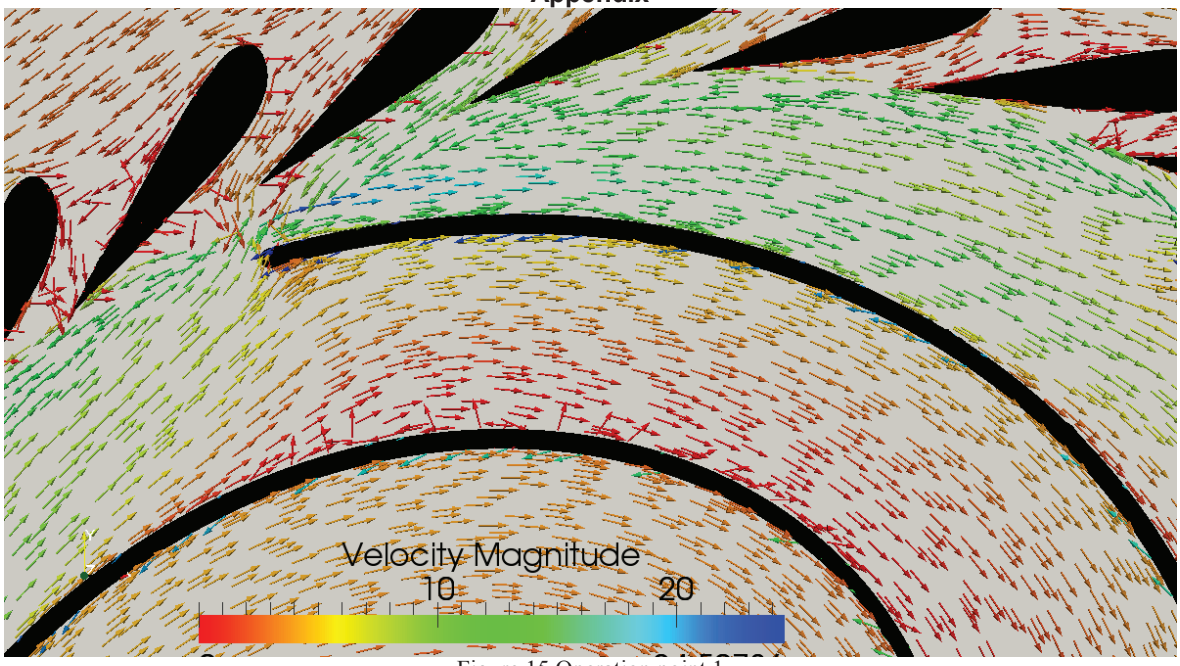

Figure 15 Operation point 1

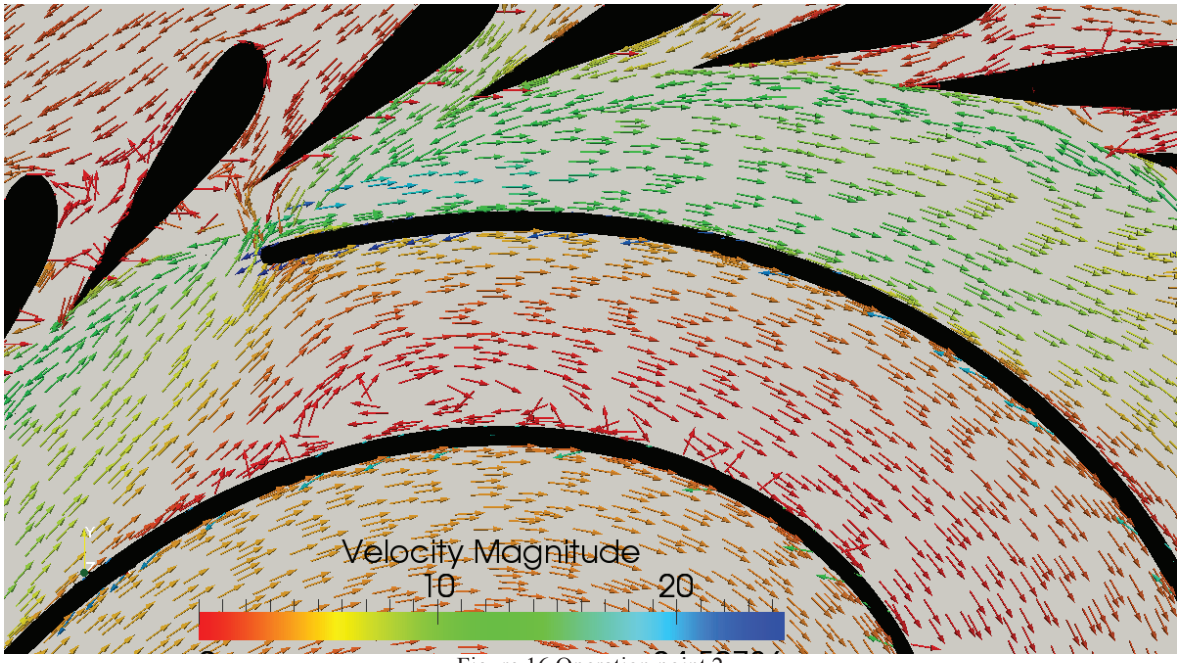

Figure 16 Operation point 2

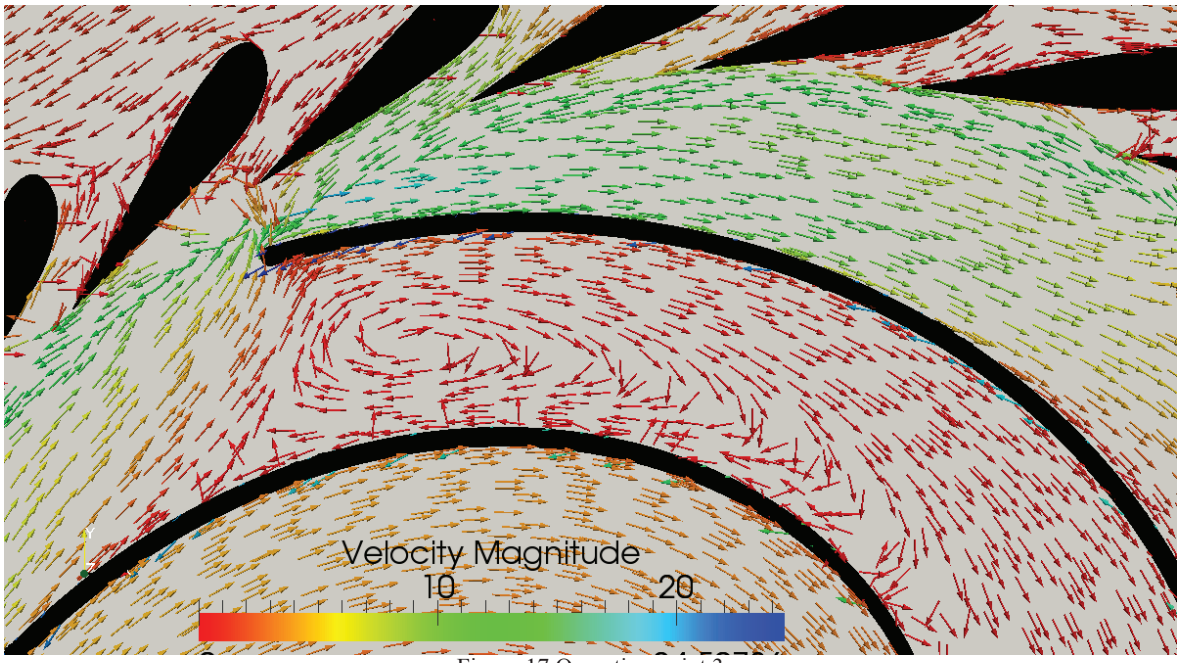

Figure 17 Operation point 3

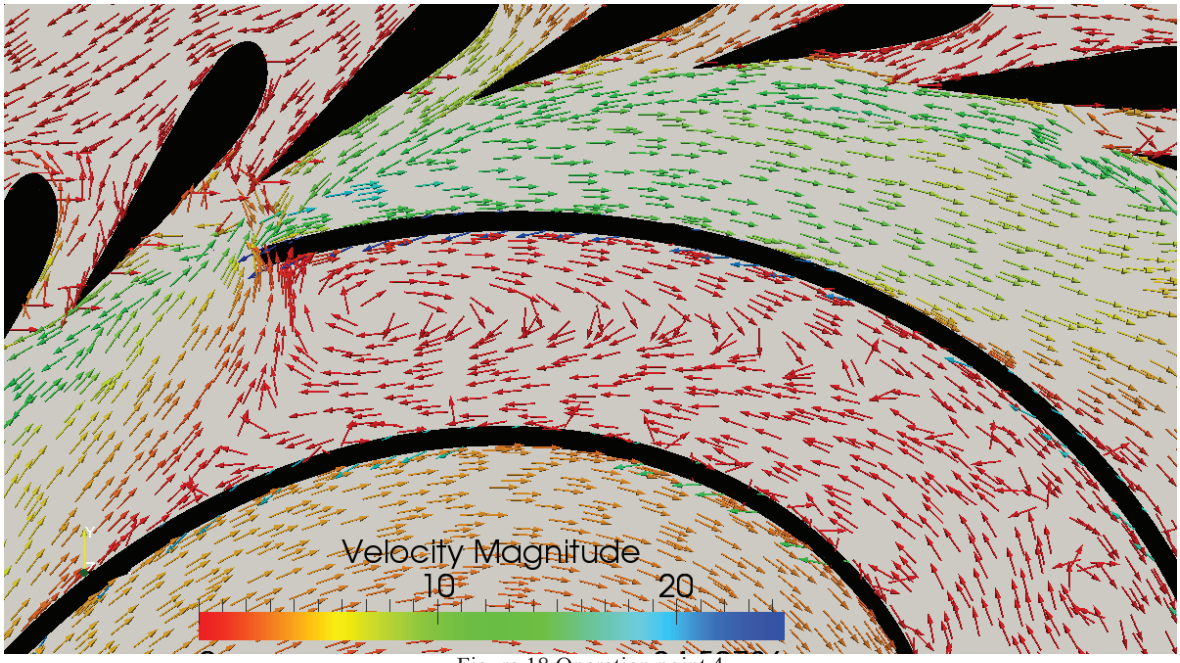

Figure 18 Operation point 4

Paper V

Olimstad, G., Børresen, B., Nielsen, T.K., 2012, “Geometry Impact on Pump-Turbine Characteristics”, in 14th International Symposium on Transport Phenomena and Dynamics of Rotating Machine, Honolulu

14th International Symposium on Transport Phenomena and Dynamics of Rotating Machinery, ISROMAC-14
February 27th - March 2nd, 2012, Honolulu, HI, USA

Geometry Impact on Pump-Turbine Characteristics

Grunde Olimstad*[1], Bjarne Børresen[2], Torbjørn K. Nielsen[1]

[1]The Waterpower Laboratory, Norwegian University of Science and Technology
Alfred Gets vei 4, Trondheim, 7491, Norway
grunde.olimstad@ntnu.no
torbjorn.nielsen@ntnu.no

[2]Energi Norge
Næringslivets Hus, Middelthunsgate 27, Oslo, Norway
bbo@energinorge.no

Abstract
New intermittent energy resources such as wind, solar and wave energy create a need for energy storing capacity. Reversible pump-turbines play an important role when the energy is stored as water with height potential. Many pump-turbines experience stability problems at start-up or when operated at low head. In this paper there has been performed a study of how different geometries impact stability of pump-turbines. Pump-turbines are unstable units if the hydraulic head decreases with increased flow rate. This corresponds to positive slope in torque characteristics and also flow characteristics. An analytic model for pump-turbine characteristics has been used to investigate the influence of inlet diameter and nominal speed. Inlet blade angles, blade profile, and internal blade angles have been investigated by means of CFD simulation. Small geometry changes are showed to have significant influence on characteristics and therewith stability.

List of Symbols

A	Area	[m^2]
B_1	Inlet Height	[m]
c_m	Meridional velocity	[m/s]
c_r	Radial velocity	[m/s]
c_μ	Turbulence model constant	[-]
D_1	Inlet diameter	[m]
D_2	Outlet diameter	[m]
F_r	Radial forces	[N]
g	Gravitational acceleration	[m/s^2]
H	Head	[m]
I	Turbulence intensity	[-]
k	Turbulent kinetic energy	[m^2/s^2]
m	Mass	[kg]
n	speed	[1/s]
Ned	Dimensionless speed	[-]
Q	Flow rate	[m/s^3]
Qed	Dimensionless Flow	[-]
R	Radius	[m]
R_q	Model parameter	[1/m]
s	Diameter relation	[m^2]
T	Torque	[Nm]
Ted	Dimensionless torque	[-]
u	Tangential velocity	[m/s]
w	Relative velocity	[m/s]
α	Guide vane angle	[Degree]
β	Blade angle	[Degree]
ε	Turbulent dissipation	[m^2/s^3]
κ	Opening degree	[-]
ω	Rotational speed	[1/s]

Subscripts

n	Nominal
1	Inlet
2	Outlet
*	Best operation point

Introduction
Pump turbines with low specific speed and high nominal head often suffer from stability problems. This instability comes forth as fluctuations in head, speed and flow. Such fluctuations create difficulties during start-up in turbine mode and during low head operation. The speed stability demand comes from the electric generators which must have fully stable speed when connecting to the turbine shaft.

The stability is traditionally connected to head-flow curves. A criterion for stability is that these curves should

have positive slope in turbine mode. Another stability criterion, Martin [1], is connected to the slope of torque or flow characteristics. These characteristics relates dimensionless torque, Ted, with dimensionless speed and dimensionless flow rate, Qed, with dimensionless speed, Ned. The pump-turbine becomes unstable if the torque characteristics have positive slope.

$$Q_{ed} = \frac{Q}{D^2\sqrt{gH}},\ N_{ed} = \frac{nD}{\sqrt{gH}},\ \mathrm{T_{ed}} = \frac{T}{\rho D^3 gH} \quad [-] \qquad (1)$$

Steep or even s-shaped characteristics are often observed for high head pump-turbines but not as often for high head Francis turbines. A significant difference between the two types of machines is the inlet diameter which is higher for pump-turbines than for Francis turbines. This is a natural result of the pumping head that is higher than the head available in turbine mode of operation. The higher pumping head may also be achieved by increasing the nominal rotational speed. Two observations should be done for the case of increased diameter or prolonged inlet. First the inlet region becomes nearly two-dimensional which makes two-dimensional simulations suitable. Second the diameter has great influence on the radial forces acting on the water inside the runner channels. By radial forces, equation (2), means here the centrifugal force and the radial component of the Coriolis force. The two forces counteract the centripetal and coriolis accelerations which depend on both diameter and speed. Since the radial forces are significantly stronger for pump-turbines than for Francis turbines it is reasonable to believe that they influence the characteristics.

$$F_{radial} = m[(2\omega \times w)\cos(\beta) + \omega^2 R] \quad [\mathrm{N}] \qquad (2)$$

The impact of diameter and speed investigated by an analytic model

An analytic model for pump-turbine characteristics is presented by Nielsen [2]. This model relates flow rate to speed at constant head by the equation (3). It is developed from the Euler turbine equation and includes one extra term for the pumping effect in pump-turbines.

$$gH = gH_n\left(\frac{Q}{\kappa Q_n}\right)^2 + s(\omega^2 - \omega_n^2) - (\omega - \omega_n)R_q(Q - Q_n)\ [\mathrm{m^2/s^2}] \quad (3)$$

The Rq, equation (4), represents the pumping effect and this term is zero at nominal operation point. The parameter s, equation (5), represents the diameter relation and the κ, equation (6), is the opening degree. The opening degree refers to the opening of the guide vanes in best operation point for each guide vane angle. It carries the value one in this article.

$$R_q = \frac{D_1}{2}\frac{1}{A_1\tan\beta_1} - \frac{D_2}{2}\frac{1}{A_2\tan\beta_2} \quad [1/\mathrm{m}] \qquad (4)$$

$$s = \frac{1}{8}D_1^2\left(1 - \frac{D_2^2}{D_1^2}\right) \quad [\mathrm{m^2}] \qquad (5)$$

$$\kappa = \frac{Q^*}{Q_n}\sqrt{\frac{H_n}{H^*}} \quad [-] \qquad (6)$$

Flow versus speed characteristics are simulated for different geometry configurations. Firstly the characteristics for different inlet diameters are compared. All other input values are kept constant. Figure 1 shows that the characteristics get steeper by increased diameter. Secondly the characteristics are shown for increased nominal speed, Figure 2. Also here the characteristics get steeper. With these two types of modification the design of the turbine is no longer ideal or consistent with the Euler-equation. Base input data for all comparisons with the analytic model are shown in Table 1.

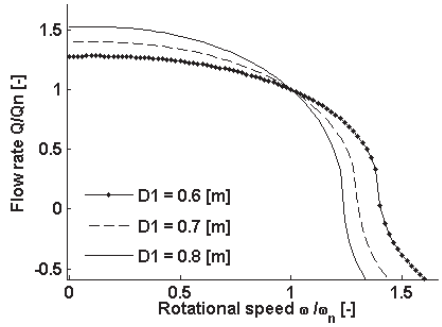

Figure 1 Inlet diameter

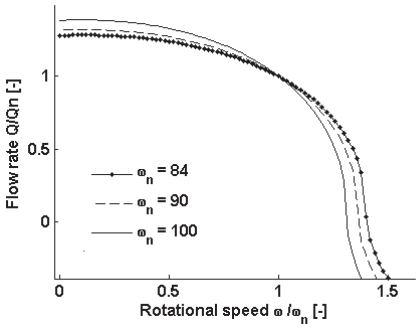

Figure 2 Rotational Speed

Table 1 Base input values

Parameter	Value	Parameter	Value
D_1	0.6 [m]	α_1	14.2 [-]
D_2	0.349 [m]	β_1	12.3 [-]
B_1	0.054 [m]	β_2	14.0 [-]
ω_n	84 [1/s]	Q_n	0.3 [m^3/s]
κ	1 [-]	H_n	30 [m]

More design relevant comparisons are performed by ensuring that the "Euler-design", the nominal flow rate and hydraulic head are preserved. The Euler-design is preserved by the Euler equation (7), where the efficiency is exact equal one.

$$uc_u = gH_n = \omega_n R_1(\omega_n R_1 - \frac{Q_n}{A_1 \tan(\beta_1)}) \quad [m^2/s^2] \qquad (7)$$

For comparison, the inlet diameter is given two new values. For those values new inlet heights, B_1 are calculated by turning around equation (7). The B_1 is contained in the inlet area, A_1. A new absolute flow angle, α_1, is calculated to complete the velocity diagram. The rotational speed is given new values in a second comparison. New values for B_1 and α_1 are calculated as in the diameter comparisons. The two new rotational speeds are chosen such that the radial forces are equal in the cases of increased diameter and speed. The coriolis acceleration has a direction perpendicular to the relative flow and the radial component is found by multiplying by cosine to β_1.

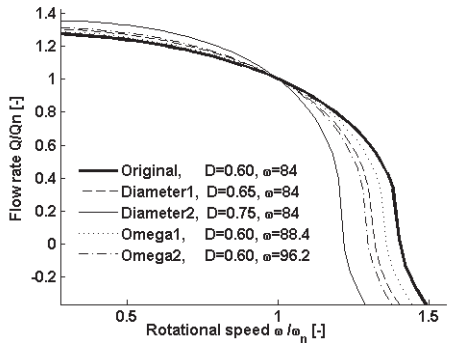

Figure 3

The characteristics get steeper by increasing the diameter or the rotational speed. It can further be seen that characteristics with equal radial forces in best operation point have different slopes. The slopes for the geometries with increased diameter are steepest. Table 2 shows the parameters that are changed in the comparisons. Figure 4 depicts the inlet velocity diagrams for the diameter comparisons. When the diameter is increased the inlet height is decreased with the result that the inlet area also is decreased. As a consequence the meridional speed gets higher. The equation (8) shows how new rotational speeds are calculated. For cases with increased speed the outlet blade angle had to be modified.

Table 2 Diameter and speed comparisons

Comparison	D_1 [m]	ω_n [1/s]	α_1 [-]	B_1 [cm]	F_r/m [m/s^2]
Original	0.6	84	14.2	5.4	4390
Diameter1	0.65	84	18.4	4.1	5066
Diameter2	0.75	84	27.3	2.6	6367
Omega1	0.6	88.4	16.8	4.7	5066
Omega2	0.6	96.2	21.7	3.9	6367

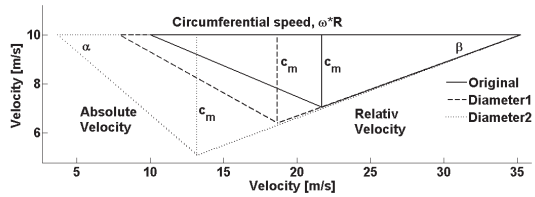

Figure 4 Velocity diagram for different diameters

$$\omega = [(k + \frac{4gH}{D_1})\frac{2}{3D_1}]^{0.5} \quad [1/s] \tag{8}$$

k=coriolis+centripetal

CFD-analysis

Characteristics are simulated by CFD-analysis on different geometries. The simulations are performed on a model presented in Olimstad [3]. The computational domain is shown in Figure 5. It contains the runner, guide vanes and a prolonged inlet region. The simulations are performed steady state with the rotation represented with extra terms for coriolis and centripetal accelerations. Boundary conditions are no-slip and log-law at the walls and symmetric at the top and bottom. At the outlet the pressure is set to a reference value and other variables, u, k and ε, have the zero gradient boundary condition. At the inlet the pressure has the zero-gradient boundary condition while the other variables have given values. The turbulent kinetic energy and dissipation of turbulent kinetic energy are calculated form equations (9) and (10) with a turbulence intensity of 7 percent. The radial velocity at the inlet is varied from 2 m/s to 0 m/s to obtain different points along characteristic curves. The rotational speed is set to 84 radians per second for best operation point. Operation points at part load are given slightly higher speeds while operation points at over load are given lower speeds. In every mesh there are approximately 100.000 cells. Their spacing have a gradient towards walls giving average y+ values of approximately 50 at nominal flow rate.

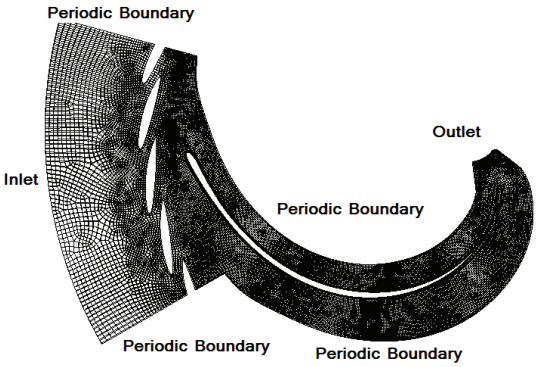

Figure 5 Computational domain

$$k = \frac{2}{3}U^2 I^2 \quad [m^2/s^2] \tag{9}$$

$$\varepsilon = c_\mu^{3/4}\frac{k^{3/2}}{0.07D_2} \quad [m^2/s^3] \tag{10}$$

During simulations the head is held constant within a range of plus minus three meter. The reason for this is to avoid unrealistic low and high head at the extremes borders of the characteristics. Initially two sets of values for inlet radial velocity and rotational speed are given as input. The small variation of head is then ensured by instructing the solver to adjust the inlet velocity. The solver runs 2000 iterations between every adjustment. Adjustments are done by equation (11), which essentially is the Torricelli's valve equation for the actual(old) state divided through a new(wanted) state with fifty meter head. When two or more geometries are compared the described adjustment is performed only for simulation of one characteristic curve. The compared simulations are given the exact same boundary values.

$$c_{r,new} = c_{r,old}\sqrt{\frac{50}{H_{old}}} \quad [m/s] \tag{11}$$

The accuracy of the simulations is demonstrated by comparisons of five runner blades. These runner blades differ only by the inlet blade angle and the comparisons are performed down to 0.1 degree difference in the blade angle. The blade shapes does not differ much and the difference is only visible when zooming in the leading edge. Figure 6 shows the geometry difference of the blades. Since the geometry difference is very small the difference in terms of flow characteristics also gets very small. This difference is therefore represented as deviation in hydraulic head. In Figure 7 the head for all geometries are compared to the head for the original blade. Higher head move points in the first quadrant of the flow–speed characteristics towards lower left and lower head move points towards upper right. Therefore it can be seen from Figure 7 that characteristics become steeper with higher inlet blade angle.

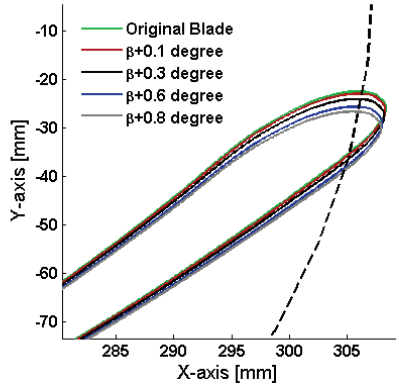

Figure 6 Small variations in β_1

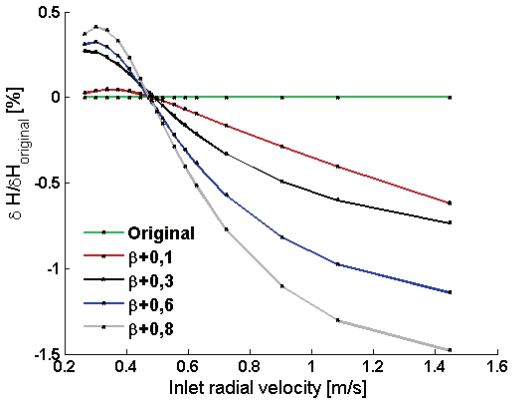

Figure 7 Head difference for small variation in β_1

To show the effect of inlet blade angle on characteristics simulations are performed for two blades with a four degree difference in inlet blade angle. For this comparison there have been simulated characteristics for four guide vane openings. The flow rate for these guide vane openings have been adjusted by equation (12).

$$Q_\alpha = Q_{\alpha_n} \frac{\sin(\alpha)}{\sin(\alpha_n)} \quad [\mathrm{m}^3/\mathrm{s}] \qquad (12)$$

The flow characteristics resulting from the simulations are shown in Figure 8.

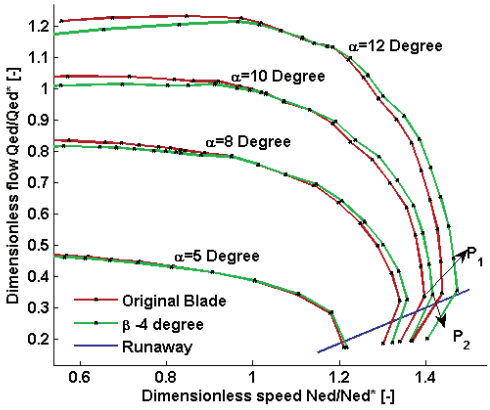

Figure 8 Characteristics for four degree difference in β_1

It can be seen that the blade with the highest inlet blade angle has the steepest characteristics. In best operation point(BEP) the two geometries give equal simulation results, such that the characteristic curves cross each other at that point. For BEP, as for other points, the given flow rate and speed of rotation were exact equal. The resulting head over the runner was H=47.47m and H=47.56m for original blade and β-4 respectively. These numbers are taken for the 10 degree guide vane opening. The efficiency in BEP for the two differed with only 0.03 percent. To simulation points P_1 and P_2 where investigated to find out why the two geometries have different characteristics. Obviously the difference is constituted by difference in hydraulic head. This is 0.9 meter(2%) higher for the original blade. Figure 9 shows streamlines for the runner flow in P_1. A large steady vortex is dominating the flow picture. This vortex can be observed for both geometries and they are equally large. However the head difference over the vortex has been found by extracting pressure and velocity at line 1 and 2 in Figure 9. The downstream hydraulic head is equal in both cases while the head difference over the vortex is 1.1 meter larger for the original blade. This is close to the total head difference of 0.9 meter.

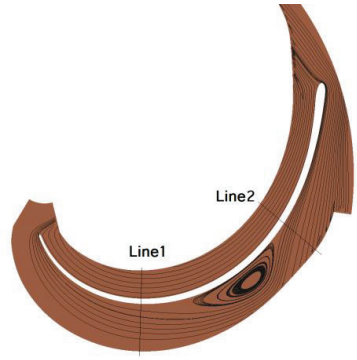

Figure 9 Streamlines in operation point P_1

In addition to the inlet blade angle two other blade shape variations are performed to see how they influence characteristics. Firstly three different shapes of the leading edge are compared. Secondly three different blade angel distributions are compared while keeping the inlet and outlet blade angles as original. The three shapes of the leading edge are depicted in Figure 10. The blades have different thicknesses close to the leading edge but this difference is gradually diminished towards the inner if the blade.

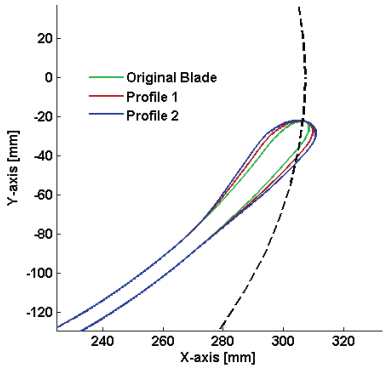

Figure 10 Leading edge profiles

The characteristics for the three profiles are shown in Figure 11. The thickest blade profile, profile 2, seems to give the steepest characteristics.

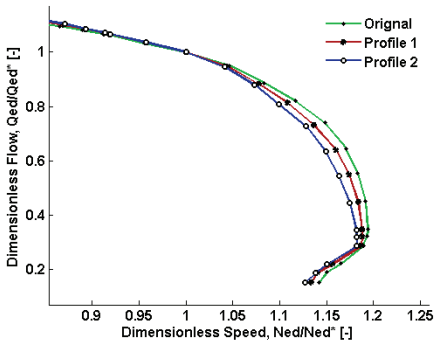

Figure 11 Characteristics for leading edge profiles

Further three geometries are compared. Here all the main geometry parameters are equal, including inlet and outlet diameters and blade angles. The differences lie in how the blade angle develops from inlet to outlet. Figure 12 shows the blade angle for the three blades as a function of blade length. Relative blade length of zero refers to the inlet and one to the outlet. The blade with β-distribution 2 gives the steepest characteristics.

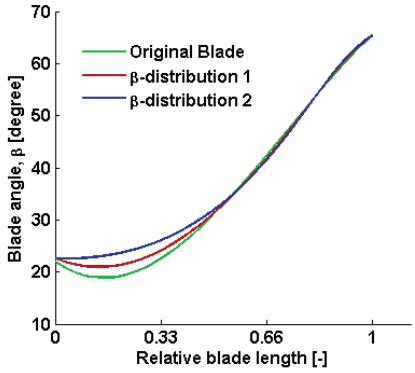

Figure 12 Blade angle distributions

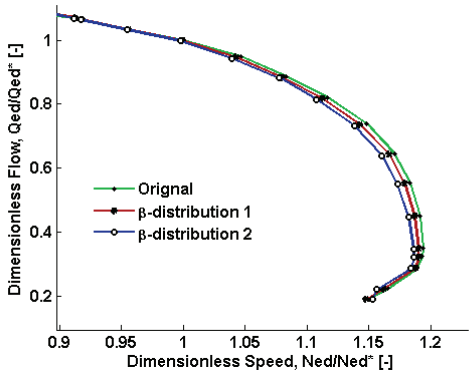

Figure 13 Characteristics for β-distributions

Conclusion

Diameter and speed both have great influence on the characteristics. Both increased speed and increased diameter give steeper characteristics. This effect is connected to the radial forces which counteracts the centripetal and coriolis acceleration. For cases where nominal flow and head are preserved and the radial forces are equal the diameter shows to have most influence. This means that regarding characteristics it is favorable to design pump-turbines with low diameter and high speed.

In CFD-comparisons very small geometry difference can be distinguished. Geometries with as little as 0.1 degree difference in inlet blade angle were tested and could be distinguished when comparing deviations in head.

The inlet blade angle influences the characteristics which becomes steeper with increasing blade angle. A vortex inside the runner channel blocks part of the flow area and is responsible for an extra pressure rise over the turbine. The vortex seems to have increased importance for blades with higher inlet blade angles. Measurements in Yamabe [4] confirms the relation between the blade angle and characteristics.

Blades with thicker inlet profiles get steeper characteristics. So does also blades where internal blade angle distribution is lifted to higher angles. The effect of increasing the internal blade angles can be compared to the effect of increasing only the inlet blade angle.

Acknowledgments

This work is financed by Norwegian power companies, consultants and equipment suppliers through Energy Norway.

References

[1] Martin, C.S. Stability of pump-turbines during transient operations. 5th International conference on pressure surges, 1986, Hannover, Germany.

[2] T. Nielsen, G.O., Dynamic Behavior of Reversible Pump-Turbines in Turbine Mode of Operation, in International Symposium on Transport Phenomena and Dynamics of Rotating Machine, 2010, Honolulu.

[3] G. Olimstad, B.B., T.K. Nielsen, A Two Dimensional Model for Pump-Turbine Instability Investigation, in 14th International Symposium on Transport Phenomena and Dynamics of Rotating Machine, 2011, Honolulu.

[4] M.Yamabe, Improvement of Hysteresis Characteristics of Francis Pump-Turbines When operated as Turbine. Journal of Basic Engineering, 1972. September 1972.

Paper VI

Nielsen, T.K, Olimstad, G., 2010, “Dynamic Behaviour of Reversible Pump-Turbines in Turbine Mode of Operation”, in International Symposium on Transport Phenomena and Dynamics of Rotating Machine, Honolulu

Paper ID No: 60

Dynamic Behaviour of Reversible Pump-Turbines in Turbine Mode of Operation

Torbjørn K. Nielsen[1], Grunde Olimstad[1]

[1] Waterpower Laboratory, Department of Energy and Process Engineering, Norwegian University of Science and Technology
Alfred Getz vei 4, 7491 Trondheim, Norway
Phone: +47 73 59 35 72, FAX: +47 73 59 38 54, E-mail: torbjorn.nielsen@ntnu.no

ABSTRACT

A reversible pump turbine is a machine that can operate in three modes of operation i.e. in pumping mode, in turbine mode and in phase compensating mode (idle speed). Reversible pump turbines (RPTs) have an increasing importance for regulation purposes for obtaining power balance in electric power systems. Especially in grids dominated by thermal energy, reversible pump turbines improve the overall governor stability. Increased use of new renewables (wind, wave and tidal power plants) will utterly demand better regulation ability of the more traditional power suppliers, enhancing the need for reversible pump turbines.

It is, however, a necessity that both machine and system is designed for maximum flexibility in changing modes of operation from pump to turbine and vice versa. A reversible pump turbine is known for having very steep speed–flow characteristics which might give stability problems.

During the design process, focus on the system dynamics in such power plants is essential. Simulation of the dynamic behaviour of the system implies a good representation of the turbine by its characteristics. It is necessary to be able to represent the characteristics before any measurements of the actual machine are available.

This paper presents an possible explanation of the reason for these steep characteristics. Based on this hypothesis, a representation of the turbine for system dynamic simulation purposes is suggested.

Symbol	Quantity	Unit
D_1	Inlet diameter, turbine mode	m
D_2	Outlet diameter, turbine mode	m
B	Runner height at inlet in turbine mode	m
H	Head	m
H_{th}	Theoretical pump head	m
β_1	Inlet angle, turbine mode	-
ω	Angular speed	1/s
v	Relative velocity	m/s
s	Diameter relation	-
u1	Peripheral velocity at inlet, turbine mode	m/s
u2	Peripheral velocity at outlet, turbine mode	m/s
g	Gravitational constant	m/s^2
κ	Guide vane opening degree	
Q	Discharge	m^3/s
cu	Absolute velocity in peripheral diameter	m/s
c	Absolute velocity	m/s
Q_c	Discharge with zero incident losses	m^3/s
H_p	Head for pump	m
H_n	Head at nominal speed	m

Introduction

The special geometry of the reversible pump turbine gives an effect of pumping in operation outside the best performance point in turbine mode. Hence, from a global point of view, the turbine will have an increased throttle effect as the rotational speed increases. As the speed increases, the flow decreases more than that of a Francis turbine with the same specific speed. This is due to the difference in geometry. A reversible pump turbine is a compromise between a turbine and a pump, where the priority is on the performance in pumping mode of operation. The steep characteristics might cause severe stability problems, especially at idle speed. Stability in idle speed is a necessity for phasing in the generator to the electric grid. Also severe water hammer pressure is known to be caused by these steep characteristics. As the turbine increase the speed because of a load rejection, the wicket gates go towards closure, giving retardation pressure in front of the turbine.

In all reaction turbines, the speed of rotation will have an influence on the flow. In general, a low specific speed Francis turbine will have steeper characteristics than a high specific speed Francis. This is mainly due to the acting centripetal forces. Dependent of the ratio between inlet and outlet diameter, the pumping effect will be different in different machines. For a low specific speed Francis, the inlet diameter is much larger than the outlet diameter, hence the centripetal forces works against the driving pressure. This results in a throttling effect, which decreases the flow when the speed of rotation increases. If the outlet diameter is the larger one, the effect will be opposite, the flow increases when the speed of rotation increase. In Figure 1 and Figure 2, this is illustrated.

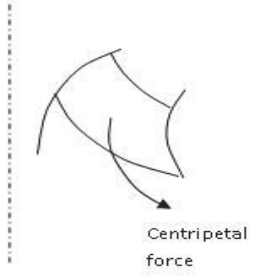

Figure 1 - The effect of centripetal force on a low specific speed Francis

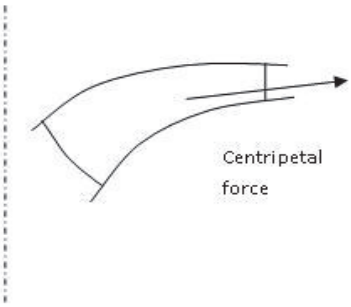

Figure 2 - The effect of centripetal force on a high specific speed Francis

By developing Euler's turbine equation, eq. (1), one can see that the speed of rotation affects the pressure so that when the inlet diameter is larger than the outlet diameter, the turbine runner will give increased throttling effect as the speed of rotation increases.

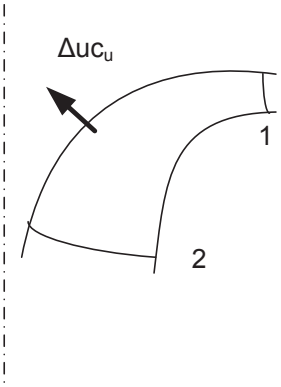

Figure 3 - Francis turbine, axial section

According to the Euler turbine equation, the pressure difference between inlet and outlet (marked 1 and 2 in Figure 3), is given by:

$$g(H_1 - H_2) = u_1 c_{1u} - u_2 c_{2u} \tag{1}$$

Applying the cosine rule on the inlet velocity triangle, Figure 4, gives:

$$\begin{aligned} v_1^2 &= u_1^2 + c_1^2 - 2u_1 c_1 \cos\alpha_1 = u_1^2 + c_1^2 - 2u_1 c_{1u} \\ u_1 c_{1u} &= \frac{1}{2}c_1^2 - \frac{1}{2}v_1^2 + \frac{1}{2}u_1^2 \end{aligned} \tag{2}$$

And accordingly for the outlet triangle, Figure 4:

$$u_2 c_{2u} = \frac{1}{2}c_2^2 - \frac{1}{2}v_2^2 + \frac{1}{2}u_2^2 \tag{3}$$

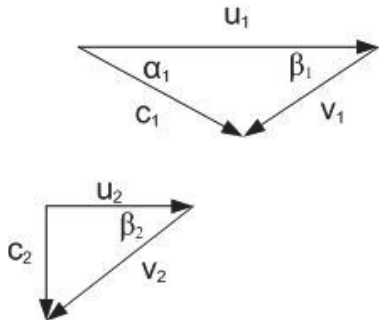

Figure 4 - Velocity triangles

Implemented in eq. (1) and substituting u with ωr gives:

$$g(H_1 - H_2) = \frac{1}{2}(c_1^2 - c_2^2) - \frac{1}{2}(v_1^2 - v_2^2) + s\omega^2 \tag{4}$$

Where s is the diameter relation defined as;

$$s = \frac{1}{8}D_1^2\left(1 - \frac{D_2^2}{D_1^2}\right) \tag{5}$$

Introducing the opening degree of the turbine, κ, defined by:

$$\kappa = \frac{\dfrac{Q}{\sqrt{2gH}}}{\dfrac{Q_n}{\sqrt{2gH_n}}} \tag{6}$$

where n denotes the design point of the turbine. Solving the equation with respect to the head H gives:

$$H = H_n\left(\frac{Q}{\kappa Q_n}\right)^2 \tag{7}$$

which in the design point is the same head as H1-H2, as expressed in eq.(4), hence:

$$gH_n\left(\frac{Q}{\kappa Q_n}\right)^2 = \frac{1}{2}(c_{1n}^2 - c_{2n}^2) - \frac{1}{2}(v_{1n}^2 - v_{2n}^2) + s\omega_n^2$$

or (8)

$$\frac{1}{2}(c_{1n}^2 - c_{2n}^2) - \frac{1}{2}(v_{1n}^2 - v_{2n}^2) = gH_n\left(\frac{Q}{\kappa Q_n}\right)^2 - s\omega_n^2$$

Implemented in eq. (1) gives:

$$gH = gH_n\left(\frac{Q}{\kappa Q_n}\right)^2 + s(\omega^2 - \omega_n^2) \tag{9}$$

When s is positive, i.e. D1>D2, the flow will decrease and if s is negative, i.e. D1<D2, the flow will increase as the speed of rotation increases, see Figure 5

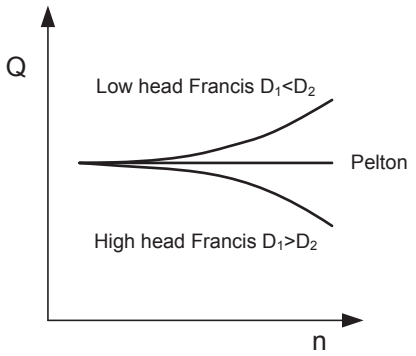

Figure 5 - Illustration of the tendency of the speed-flow characteristics.

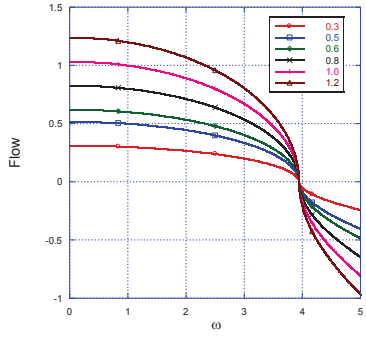

Figure 6 - Speed–flow characteristics according to the Euler turbine equation for different opening degrees, κ.

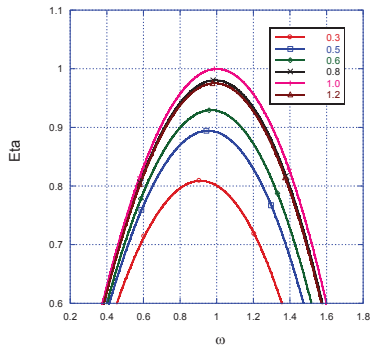

Figure 7 - Efficiency according to the Euler turbine equation

This is all according to the Euler turbine equation. Simulations of the turbine characteristics and efficiency of a high head Francis turbine with this model are shown in Figure 6 and Figure 7. It can be observed that the flow characteristics end up in one point for the different guide vane opening. As there is no loss involved, the peak efficiency will be 1 for best operational point, κ=1.

For high head Francis turbines, and especially for RPTs, the speed-flow characteristics are in fact much steeper. Even for low head RPTs, where the inlet diameter is equal or even smaller than the outlet diameter, the speed-flow characteristics is decreasing. This indicates that it is not only the diameter ratio that decides the characteristics.

The flow dependency of the speed of rotation is often referred to as "pumping effect" because as the speed increases, the turbine will act like a pump, throttling the flow through the turbine. There are reasons to model the turbine in accordance with the Euler turbine equation, adding a term based on the pump equation in order to include this "pumping effect".

Pump characteristics

A centrifugal pump and a Francis turbine is in fact the same kind of machine, both obeying the Euler equation. Assuming rotation free inlet, the theoretical head of a pump may be expressed by the Euler equation:

$$gH_{th} = u_2\left(u_2 - \frac{c_{2m}}{\tan\beta_2}\right) = u_2\left(u_2 - \frac{Q}{\pi B_2 D_2 \tan\beta_2}\right) \quad (10)$$

At a given speed of rotation, i.e. for a given u_2, The QH-characteristics will be ascending if the outlet angle $\beta>90^o$ and descending if $\beta<90^o$, i.e. forward or backward leant runner blades as illustrated in Figure 8. In order to get stabile pump characteristics, centrifugal pumps must have backward leant runner blades. This is also the case for a RPT, when running as a pump. However, when the speed of rotation changes direction to turbine mode of operation, the pump effect will be even stronger because of forward leant blades.

In eq. (10), it is assumed no rotation at the pump inlet. For this case, there is rotation at the inlet because of the guide vanes. This rotation term is included in eq. (11) below.

$$gH_{th} = u_2 c_{2u} - u_1 c_{1u} = u_2\left(u_2 - \frac{c_{2m}}{\tan\beta_2}\right) - u_1\left(u_1 - \frac{c_{1m}}{\tan\beta_1}\right)$$
$$gH_{th} = u_2\left(u_2 - \frac{Q}{A_2\tan\beta_2}\right) - u_1\left(u_1 - \frac{Q}{A_1\tan\beta_1}\right) \quad (11)$$

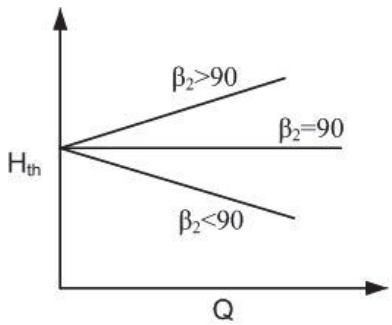

Figure 8 - Theoretical QH-characteristics of centrifugal pumps. They are dependent on the outlet angle β_2.

Pumping effect in a Francis turbine

Because of the pumping effect in a Francis turbine, the turbine will behave in the same way as a centrifugal pump. The water flows through the turbine from upper to lower reservoir and will give rotational power on the turbine shaft according to the Euler turbine equation. At the same time, the pump equation will also apply, but with the direction of the rotation as in turbine mode of operation. Seen from the pump equation, the flow will be negative until the flow really turns, which will happen if one increases the speed of rotation sufficiently. As pump regarded, this will be a pump with forward leant blades, i.e. with increasing characteristics, (see Figure 8). Using notations common for turbine mode, the pump equation will be:

$$gH_p = u_1 c_{1u} - u_2 c_{2u} = u_1\left(u_1 - \frac{c_{1m}}{\tan\beta_1}\right) - u_2\left(u_2 - \frac{c_{2m}}{\tan\beta_2}\right)$$
$$gH_p = u_1\left(u_1 - \frac{Q}{A_1 \tan\beta_1}\right) - u_2\left(u_2 - \frac{Q}{A_2 \tan\beta_2}\right) \quad (12)$$

Introducing the angular speed of rotation, ω:

$$gH_p = s\omega^2 - \omega\left(\frac{D_1}{2}\frac{Q}{A_1 \tan\beta_1} - \frac{D_2}{2}\frac{Q}{A_2 \tan\beta_2}\right) \quad (13)$$

The first term is identical with the term that one gets when developing the turbine equation, se eq. (9). The last terms enhance the pumping effect dependent on the difference in diameters and the blade angle. Implemented in eq.(9), adding the term Hp, gives:

$$gH = gH_n\left(\frac{Q}{\kappa Q_n}\right)^2 + s(\omega^2 - \omega_n^2) - (\omega - 1)R_q(Q - Q_c) \quad (14)$$

$$R_q = \frac{D_1}{2}\frac{1}{A_1 \tan\beta_1} - \frac{D_2}{2}\frac{1}{A_2 \tan\beta_2} \quad (15)$$

The same Francis turbine as in Figure 6 in is now simulated with the pumping effect included. The turbine characteristics are now steeper, as shown in Figure 9.

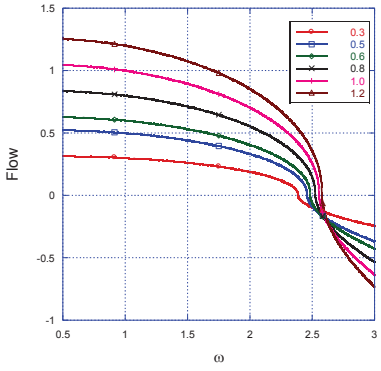

Figure 9 - Speed-flow characteristics for corrected model

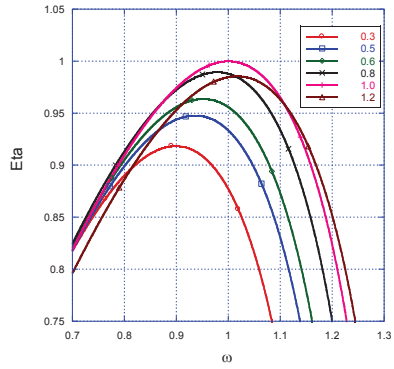

Figure 10 - Efficiency for the corrected model

Design principles for reversible pump-turbines

Bigger difference between inlet and outlet diameter gives a higher pumping effect and thereby steeper characteristic is to be anticipated. The difference of diameters does not explain that the characteristics become significant steeper. Also low head RPTs, where the diameters are nearly equal, have very steep characteristics. The explanation must be on the blade angle i.e. the outlet blade angle seen from the pumping point of view.

In RPTs, the blade angle is back leant in pumping mode of operation in order to have stabile pump characteristics. Compared with a turbine with given head, flow and speed of rotation, the outlet diameter of a pump must be increased to be able to pump the same flow back to the upper reservoir. See Figure 11.

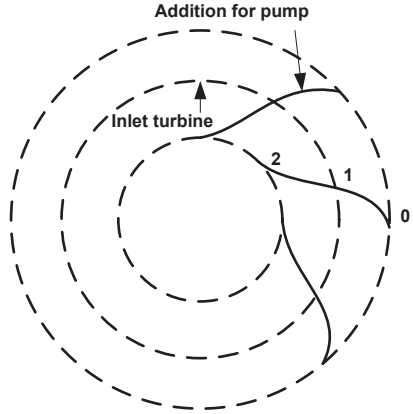

Figure 11 - Design principle for a RPT, 0 marks inlet RPT, 1 inlet for a comparable Francis turbine and 2 is outlet.

In turbine mode, the pumping part of the runner is somewhat unnecessary. In order not to disturb the turbine behaviour, it is reasonable to design the addition in diameter uc_u neutral. Figure 12 shows simulated RPT characteristics based on this model. The speed-flow characteristics are much steeper than for a Francis turbine, see Figure 9.

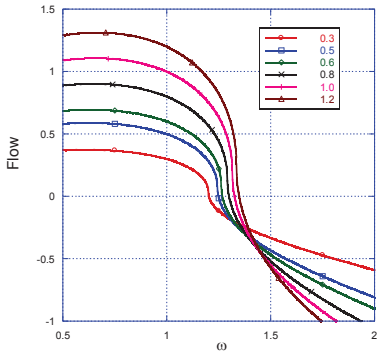

Figure 12 - Simulated speed –flow characteristics of RPT

Simulated and measured characteristics

The new model shows reasonable good agreement with measured characteristics. The simulated characteristics are plotted against measured data from the corresponding model turbine in Figure 10.

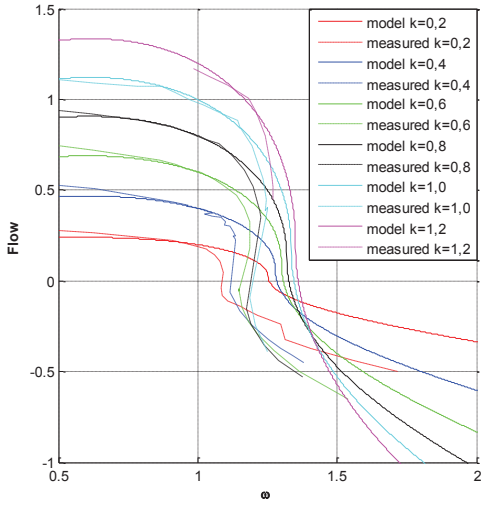

Figure 13 - Comparison for different opening degrees

Conclusion

The model seems to have good overall agreement with measured characteristics, as Figure 13 indicates. The model is a quadratic algebraic equation and it is then impossible to have an s-shaped curve as in the measured characteristics. There are reasons to believe that there is a hysteresis effect in the measurements for the s-shaped region and the s-shape is subject to discussion among turbine experts. As the flow approaches zero, the deviation between the model and the measured characteristic curve is highest. At least, the similarity is good enough for a priori simulations, i.e. before the turbine design is complete and no model measured characteristics are available.

References

Dörfler. P.K., el al "Stable operation achieved on single-stage reversible pump turbine showing instability at no-load operation". Proceeding of the 19th Symposium on Hydraulic Machinery and Systems (Singapore, 1998)

Martin C.S. "Instability of pump-turbines with s-shaped char acteristics". Proceedings of 20th Symposium on Hydraulic Machinery and Systems (Charlotte, USA,2000)